The Pennsylvania State University

The Graduate School

WATER UPTAKE, MORPHOLOGY, AND COMPOSITION MEASUREMENTS OF SECONDARY ORGANIC AND ANTHROPOGENIC AEROSOL PARTICLES

A Dissertation in

Chemistry

by

Joseph Nelson Dawson

© 2020 Joseph Nelson Dawson

Submitted in Partial Fulfillment
of the Requirements
for the Degree of

Doctor of Philosophy

December 2020

The dissertation of Joseph Nelson Dawson was reviewed and approved by the following:

Miriam Freedman
Associate Professor of Chemistry
Dissertation Advisor
Chair of Committee

Christine Keating
Distinguished Professor of Chemistry

Raymond Schaak
DuPont Professor of Materials Chemistry

Donghyun Rim
Associate Professor of Architectural Engineering

Philip Bevilacqua
Distinguished Professor of Chemistry and of Biochemistry and Molecular Biology
Head of the Department of Chemistry

ABSTRACT

Aerosol particles are ubiquitous in the atmosphere. They originate from both natural and anthropogenic sources. While aerosol particles exist in many forms such as mineral dust from deserts, sea salt from the oceans, and soot and ash from volcanos, most fine aerosol particles (< 2.5 microns) in the continental mid-latitudes are composed of organic matter, by mass. Aerosol particles are known to affect the climate by the absorption and/or scattering of solar radiation. This occurs through the direct interaction of light with particles (aerosol direct effect), or by particles serving as cloud nuclei and the clouds interacting with light (aerosol indirect effect). These climate interactions result in a net cooling of the Earth. However, there is much uncertainty in the extent that they cool, which originates from a fundamental and incomplete understanding of the physical and chemical properties of aerosol particles. Furthermore, due to being ubiquitous in the air, humans often breathe in aerosol particles; the smallest particles can enter deep into the lungs and cause adverse health effects. Similarly, the extent of these health effects are not well understood due to a lack of understanding the fundamental properties of these aerosol particles, such as composition. These negative health effects are correlated to particle concentration, and when indoors, humans can be exposed to very high concentrations of aerosol particles of varying compositions.

In this work, we focused on two major objectives, the first of which was the characterization of the hygroscopicity, cloud condensation nucleating ability, and optical properties of secondary organic aerosol (SOA) and water soluble organic compounds (WSOCs). We worked in collaboration with nearby universities to apply multiple techniques to the same laboratory samples to calculate the single hygroscopicity parameter κ with three different experimental techniques. One of the goals of this project was to provide insight into the differences in the values obtained by these techniques in order better understand κ measured by a

single technique. We applied cavity ring-down spectroscopy (CRDS), hygroscopic tandem differential mobility analysis (H-TDMA), and cloud condensation nuclei counting (CCNC) to non-surface active (WSOCs) and SOA. The WSOCs studied consisted for four viscous sugars. SOA has been shown to be viscous, and to probe the effect of viscosity on water uptake, the system was simplified to use single component systems, in this case sugars. We showed that the hygroscopicity of compounds is governed by their molecular weight in accordance to κ-Kohler theory and provide a comparative analysis of the results from the three techniques.

To increase the complexity of our system and further investigate water uptake by SOA, we generated laboratory samples for SOA using pure precursors. Both α-pinene and *trans*-caryophyllene SOA was formed under four conditions. These conditions reflect some of the conditions SOA is created under in the atmosphere including high humidity, low humidity, high humidity with seed particles, and low humidity with seed particles. As before, three techniques were applied to the same samples and compared with each other. The major findings in this study were that a viscous SOA coating inhibits water uptake of ammonium sulfate seeds when below the deliquescence point of the SOA, and fortify the understanding that composition of SOA plays a role in its hygroscopicity.

The second major objective of this work was to characterize indoor air pollutants. In this study, hairdryers were selected as a household source of indoor air pollution. Of the hairdryers tested all generated ultrafine particulate matter, which has been shown to be harmful to human health in high concentrations. Furthermore, some hairdryers were shown to generate silver nanoparticles in the ultrafine range. Silver nanoparticles are well known to cause oxidative stress within living organisms. Due to their small size, they can penetrate deep into the lungs and pass into the blood stream via the blood-air interface. Emission rates for the hairdryers are calculated and found to generate particles an order of magnitude greater than burning candles, a well-known

indoor air pollutant. The results presented herein can help improve climate modeling, increase visibility by reducing haze events, and mitigate the adverse health effects caused by indoor air pollutants.

TABLE OF CONTENTS

LIST OF FIGURES

LIST OF TABLES

LIST OF ABBREVIATIONS

AER ..... Air Exchange Rate

CCN ..... Cloud Condensation Nuclei

CCNC.....Cloud Condensation Nuclei Counter

CPC .....Condensation Particle Counter

CRDS .....Cavity Ring-Down Spectroscopy

DMA .....Differential Mobility Analyzer

DMT..... Droplet Measurement Technologies

d_{p50} .....Critical Activation Diameters

EDB .....Electrodynamic Balance

EDS .....Energy Dispersive Spectroscopy

EPA ..... Environmental Protection Agency

*f*RH .....Optical Growth Factor

G_f ..... Growth Factor

HPLC .....High Performance Liquid Chromotography

H-TDMA ..... Hygroscopic Tandem Differential Mobility Analyzer

ICP-AES ..... Inductively Coupled Plasma Emission Spectroscopy

NAAQS..... National Ambient Air Quality Standards

OA ..... Organic Aerosol

OPS .....Optical Particle Spectrometer

OSHA.....Occupational Safety and Health Administration

$PM_{0.1}$ .....Particulate Matter less than 100 nanometers

PM_{10} ..... Particulate Matter less than 10 microns

$PM_{2.5}$ ..... Particulate Matter less than 2.5 microns

POA ..... Primary Organic Aerosol

RH ..... Relative Humidity

SMCA ..... Scanning Mobility CCN Analysis

SMPS ..... Scanning Particle Mobility Sizer

SOA ..... Secondary Organic Aerosol

SVOC ..... Semi-Volatile Organic Compound

TEM ..... Transmission Electron Microscopy

VOC ..... Volatile Organic Compound

WSOC ..... Water Soluble Organic Compound

κ ..... Single-parameter Hygroscopicity

ACKNOWLEDGEMENTS

For all her encouragement, support, guidance, and instruction, I thank my graduate advisor, Dr. Miriam Freedman. Miriam has supported me through every struggle of my graduate career and provided me with every possible opportunity for personal and professional development within her capability. She has encouraged me through even the toughest times when work life and private life clashed as a perfect storm. She will forever have my most sincere gratitude. I truly think that I could not have had a better mentor. Furthermore, I would like to thank my graduate committee for their support in my professional development. Dr. Christine Keating, Dr. Raymond Schaak, Dr. Frank Dorman, and Dr. Donghyun Rim have all provided me with valuable insight during the course of my thesis work, providing suggestions, ideas, and feedback during critical times. I would also like to thank all of my collaborators over the years; Dr. Rim, Dr. Murray Johnston, Dr. Akua Asa-Awuku, Dr. Timothy Raymond, Dr. Dabrina Dutcher, Devan Kerecman, Patricia Razafindranbinina, and Kotiba Malek. Not only did they assist with my thesis work by providing suggestions, ideas, and contributions to research, but they were all a genuine pleasure to work with. I would like to thank the wonderful staff at Penn State's Materials Research Institute for sharing their experience and knowledge while training me on research equipment and discussing experiments with a special shout-out to Dr. Jenn Gray who was always exceptionally kind and understanding. I offer a very heartfelt thanks to all the Freedman Lab members present and past that have been great friends and helped me along the way with a special thanks to Dr. Muhammad Altaf who trained me when I first joined the lab and mentored me until he graduated. Finally, I would like to thank those who have supported me even before I began my graduate career. My undergraduate advisors Dr. Craig Sockwell and Dr. Chong Qiu deserve more thanks than I can give. Not only did they support and encourage me, but if not for them I would have never of seen graduate school as a possibility. My family has provided continual love, support,

and most importantly understanding as I have ventured on this endeavor. My mother, Candy Dawson, has prioritized and encourage my education from the very start often providing for that education on her own. My grandparents, Ruth and Nelson Tucker, deserve a very special thanks as well, in a way I cannot even begin to articulate. The love and support of my family crosses any distance to find a way to help me pursue my dreams.

I gratefully acknowledge support from the NSF CAREER program (CHE-1351383) and a seed grant from Penn State's Institute of Energy and the Environment. I also acknowledges funding from the NSF GRFP (NSF 1255832). All findings and conclusions in this work do not necessarily reflect the view of the funding agencies.

Chapter 1

Introduction

1.1 Aerosol Particles in the Atmosphere

The atmosphere consists of a complex mixture of aerosols which vary in size and composition. Due to this diverse mixture of compounds in the atmosphere, aerosol particles themselves are often composed of multiple organic and inorganic compounds. In addition to being complex mixtures, aerosol particles vary greatly in size and distribution. Aerosol particles in the atmosphere are often divided into three size regimes; Aitken mode, accumulation mode, or coarse mode. Coarse mode particles are those between 2 and 100 microns and they are readily removed from the air by sedimentation.[1] The Aitken mode are particles less than 90 nm which coagulate into larger particles. The accumulation mode are particles ranging from 90 nm to 2 microns and are not as easily removed from the atmosphere as coarse mode particles because they do not sediment as quickly. For this reason, aerosol particles less than 2 microns are of particular interest due to the long times they spend in the atmosphere and therefore the long distances they can travel.[2, 3]

Aerosol particles are ubiquitous in the atmosphere and are generated from a number of sources. The some of the ones we recognize most commonly are dust particles, soot from exhaust, and pollen. However, aerosol particles are much more expansive than the ones we recognize in our daily lives. Volcanoes, forest fires, coal powered power plants, wood burning cook stoves, and other combustion sources all generate soot and ash known as black carbon. Windblown dust from deserts produce mineral dust aerosols. Factories and other industrial sources produce sulfates, and nitrates. Trees and other vegetation produce semi-volatile organic compounds, and

when these compounds react in the highly oxidizing environment of the Earth's atmosphere, brown carbon aerosol particles are formed. The breaking of waves produces salt aerosol as well as releases a number of organic compounds into the atmosphere. While these generation methods do not account for all of the aerosol particles in the atmosphere, they do exemplify the complexity of aerosol science. Each particle, based on size, shape, composition, and reactivity, affect our environment in a number of ways. Some of these ways include adversely effecting human health, interacting with solar radiation to influence our climate, forming haze which limits visibility, acting as cloud condensation nuclei, acting as ice nuclei, and influencing the heterogeneous chemistries of the atmosphere.

1.2 Aerosol Particles' Influence on the Climate and Associated Uncertainties

The IPCC report shows that even with the collective knowledge of the atmospheric chemistry community, there is still great uncertainty with regard to aerosol particles.[4] On the other hand, greenhouse gasses like water, carbon dioxide, and methane are relative well understood. Unlike greenhouse gasses that have a positive radiative forcing (a warming effect), aerosol particles are reported to have a net cooling effect. For reference, a radiative forcing value of 0 W m^{-2} indicates a lack of change in the amount of solar radiation absorbed by the Earth relative to the amount of solar radiation that was absorbed in 1750 under preindustrial conditions. Aerosol particles that are the result of direct emission (mineral dust, sulfates, nitrates, organic carbon, and black carbon) have a reported radiative forcing of 0.23 W m^{-2}. The uncertainty in this measurement results in a range of radiative forcing values from -0.77 W m^{-2} to 0.23 W m^{-2} which is important since, on the extreme end of this range, radiative forcing values are in the "warming" category. The interactions of aerosol particles with incoming solar radiation is known as the direct effect (Figure 1-1). Compounding on the uncertainty of aerosol particle's influence on the

radiative budget is the indirect effect. The indirect effect is when aerosol particles uptake water and lead to cloud formation (Figure 1-1). The uncertainty in cloud adjustments due to aerosols is even greater than that of the particles themselves with radiative forcing values ranging from -1.33 W m^{-2} to -0.06 W m^{-2}. Much of the uncertainty in current radiative forcing calculations is due to the influence of secondary organic aerosol particles. SOA have complex compositions and often contain surface active organic compounds. Additionally, some SOA have been shown to be hygroscopic, and as a result, contributes to both uncertainty in the aerosol direct effect, and the aerosol indirect effect. Not only is the contribution of SOA to the radiative budget not well understood, SOA also pose a number of environmental concerns. For example, one other effect of atmospheric SOA is the potential for forming visibility reducing.[5]

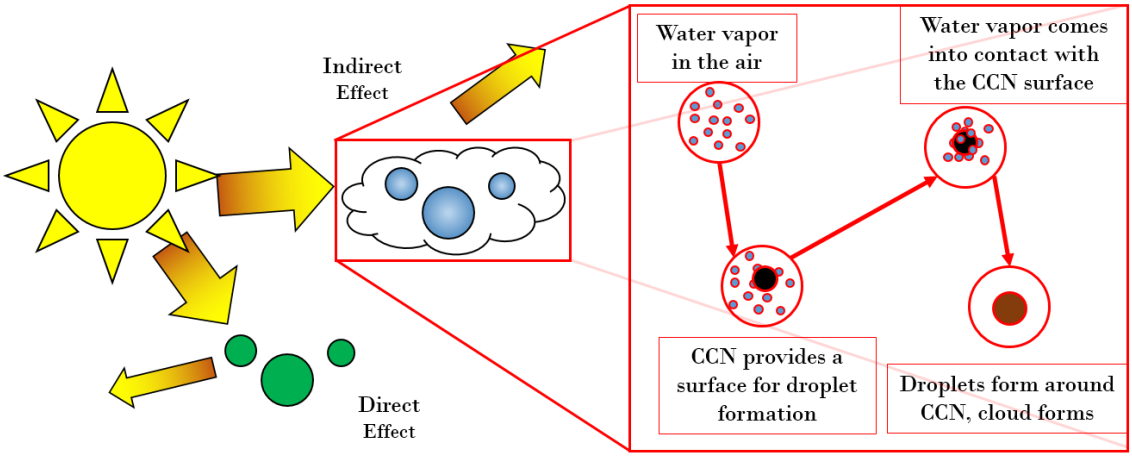

Figure 1-1: Illustration of the aerosol direct effect and aerosol indirect affect with an excerpt showing the formation of a cloud by a cloud nucleating particle.

1.3 Formation and Complexity of Secondary Organic Aerosol Particles

Particulate organic matter makes up 20% - 60% of the particulate mass in the continental mid-latitudes and is often the dominant fraction of fine particulate matter.[6-8] Fine aerosols are expected to have a stronger impact on the climate because their sizes are close to the wavelengths of light in the visible spectrum.[7] This particulate matter exists in two forms - primary organic

aerosol (POA), and secondary organic aerosol (SOA). POA is directly emitted aerosol, while SOA is aerosol that forms from precursors in the atmosphere. The compositions of particulate matter are poorly understood, despite its relative abundance.[9] An understanding of the composition of atmospheric particulate matter is important for the development of efficient air quality management. With a proper understanding of the climate effects and adverse health effects of these aerosols particles, policy can be in enacted to mitigate these negative effects.[10] While POA, which is easier to know the composition of, remains a concern for their influence on the climate, it only composes about 20% of the total organic aerosol mass in the global atmosphere.[7, 11, 12] SOA often forms by gas phase photochemistry followed by either new particle formation, absorption of semi-volatile products into preexisting OA mass, or nucleation by a seed particle.[13, 14] Interestingly, POA can also be converted into SOA; POA often contains semi-volatile organic compounds that evaporate after direct emission and undergo atmospheric reactions to become SOA.[15]

Much of the complexity of SOA lies in its composition. Regulation targets the control of SOA precursors like, nitrogen oxides, sulfates, and POA, but knowing the compositions of the precursor does not provide a full perspective of the SOA compositions. For example, β-Pinene is a common SOA precursor released by vegetation in the eastern hemisphere, and under very well defined conditions, it alone has been shown to produce dozens of derivative compounds; however, the conditions of the atmospheric are not well controlled and studies like these only give a limited understanding of SOA composition.[16] The greatest uncertainties of SOA come from the following: a lack of knowledge of the SOA precursor gases, not understanding the relative importance of those gases in the atmosphere (e.g. their abundance), not understanding the importance of organic nucleation on a global scale, the hygroscopic uncertainties of SOA and their involvement in cloud formation, the uncertainties of the optical properties of SOA and the effect of particle aging on those properties, and a lack of understanding of how aerosols are

mixed in the atmosphere and if that mixing alters their properties.[7] In this thesis, work we explore the hygroscopicity and optical properties of laboratory generated SOA with the goal of furthering the understanding of SOA and improving climate models.

1.4 Health Effects of Aerosol Particles

Since aerosol particles are ubiquitous in the atmosphere, they are frequently inhaled by humans. Some aerosol particles have been shown to have negative effects on human health. The most notable of these effects is usually thought of in terms of air pollutants like smog and major air pollution events such as the 1948 Donora smog disaster. Repeated smog events and the deaths associated with those events eventually lead to the formation of the Clean Air Act in 1963. As particulate matter continued to be a growing concern, the Clean Air Act was amended in 1977 to set new goals in air pollution reduction in the form of the National Ambient Air Quality Standards (NAAQS).[17] While air pollution reduction has come a long way, the influence of aerosol particles on health is still only regulated in terms of size. Specifically, particulate matter is classified into three main categories: coarse particles, fine particles, and ultrafine particles. Coarse, fine, and ultrafine particulate matter consist of particles less than 10 microns, 2.5 microns, and 100 nm in diameter, respectively, but are more commonly referred to by the abbreviations PM_{10}, $PM_{2.5}$, and $PM_{0.1}$. The EPA regulations for these particle groupings are shown in Table 1-1. It is of note that $PM_{0.1}$ currently has no federal limitation to its emission, which is in part due to the difficulty in measuring it.

Table 1-1: EPA emission regulations for particulate air pollution for coarse and fine aerosol particles.

Particle Pollution (PM)	$PM_{2.5}$	Primary	1 Year	12.0 μg m^{-3}	Annual mean, averaged over 3 years
		Secondary	1 Year	15.0 μg m^{-3}	Annual mean, averaged over 3 years
		Primary and Secondary	24 Hours	35 μg m^{-3}	98th percentile, averaged over 3 years
	PM_{10}	Primary and Secondary	24 Hours	150 μg m^{-3}	Not to be exceeded more than once per year on average over 3 years

Table adapted from https://www.epa.gov/criteria-air-pollutants/naaqs-table.[17]

EPA has issued guidelines are set to limit the amount of particulate matter emissions in the outdoor environment with daily limits set to 150 μg m^{-3} day^{-1} for coarse particles and 35 μg m^{-3} day^{-1} for fine particles. The reason that the larger particles allow for a greater daily emission is because that the health impacts of aerosols are grouped by size and the divisions made are set to reflect the potential health impact of each size regime. That is, the smaller a particle is, the greater the risk it imposes.

Aerosol particles consist of more than just smog, however. Part of the reason that aerosol particles are ubiquitous is because they are naturally generated in addition to the anthropogenically generated particles. Volcanoes, windblown dust from deserts, and sea spray all produce coarse aerosol particles as well as plant life producing pollen. These particles act as irritant, and result in coughing when inhaled as coughing being our bodies' natural method of removing irritants. Fine particulate matter is more hazardous than course aerosol particles due to the fact that they are easily breathed in and penetrate deep in the lungs. These particles become trapped in the alveoli as our bodies do not have the means to remove them. Some sources of fine aerosol particles include soot, secondary organic aerosol, and sulfate or nitrate particles. While they are neither well studied nor regulated explicitly by the EPA, ultrafine particulate matter has the highest potential for negative health effects. Due to their small size, they are capable of not only entering the lung, but can enter the bloodstream through the blood-air barrier. The

production of ultrafine aerosol particles is not well characterized as they are more difficult to measure and detect than larger particles. Some known common sources of ultrafine particles include biogenic sources such as the oxidation of gas-phase species leading to new particle formation, and anthropogenic sources such as cook stove, burning candles, and heated metal surfaces.

While the full extent of the health impacts of aerosol particles is not understood, many studies have been done to correlate these particles with adverse health effects such as cardiopulmonary disease. One of the most cited studies is the Harvard Six Cities study which demonstrated a correlation between particulate matter and increased mortality rates.[18] The study presented a strong linear correlation between mortality rates and fine particulate matter while factoring in considerations such as age; that is, they identified the risk factors already associated with some populations to extrapolate a mortality ratio without the interference of those risks.

What these studies lack, however, is a consideration of particle composition. Particles size does not sufficiently describe their influence on the body. Shape, composition, and phase all play an important role in their health hazards. Furthermore, regulations from the EPA only consider the concentrations of particles outdoors whereas people may be subjected to much higher particle concentrations while indoor. Recent events like the COVID-19 outbreak have made people more aware of the air they breathe while indoors. Studies have shown that Americans spend approximately 87% of their time indoors. The indoor environment is often poorly ventilated, and even pollution source with low generation rates can lead to particle concentrations that exceed the outdoor standards. Another factor leading to hazardous indoor conditions is the relative distance to emission sources. Ultrafine particles have a very high mobility due to their small size which results in them colliding with each other and growing to larger sizes very quickly. However, when near the emission source, this may not occur quickly enough. Some examples of these activities include cooking, cleaning, cigarette smoking, and

combustion (such as candle burning). The uncertainties in our understanding of the health impacts of indoor air pollution has resulted in a lack of regulation or concern by the general populace. The study of indoor air pollution and its sources may improve air quality, and quality of life.

1.5 Overview of Dissertation

This thesis work focuses on the characterization of aerosol particles' fundamental properties with the goal of improving air quality and better predicting the optical properties and cloud nucleating abilities of aerosol particles. Chapter 2 focuses on the instruments and techniques used to generate and study aerosol particles, specifically outlining the tools we use to characterize particle composition, size, concentration, optical properties, hygroscopic growth, and cloud condensation nuclei activity.

In chapter 3, highly viscous sugars are used in a multi-university collaboration as proxies for SOA. We used three complimentary laboratory techniques to study the hygroscopic growth of these sugars in an attempt to elucidate the impacts of viscosity on water uptake. Additionally, the optical properties, and CCN activities of these sugars are measured. Finally, we explore two methods of determining κ-factor using the CRDS and compare those values with the κ-factors obtained from CCNC, H-TDMA, and theory.

Chapter 4 is a continuation of the collaborative study performed in chapter 3. In this study, we increase the complexity of our system by moving from SOA proxies to study laboratory generated SOA. The SOA is generated in four ways using two different precursors. Here, again, CRDS, H-TDMA, and CCNC are used to analyze the same sample with the goal of being able to relate κ-factors acquired by different measurements, with each other as well as explore their systematic limitations in obtaining these values.

Chapter 5 focuses on the health impacts of aerosol particles in the indoor environment. Specifically, we use TEM, SMPS, and EDS to characterize the size, composition, and emission strength of particulate matter released during the operation of hairdryers. After finding silver nanoparticles released by some of the hairdryers, they are further studied in an attempt to find the component that releases these particles.

Finally, chapter 6 is a summary of the main finding of this dissertation and outlines our continuing goals. It includes a description of the next phase of the collaboration from chapters 3 and 4 with our proposed experimental approach.

References

1. Zhao, T. L.; Gong, S. L.; Zhang, X. Y.; McKendry, I. G., Modeled size-segregated wet and dry deposition budgets of soil dust aerosol during ACE-Asia 2001: Implications for trans-Pacific transport. *Journal of Geophysical Research: Atmospheres* **2003**, *108*, (D23).

2. Duncan Fairlie, T.; Jacob, D. J.; Park, R. J., The impact of transpacific transport of mineral dust in the United States. *Atmospheric Environment* **2007**, *41*, (6), 1251-1266.

3. Cahill, C. F., Asian aerosol transport to Alaska during ACE-Asia. *Journal of Geophysical Research: Atmospheres* **2003**, *108*, (D23).

4. Stocker, T. F.; Qin, D.; Plattner, G.-K.; Tignor, M. M.; Allen, S. K.; Boschung, J.; Nauels, A.; Xia, Y.; Bex, V.; Midgley, P. M., Climate Change 2013: The physical science basis. contribution of working group I to the fifth assessment report of IPCC the intergovernmental panel on climate change. In Cambridge University Press: 2014.

5. Tanner, R. L.; Parkhurst, W. J., Chemical Composition of Fine Particles in the Tennessee Valley Region. *Journal of the Air & Waste Management Association* **2000**, *50*, (8), 1299-1307.

6. Carlton, A. G.; Turpin, B. J.; Altieri, K. E.; Seitzinger, S.; Reff, A.; Lim, H.-J.; Ervens, B., Atmospheric oxalic acid and SOA production from glyoxal: Results of aqueous photooxidation experiments. *Atmospheric Environment* **2007**, *41*, (35), 7588-7602.

7. Kanakidou, M.; Seinfeld, J. H.; Pandis, S. N.; Barnes, I.; Dentener, F. J.; Facchini, M. C.; Van Dingenen, R.; Ervens, B.; Nenes, A.; Nielsen, C. J.; Swietlicki, E.; Putaud, J. P.; Balkanski, Y.; Fuzzi, S.; Horth, J.; Moortgat, G. K.; Winterhalter, R.; Myhre, C. E. L.; Tsigaridis, K.; Vignati, E.; Stephanou, E. G.; Wilson, J., Organic aerosol and global climate modelling: a review. *Atmospheric Chemistry & Physics* **2005**, *5*, (4), 1053-1123.

8. Yu, F.; Luo, G., Simulation of particle size distribution with a global aerosol model: contribution of nucleation to aerosol and CCN number concentrations. *Atmospheric Chemistry & Physics Discussions* **2009**, *9*, (2).

9. Turpin, B. J.; Saxena, P.; Andrews, E., Measuring and simulating particulate organics in the atmosphere: problems and prospects. *Atmospheric Environment* **2000**, 34, (18), 2983-3013.

10. Carlton, A.; Wiedinmyer, C.; Kroll, J., A review of Secondary Organic Aerosol (SOA) formation from isoprene. *Atmospheric Chemistry & Physics* **2009**, *9*, (14), 4987-5005.

11. Spracklen, D.; Jimenez, J.; Carslaw, K.; Worsnop, D.; Evans, M.; Mann, G.; Zhang, Q.; Canagaratna, M.; Allan, J.; Coe, H., Aerosol mass spectrometer constraint on the global secondary organic aerosol budget. *Atmospheric Chemistry & Physics* **2011**, *11*, (23), 12109-12136.

12. Ervens, B.; Turpin, B.; Weber, R., Secondary organic aerosol formation in cloud droplets and aqueous particles (aqSOA): a review of laboratory, field and model studies. *Atmospheric Chemistry & Physics Discussions* **2011**, *11*, (8).

13. Pankow, J. F., An absorption model of the gas/aerosol partitioning involved in the formation of secondary organic aerosol. *Atmospheric Environment* **2007**, *41*, 75-79.

14. Odum, J. R.; Hoffmann, T.; Bowman, F.; Collins, D.; Flagan, R. C.; Seinfeld, J. H., Gas/Particle Partitioning and Secondary Organic Aerosol Yields. *Environmental Science & Technology* **1996**, *30*, (8), 2580-2585.

15. Shrivastava, M. K.; Lipsky, E. M.; Stanier, C. O.; Robinson, A. L., Modeling Semivolatile Organic Aerosol Mass Emissions from Combustion Systems. *Environmental Science & Technology* **2006**, *40*, (8), 2671-2677.

16. Ma, Y.; Marston, G., Multifunctional acid formation from the gas-phase ozonolysis of β-pinene. *Physical Chemistry Chemical Physics* **2008**, *10*, (40), 6115-6126.

17. U.S. EPA National Ambient Air Quality Standards for Particulate Matter. www.epa.gov/criteria-air-pollutants/naaqs-table (November 27, 2020),

18. Dockery, D. W.; Pope, C. A.; Xu, X.; Spengler, J. D.; Ware, J. H.; Fay, M. E.; Ferris, B. G.; Speizer, F. E., An Association between Air Pollution and Mortality in Six U.S. Cities. *New England Journal of Medicine* **1993**, *329*, (24), 1753-1759.

Chapter 2

Instrumentation

2.1 Aerosol Particle Generation Techniques

Two main aerosol particle generation techniques are used in this work, solution atomization and chamber generation. In solution atomization an aqueous of the analyte is formed by dilution with HPLC grade water. The aqueous solution is pumped by a syringe pump into a constant output atomizer (TSI 3076). By varying the solution concentration, syringe pump flow rate, and atomizer carrier gas flow rate, the distribution of atomized particles can be controlled. The syringe pump flow rate is maintained between 0.03 mL min^{-1} and 0.06 mL min^{-1} as faster injection rates provide diminishing returns in particle concentrations below 500 nm and slower injection rates can cause instability in the aerosol particle production. Solutions are atomized using either pre-purified nitrogen or purified house air as the carrier gas. Atomizer flow rates can vary greatly to maintain sufficient air flow for the analytical equipment to sample from.

In many cases aerosol particles generated in this method are dried with one of two methods: using a home-built diffusion dryer, or a Tedlar® chamber. The diffusion dryer is an approximately 3 ft long hollow cylinder with an approximate 3 in radius is filled with molecular sieve. The container has a cylindrical metal mesh of equal length running through the middle to prevent sieve from entering directly into the flow of air. Aerosolized sample is flowed through this diffusion dryer at a typical rate of 1.5 L min^{-1}. This system removes relative humidity at a rate of 98% RH s^{-1}.[1] When using higher flow rates than 1.5 L min^{-1}, multiple of these diffusion dryers can be used in series to ensure the particles are dry. The other method of aerosol particle drying is by dilution in a small Tedlar® chamber. The chamber is filled to about one quarter

capacity with the generated aerosol particles and then filled to capacity with dry nitrogen. This drying method is much slower (0.08% RH s^{-1}).[1]

Aerosol particles can also be generated by performing gas-phase reaction chemistry in large Tedlar® reaction chamber (Welsh Fluorocarbon®). The chamber is 1 m^3 when completely filled. The clean, empty chamber is filled with clean air that is either dry or humidified depending on the experimental conditions. To verify that the chamber is clean, it can be connected to a condensation particle counter to ensure there are fewer than 100 particles cm^{-3}. The clean chamber can be filled ozone using an arc ozone generator (Ozotech Inc. Poseidon Model) and the concentration of ozone is monitored with an ozone analyzer (Teledyne Model 430). Semivolatile biogenic precursor can be added to the high ozone environment within the chamber where it reacts with the ozone to produce SOA. The entire chamber is covered with a thick black cover to prevent light exposure to the sample.

2.2 Differential Mobility Analyzer

An electrostatic classifier (TSI 3080) and differential mobility analyzer (DMA, TSI 3081) can be used to size aerosol particles based on particle charge. A polydisperse aerosol particle flow goes through an impactor that removes large (>700 nm) particles by inertial impaction. The particle flow then enters into the electrostatic classifier where it passes through a 2 mCi ^{85}Kr neutralizer. Within the neutralizer particles reach a charge equilibrium due to their exposure to ionizing radiation such that they can be described by a charge distribution equation:

$$f(N) = 10^{\left[\sum_{i=0}^{5} a_i(N)(log\frac{D_p}{nm})^i\right]} \quad (2\text{-}1)$$

where a_i is the coefficient based on the Fuchs charge distribution model, D_p is the particle diameter, and $f(N)$ is the fraction of particles containing a given charge, N.[2, 3] For this thesis work,

the fraction of particles containing a +1 charge, and the fraction containing a +2 charge are calculated using Equation 2-1. After they are charged, the particles pass into the DMA column which creates an electrical field between a negatively charged rod and a grounded cylindrical column. This electric field separates the charged aerosol particles based on their electrical mobility. The electrostatic classifier controls the voltage of the charged rod which selects the particles of a given electrical mobility to pass. Generally, this electrical mobility selection is viewed as a "size selection" as when the electrostatic classifier is set to a given particle diameter, spherical particles with that diameter and a +1 charge are allowed to pass as described by

$$\frac{D_p}{C} = \frac{2neVL}{3\mu q_{sh} ln\frac{r_2}{r_1}} \tag{2-2}$$

where D_p is the particle diameter selected, C is the Cunningham slip correction, n is the number of elementary charges on the particle, e is the elementary charge, V is the average voltage of the rod, L is the length between the exit slit and the aerosol particle inlet, μ is the gas viscosity, q_{sh} is the sheath air flow rate, r_2 is the outer radius of annular space, and r_1 is the inner radius of annular space. However, it should be noted that particles other than those of the size selected can pass through the DMA column. Specifically, particles with a charge other than +1 will pass through the column if their electrical mobility is equal to that of the selected size with a +1 charge.[4]

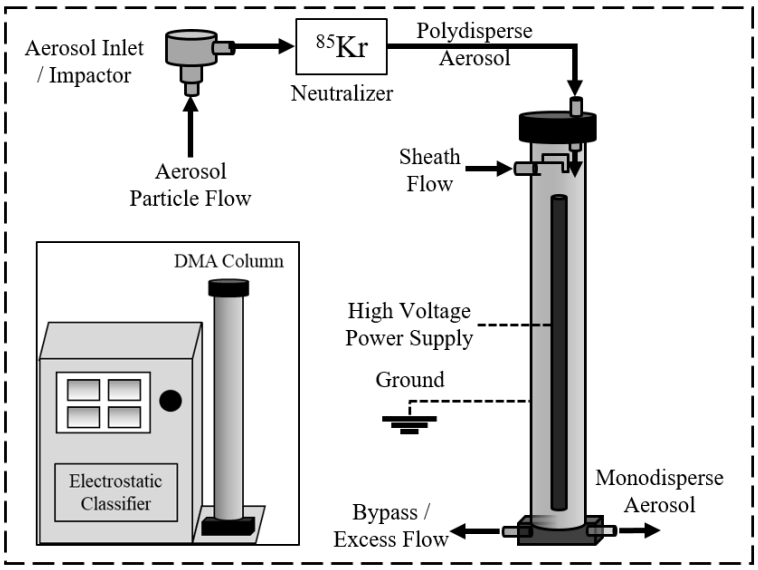

Figure 2-1: Schematic of electrostatic classifier and DMA.

2.3 Condensation Particle Counter

Aerosol particle concentrations can be measured with a condensation particle counter (CPC, TSI 3775). The CPC functions by condensing vapor onto existing particles causing them to grow. Once they have grown, they can be easily detected with an optical detector. The CPC is composed of a sensor, signal processing electronics, and a flow system. A saturator, a condenser, and an optical detector make up the sensor itself. The CPC functions starting at the aerosol inlet, where aerosol particles enter the saturator and pass through a heated, butanol-soaked wick. The butanol from the wick evaporates as it is heated, and as it cools it then saturates the carrier gas flow. The butanol then cools and condenses onto the aerosol particles as the flow enters the condenser, causing the particles grow to a detectable size.[5] The aerosol particles are then detected by light scattering. Specifically, light scattered by the particles is collected at an angle orthogonal to the incidence light and focused onto a low-noise photodiode.

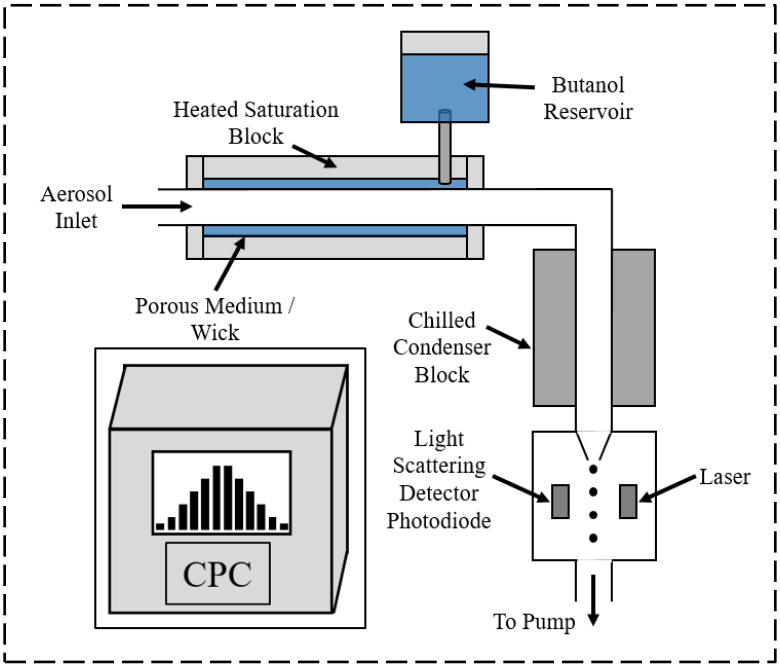

Figure 2-2: Schematic of condensation particle counter.

2.4 Cavity Ring-Down Spectroscopy

Cavity ring-down spectroscopy (CRDS) is an optical technique often applied to light absorbing gasses.[6] In this work CRDS is applied to aerosol particles to determine their optical properties and optical growth.[7-9] CRDS has a long effective path length making it a highly sensitive technique and ideal for this body of work. The CRDS consists of two 91 cm long stainless-steel cavities that are capped at both end with highly reflective mirrors (> 99.9985% reflective @ 640 nm; ATFilms, Boulder, CO) and each cavity had an effective path length of approximately 48 km. a 643 nm diode laser is split and pulsed in each cavity simultaneously. The light propagates through the cavity and upon each pass loses intensity. This intensity is measured by a photomultiplier tube with detects the light that is transmitted through the back mirror and a rate of decay is measure. When a sample enters the cavity the rate of decay increases due to the scattering and/or absorption of light by the sample. Extinction coefficients are determined from

these first order decay constants which quantifies the sum of both light scattering and light absorption by the sample. For aerosol particles, the particle concentration can be measured, and with that measurement and particle size information an extinction cross-section can be determined for a sample.[10] Furthermore, by humidifying the second cavity and comparing the two extinction cross-sections, an optical growth factor can be determined. The CRDS and its application to viscous organic aerosol particles is further described in Chapter 3.

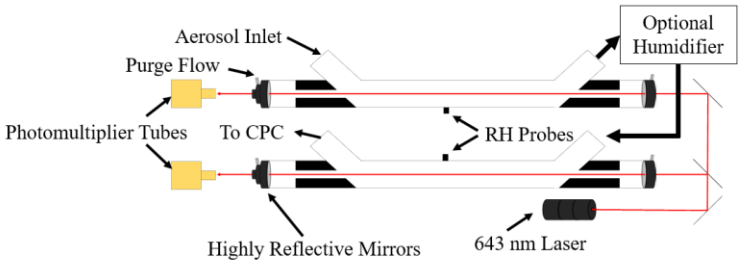

Figure 2-3: Simplified schematic of a cavity ring-down.

2.5 Cloud Condensation Nuclei Counter

In addition to CRDS, cloud condensation nuclei counting (CCNC) is another useful technique in the determination of the properties of aerosol particles. Specifically, CCNC measures the activation of hygroscopic aerosols that can serve as cloud condensation nuclei. A CCNC can be used to measure the concentration of aerosol particles that activate and act as CCN. A Droplet Measurement Technologies (DMT, Boulder, Colorado) CCNC is used in this thesis work to study the hygroscopic properties of SOA and SOA proxies. A DMT CCNC is contains a column with a thermal gradient. Aerosol particles and sheath air flow from the top of this cylindrical column to the bottom where temperature increases. Within the column, water vapor diffuses form the heated, humidified walls toward the centerline at a faster rate than heat. Thus, a thermodynamically unstable supersaturated water vapor state is reached. The CCNC manipulates this difference in diffusion rates to expose aerosol particles to supersaturated conditions. While in

these conditions supersaturated water vapor condenses onto the aerosol particles which eventually results in the formation of droplets. The size and number of particles are analyzed by the CCNC using an optical particle counter, and when paired with a DMA and a CPC the fraction of particles that are CCN activated as a function of water supersaturation and particle size is determined.[11]

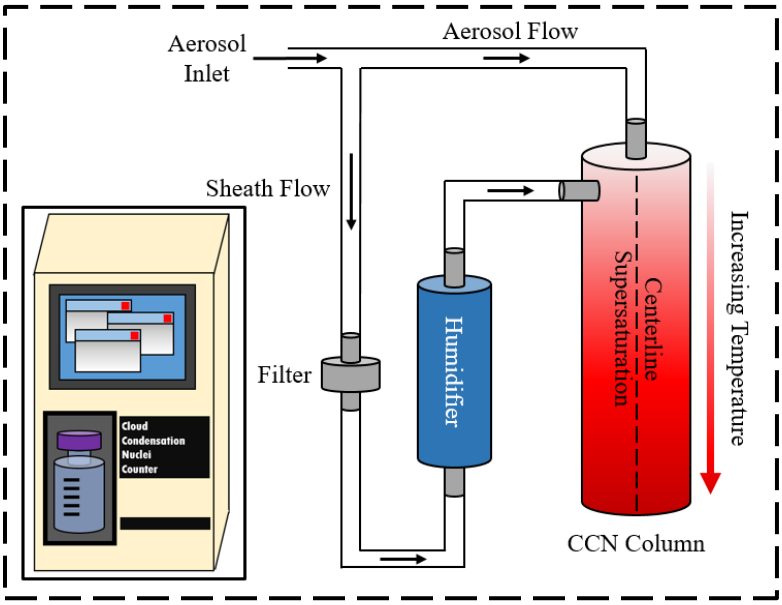

Figure 2-4: Simple Schematic of a cloud condensation nuclei counter including the temperature gradient within the CCNC column

2.6 Transmission Electron Microscopy and Accompanying Techniques

Transmission electron microscopy (TEM) is a robust imaging technique that operates at high magnification and resolution providing an advantage over light microscopes. Briefly described here, a TEM is composed of four primary systems: an electron optical column, a vacuum system, electronics, and an electron source.[12] Two TEMs are used in this work both of which use a LaB_6 electron source. The LaB_6 field emission gun generates and electron beam from the top of the optical column. This beam is condensed by the condenser lens into a nearly parallel beam at the sample. If the sample is sufficiently thin, then the electrons from the beam will

transmit through the sample where they are then collected and focused onto a detector where an image can be captured.[12]

While the process of transmission provides imaging data, the system itself is capable of much more. When electrons from the beam interact with the sample they can diffract and reveal crystallographic information in the form of a diffraction pattern. Additionally, when the high energy electron beam interacts with the sample the energy is absorbed and then rereleased in the form of X-rays. The energy of these X-rays corresponds to the element that absorbed the energy and as such elemental data can be acquired. This process is known as energy dispersive X-ray spectroscopy (EDS).[12] Generally, EDS is conducted by focusing the electron beam onto a point on the sample providing compositional information in that one spot on the sample, but by passing the beam along the sample a compositional map can be created in a process known as EDS mapping.

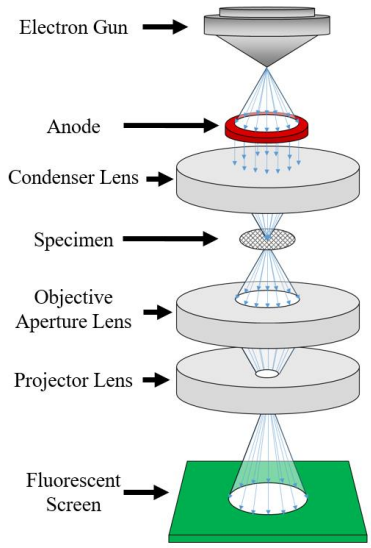

Figure 2-5: Schematic of the main components of a transmission electron microscope.

References

1. Altaf, M. B.; Freedman, M. A., Effect of Drying Rate on Aerosol Particle Morphology. *The Journal of Physical Chemistry Letters* **2017**, *8*, (15), 3613-3618.

2. Fuchs, N. A., On the stationary charge distribution on aerosol particles in a bipolar ionic atmosphere. *Geofisica pura e applicata* **1963**, *56*, (1), 185-193.

3. Wiedensohler, A., An approximation of the bipolar charge distribution for particles in the submicron size range. *Journal of Aerosol Science* **1988**, *19*, (3), 387-389.

4. Knutson, E. O.; Whitby, K. T., Aerosol classification by electric mobility: apparatus, theory, and applications. *Journal of Aerosol Science* **1975**, *6*, (6), 443-451.

5. Stolzenburg, M. R.; McMurry, P. H., An Ultrafine Aerosol Condensation Nucleus Counter. *Aerosol Science and Technology* **1991**, *14*, (1), 48-65.

6. Friedrichs, G., Sensitive Absorption Methods for Quantitative Gas Phase Kinetic Measurements. Part 2: Cavity Ringdown Spectroscopy. *Zeitschrift für Physikalische Chemie* **2008**, *222*, (1), 31.

7. Freedman, M. A.; Hasenkopf, C. A.; Beaver, M. R.; Tolbert, M. A., Optical Properties of Internally Mixed Aerosol Particles Composed of Dicarboxylic Acids and Ammonium Sulfate. *The Journal of Physical Chemistry A* **2009**, *113*, (48), 13584-13592.

8. Abo Riziq, A.; Erlick, C.; Dinar, E.; Rudich, Y., Optical properties of absorbing and non-absorbing aerosols retrieved by cavity ring down (CRD) spectroscopy. *Atmospheric Chemistry and Physics* **2007**, *7*, (6), 1523-1536.

9. Rudich, Y.; Donahue, N. M.; Mentel, T. F., Aging of Organic Aerosol: Bridging the Gap Between Laboratory and Field Studies. *Annual Review of Physical Chemistry* **2007**, *58*, (1), 321-352.

10. Berden, G.; Engeln, R., *Cavity ring-down spectroscopy: techniques and applications*. John Wiley & Sons: 2009.

11. Roberts, G. C.; Nenes, A., A Continuous-Flow Streamwise Thermal-Gradient CCN Chamber for Atmospheric Measurements. *Aerosol Science and Technology* **2005**, *39*, (3), 206-221.

12. Williams, D. B.; Carter, C. B., The Transmission Electron Microscope. In *Transmission Electron Microscopy: A Textbook for Materials Science*, Springer US: Boston, MA, 1996; pp 3-17.

Chapter 3

Direct Comparison of the Hygroscopicity of Water-Soluble Sugars

This chapter has been adapted from Joseph Nelson Dawson, Kotiba A. Malek, Patricia N. Razafindrambinina, Timothy M. Raymond, Dabrina D Dutcher, Akua Asa-Awuku, and Miriam Arak Freedman, "Direct Comparison of the Hygroscopicity of Water-Soluble Sugars", *Submitted*, **2020**.

Author Contributions: I contributed to this work by structuring experiments, operating the CRDs, preforming relevant calculations of κ, and writing the manuscript.

Abstract

Water-soluble organic compounds (WSOCs) readily uptake water and form atmospheric droplets. Understanding the water uptake ability of these WSOCs can improve our understanding of their radiative effects, and thus can improve current climate models. In this study, we measure the subsaturated and supersaturated droplet growth of four WSOCs: levoglucosan, sucrose, raffinose, and trehalose. Specifically, we use three distinct nanoscale droplet growth methods: cavity ring-down spectroscopy (CRDS), hygroscopic tandem differential mobility analysis (H-TDMA), and cloud condensation nuclei (CCN) counting; and report optical growth factor (*f*RH), growth factor (G_f), refractive indices, and critical activation diameters (d_{p50}) for each aerosol system. Ideal thermodynamic Köhler theory is applied and the single parameter hygroscopicity, κ, is reported for the four WSOCs. Additionally, we compare two methods for calculating the κ-values from *f*RH data. Results are compared to droplet activation theory and hygroscopicity parameterizations and discussed within the context of current findings in literature. We show that the single parameter hygroscopicity term for water-soluble sugars is dependent on molecular weight. The three experimental methods have comparable precision with systematic deviations in the average mean for each method. Better hygroscopicity comparisons can be made with

literature values by understanding the relationship between the κ-values obtained via different techniques.

3.1 Introduction

Aerosol particles affect the radiative budget of the Earth through their interactions with solar radiation. Specifically, aerosol particles influence the radiative budget via direct and indirect effects. The direct effect results from the scattering or absorption of light by the particles themselves.[1] In addition, many aerosol particles are hygroscopic; and, therefore, may act as cloud condensation nuclei (CCN), taking up water and leading to the formation of droplets and clouds; this interaction is known as the indirect effect. Changes in the amount of water adsorbed subsequently affect the reflection and absorption of light. Thus, the ability of water to condense and partition from gas to liquid on particle surfaces has significant implications for visibility, air quality, and climate.[2, 3]

Organic aerosols are ubiquitous in the atmosphere; their interactions with water (water-uptake, diffusivity, etc.), however, are poorly understood.[4] Specifically, water-soluble organic compounds (WSOCs) make up a large fraction of the organic composition and are emitted by large aerosol sources such as biogenic and biomass burning sources.[5-8] WSOCs with solubilities above 100 gL^{-1} are assumed to fully dissolve and readily uptake water.[9, 10] However, solubility does not fully describe hygroscopicity and, thus, understanding other chemical and physical properties of WSOCs (e.g., structure, solubility, molecular weight, density, molality) are critical to predicting particle water uptake.

In this work, we measure droplet growth of four WSOCs: levoglucosan, an anhydrosugar, and three disaccharides (sucrose, raffinose, and trehalose). Levoglucosan is one of the most abundant atmospheric carbohydrates and is a well-studied marker of biomass burning.[11-13] The

ability of levoglucosan to promote atmospheric droplet formation has been measured with different techniques. Rosenørn et al. (2006) used a static-thermal gradient type cloud condensation nuclei counter (CCNC) and Svenningsson et al. (2006) used a hygroscopic tandem differential mobility analyzer (H-TDMA) and CCNC to measure the droplet growth of levoglucosan particles in sub and supersaturated environments.[14, 15] Water-uptake behavior has been measured for levoglucosan with an electrodynamic balance (EDB); however, these experiments deal with micron-sized particles, unlike the methods used in this work, which investigate the more atmospherically relevant submicron aerosol particles.[16, 17] Lei et al. (2014), Mochida and Kawamura (2004), and Svenningsson et al. (2006) all observed no deliquescence phase transition for levoglucosan below 100% relative humidity (RH). Levoglucosan particles retained water as low as 5% RH.[15, 18, 19]

In addition to levoglucosan, three sugars (sucrose, raffinose, and trehalose) are studied. Sucrose, though less atmospherically prevalent than levoglucosan, has been measured in the ambient and is also thought to be a good proxy for highly soluble and viscous WSOCs.[20-22] The ability of highly viscous "glassy" sucrose nanoparticles to uptake water is of recent interest and has been well studied.[23-31] Sucrose particles have been identified as glassy at room temperature with an RH less than 25%.[29] Furthermore, Koop et al. (2011) published that the thermal glass transition temperature, the relative magnitude of which indicates the relative amount of hygroscopic growth, depends strongly on molecular weight more than functional groups or O:C ratio.[32] Rosenørn et al (2006) measured the CCN activity of sucrose and other saccharides and identified differences in molecular weight as a source of significant change in hygroscopicity.[14] Lee et al. (2018) took H-TDMA measurements of sucrose to compare atomic force microscopy techniques to other viscosity measurements.[33] Hence, we probed the water uptake of two additional sugars with higher molecular weight than sucrose (raffinose and trehalose, Table 3-1). Trehalose is atmospherically relevant and can be used as a marker for biogenic secondary organic

aerosol (SOA) or biologically active surface soils.[34, 35] Raffinose is an oligosaccharide with higher molecular weight and lower solubility (Table 3-1). Sucrose, raffinose, and trehalose have been recently identified as amorphous particles in the subsaturated regime.[29] To our knowledge, CCNC and H-TDMA measurements have not been conducted for raffinose or trehalose although some work with the water uptake of super-micron particles has been performed.[29]

A recent article has summarized the available experimental techniques for hygroscopicity measurements including techniques for micron-sized particles such as EDB.[36] While several submicron WSOCs hygroscopicity measurements have been conducted with H-TDMA or CCNC, fewer studies report optical growth factor, *f*RH.[37-40] Optical growth factor measurements of laboratory WSOCs are rare in the literature and much of the hygroscopicity data of levoglucosan, sucrose, raffinose, and trehalose has been obtained with H-TDMA. To our knowledge, only two studies have measured the *f*RH of levoglucosan and only one study has measured *f*RH for sucrose and raffinose.[38, 41, 42] Traditionally, cavity ring-down spectroscopy (CRDS) has been used to measure gas-phase spectra and more recently was developed to measure the extinction of light by small particles.[43] In this work, we used two cavities in series to measure the water uptake of the WSOCs. Unlike H-TDMA, which measures a geometric growth factor (G_f) based on particle size, CRDS measures an optical growth factor (*f*RH) based on light scattering and absorption. Therefore, CRDS provides intrinsic optical data in addition to water uptake data.

In the work cited above, rarely are more than two droplet growth measurements simultaneously published. Only one study, Wex et al. (2009), used an optical particle spectrometer (OPS) with H-TDMA and CCNC measurements to study the hygroscopic growth of α-pinene SOA.[44] Here, droplet growth (on the nanoscale) is measured in the sub-saturated relative humidity regime with both an optical particle spectrometer and a H-TDMA as well as being measured in the supersaturated regime with a CCNC. Using these data, the single-parameter

hygroscopicity (κ) was calculated from all three methods and compared with one another method of converting fRH to κ.[45]

Table 3-1: Information for Each Water Soluble Organic Compounds with Calculated Refractive Indices.

	Structure	Molecular Weight [g mol^{-1}]	Solubility @ 298 K [g L^{-1}]	Density [g mL^{-1}]	O:C	RI_{exp}	κ Ideal
Levoglucosan		162.1	62.3[a]	1.7[b]	0.833	1.550 ± 0.006	0.190
Trehalose	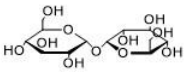	342.3	689[c]	1.58[d]	0.917	1.495 ± 0.005	0.083
Sucrose	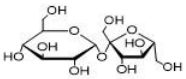	342.3	2040[d]	1.58[d]	0.917	1.510 ± 0.012	0.084
Raffinose	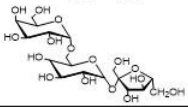	504.4	143[d]	1.465[d]	0.889	1.492 ± 0.016	0.064

[a]The Human Metabolome Database. http://www.hmdb.ca/ (accessed October 9, 2019).
[b]Value predicted by ACS/Labs Percepta Platform – PhysChem Module.
[c]Higashiyama, T., Novel functions and applications of trehalose. In Pure and Applied Chemistry, 2002; Vol. 74, p 1263.

3.2 Experimental Methods

The ability of a submicron particle to uptake water and form a droplet was estimated via optical growth factor (fRH), geometric growth factor (G_f), and supersaturated (CCN activity) measurements. Each experimental set-up was calibrated with ammonium sulfate aerosol. Ammonium sulfate and each of the four WSOCs aerosols were generated from bulk solutions using a constant output atomizer (TSI 3076) (Fig. 3-1). A dilute solution (0.1 wt% – 0.8 wt%) of the analyte was formed by dissolving the commercially obtained chemical (ammonium sulfate, 98%, Millipore™; sucrose, 99% Fisher Chemical™; D(+)-raffinose (pentahydrate), 97%, Dot Scientific Inc.™; D-trehalose (di-hydrate), 99%, Sigma-Aldrich™; 1,6-anhydro-beta-d-glucopyranose (levoglucosan), 99%, ACROS Organics™) in ultrapure water (high-performance liquid chromatography grade or Millipore(R) Water >18 MΩ). The solution was then atomized by a 3.6 L min^{-1} carrier gas of medical air (purified air with H2O < 67 ppmv) that underwent further

purification to remove particulate matter and trace gasses. Subsequently, the aerosol particles were dehydrated through the use of a diffusion dryer filled with silica gel such that particles were dry (< 10% RH) when exiting the diffusion dryer. Specifically, the removal rate (which has previously been measured) was 98% RH sec^{-1}.[46] The dry aerosol flow was split to the separate systems and measured for optical growth, geometric growth, and CCN activity (Figure 3-1). The sections below briefly describe the methods and calculations presented in this study. The three experimental methods can be directly compared with the calculation of a single-hygroscopicity parameter derived from Köhler theory (Section 3.3). The sections below briefly describe the methods and calculations presented in this study.

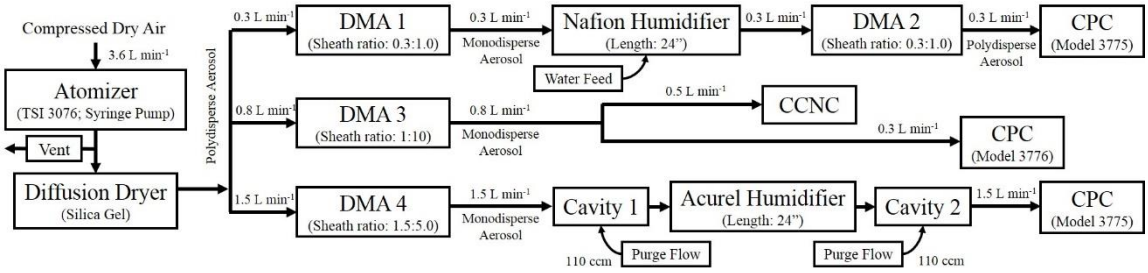

Figure 3-1: Combined experimental set-ups for a) H-TDMA b) CCNC c) CRD. DMA 1 and DMA 3 are the same piece of laboratory equipment, but reconfigured for the separate experimental methods.

3.2.1 Cavity Ring-Down Measurements

Each of the four WSOCs were atomized and dried as described above (Section 3.2). The dried particles were then analyzed using cavity ring-down spectroscopy. The cavity ring-down system consists of a few key components previously described and only briefly covered here.[47-49] A 643 nm continuous-wave diode laser (Power Technologies) was modulated at 500 Hz and was coupled to two 91 cm long cavities. The cavities were capped at both ends with highly reflective mirrors (> 99.9985% reflective @ 640 nm; ATFilms, Boulder, CO) and each cavity had an effective path length of approximately 48 km. The light transmitted through the CRDS cavity was measured by a photomultiplier tube. The first-order decay constant fitted to the decay of light is

known as the ring-down time, τ. Extinction coefficients (α_{ext}) were then calculated using Eq (3-1) from the ring-down times within the cavity,

$$\alpha_{ext} = \frac{R_L}{c}\left(\frac{1}{\tau} - \frac{1}{\tau_0}\right) \quad (3\text{-}1)$$

where R_L is the ratio of cavity length to the length of the cavity that the sample occupies, c is the speed of light, and τ, τ_0 are the ring-down times (first-order decay constants) with and without sample, respectively. A purge flow (55 sccm) was maintained across each mirror to prevent dust or sample from accumulating on them. This flow rate diluted the sample to a known degree which is accounted for using simple dilution calculations when determining particle concentrations. The laser was pulsed while the purified air flowed through the cavity at a rate of 1.5 L min^{-1}. The background ring-down time was established when no sample was present in the cavity. An aerosolized sample was dried by the diffusion dryer and then size selected with an electrostatic classifier (TSI 3080) and a differential mobility analyzer (DMA, TSI 3081) maintaining an aerosol to sheath flow of 1.5:5.0. The aerosol to sheath flow is recommended to be 1:10; however, in our experience a ratio of 1.5:5.0 is required to get the best range of sizes while leaving the sheath flow constant in the CRDS. The sample was then directed into the cavity to obtain the extinction coefficient of the sample. After passing through the cavity, particles were directed into the condensation particle counter (CPC, TSI 3775) where particle concentration was obtained.

3.2.1.1 Refractive Index Measurements

Once the extinction coefficients and the particle concentrations were obtained, the extinction coefficients, determined from each laser shot, were averaged to determine the average extinction coefficient for each selected size. Simultaneously, the concentration of particles was monitored and subsequently averaged. Due to the purge flow within each cavity of the CRDS, the

concentration of particles was slightly diluted. Using the known flow rates of both the experiment and the purge flow, the concentration of particles was corrected to account for the purge flow. It should be noted that particles selected by the DMA can be multiply charged. For this reason, we corrected the experimental data for these multiply charged particles as described by Freedman et al. (2009).[50] The extinction cross-section (σ) was calculated by Eq. (3-2) from the experimentally determined values as follows,

$$\sigma_{exp} = \frac{\alpha_{exp,avg}}{N_{avg}} \tag{3-2}$$

where $\alpha_{exp,ave}$ is the average extinction coefficient and N_{avg} is the averaged particle concentration. Extinction cross-section is related to extinction efficiency, Q_{ext} by,

$$Q_{ext} = \frac{\sigma_{ext}}{\pi r^2} \tag{3-3}$$

where r is the particle radius. The refractive index of the sample was calculated with Mie theory using the average extinction coefficient for each size. In Eq (3-4), the cumulative fractional difference (CFD_R) is calculated to determine the refractive index that is the best fit to the measured extinction cross-sections,

$$CFD_R = \frac{1}{P}\sum_{All\ Sizes} \frac{|b_{ext,measured} - b_{ext,Mie}|}{b_{ext,measured}} \tag{3-4}$$

where P is the number of particle sizes selected. The best fit refractive index is that which has the lowest CFD_R.[50,51]

3.2.1.2 Optical Growth Measurement

The dual cavity CRDS system is shown in Figure 3-1. In this system, two CRDS cavities were connected in series with a custom-built humidifier (Membrane: Accurel V8/2) between them. The background ring-down time was measured for both cavities as for the refractive index calculations. Size selected dried aerosol particles (< 10% RH) were then flowed through the first

cavity at 1.5 L min^{-1}. The extinction of light by the introduction of the dry particles into the first cavity was measured. Then the particles passed through the humidifier where the relative humidity of the particles was increased to 85% ± 3%. The extinction of light by the humidified particles was then measured in the second cavity before the concentration of particles was measured by the condensation particle counter (TSI 3775). Eq. (3-5) expresses that the optical growth factor (*f*RH) is calculated, in this work, by dividing the extinction cross-section of the humidified particles ($\sigma_{ext,a}$) by the extinction cross-section of the dry particles ($\sigma_{ext,b}$)

$$f\mathrm{RH}(a,b) = \frac{\sigma_{ext,a}}{\sigma_{ext,b}} \tag{3-5}$$

where *a* is relative humidity of the humidified particles, and *b* is the relative humidity of the dry particles (<10 % RH). The *f*RH was determined for each compound at seven different sizes (200 nm through 500 nm with a 50 nm interval) and then averaged together for a single value.

3.2.3 Humidified Tandem Differential Mobility Analysis Measurements

A humidified tandem differential mobility analyzer (H-TDMA) was used to measure the subsaturated growth factor of ammonium sulfate and the WSOCs. The H-TDMA is widely used for aerosol hygroscopic measurement and a detailed setup has been previously described (Figure 3-1) (e.g. but not limited to, (Cruz & Pandis, 2000; Rader & McMurry, 1986; Swietlicki et al., 2008)).[52-54] The dry aerosol was size selected with an electrostatic classifier (TSI 3081) at three particle electrical mobility diameters; 200, 250, and 300 nm. The aerosol flow rate was 0.3 L min^{-1} and the sheath flow was 1.0 L min^{-1}. The size selected particles were then humidified up to 95% RH with a Nafion humidification line (PermaPure® MH series). The size distribution and concentration of the humidified particles were subsequently measured with a second DMA (TSI 3081) and a condensation particle counter (TSI 3775) (See Supplemental Fig. 3-S1).

3.2.4 Cloud Condensation Nuclei Measurements

The critical activation diameters (d_{p50}) of ammonium sulfate and the four WSOCs were measured at varying supersaturations. The dry aerosol size distributions were measured with a scanning mobility particle sizer (SMPS, TSI 3081) and a condensation particle counter (TSI 3776). A cloud condensation nuclei counter (CCNC; Droplet Measurement Technologies, DMT©) was operated downstream of the SMPS in parallel with the CPC. The size selected aerosol was sampled by the CCNC at 0.5 L min^{-1} flowrate. The activated fraction, the CCN concentration divided by the aerosol number concentration, was measured between supersaturations of 0.3 – 1.2% for different particle dry diameters. Scanning mobility CCN analysis (SMCA) was employed and used to calculate the critical activation diameters for each supersaturation.[55] The CCNC was calibrated with $(NH_4)_2SO_4$ aerosol to determine the RH (see Supplemental).

Initially, dry particles were also size selected with a SMPS for CCN measurement.[56] After size selection, the monodisperse particle stream was split. A condensation particle counter (TSI 3776) sampled at a rate of 1.5 L min^{-1} and provided total particle concentration information. The second stream was sent to a continuous flow streamwise thermal gradient DMT CCNC at a rate of 0.5 L min^{-1}.

3.2.5 Hygroscopicity Analysis

The equilibrium vapor pressure at the surface of a droplet was calculated by Eq. (3-6) as a function of the ambient relative humidity

$$\frac{RH}{100} = a_w e^{\frac{4\sigma_{s/a} M_w}{RT\rho_w D}} \tag{3-6}$$

where, a_w is the water activity of the droplet, $\sigma_{s/a}$ is the surface tension of the droplet at the air droplet interface, R is the universal gas constant, T is the temperature of the droplet, and M_w and

ρ_w are the molecular weight and density of water, respectively.[45] By rearranging Eq. (3-7) and assuming that the solute is sufficiently dilute in the droplet, aw can be simply defined with a single parameterization

$$\frac{1}{a_w} = 1 + \kappa\frac{V_{dry}}{V_w} \tag{3-7}$$

where V_{dry} and V_w are the volumes of the dry and wet particle respectively, and κ represents a single hygroscopicity parameter reflective of the aerosol chemical.[45] The parametrization by Petters and Kreidenweis (2007) suggests that κ can be calculated at both subsaturated and supersaturated conditions. Kreidenweis and Asa-Awuku (2014) and the references therein provide a full derivation of κ under both conditions.[45, 57] Briefly described here, if the wet and dry particles are assumed to be spherical, then volume can be converted to particle diameter, D, and the growth factor, G_f, as defined by Eq. (3-8) can be calculated

$$G_f(a,b) = \frac{D_a}{D_b} \tag{3-8}$$

where the diameter of the humidified particle (D_a) was divided by the diameter of the dry particle (D_b).

At high relative humidities (>85%), the vapor pressure of water approaches that of a flat surface (the Kelvin effect is assumed to be negligible) and the a_w can be approximated with RH. Thus, G_f is simplified to Eq. (3-9) as follows

$${G_f}^3 = 1 + \kappa\left(\frac{RH/100}{(1-RH)/100}\right) \tag{3-9}$$

For supersaturated CCN measurement, κ factor is calculated via

$$\kappa = \frac{4\left(\frac{4\sigma_{s/a}M_w}{RT\rho_w}\right)^2}{27\left(D_{dry}\right)^3 ln^2 s_c} \tag{3-10}$$

where s is the instrument supersaturation and the critical dry diameter is substituted for d_{p50}. Unlike for H-TDMA and CCNC measurements, the equations for single hygroscopicity optical growth measurements, fRH, have not been explicitly derived. Previous studies have proposed two

and three empirical parameter relationships between *f*RH and RH.[39, 41, 57] Currently, two techniques are available to obtain a single hygroscopicity parameter and are described below.

In the first method, optical growth factor was converted to geometric growth factor using Mie theory, and the experimentally derived refractive indices. The mobility diameter of the dry aerosol particles was experimentally selected with the DMA. However, the diameter of the humidified particles was calculated by extrapolating the water content of the humidified particle from the optical growth factor calculation and Mie theory. First, the volume-weighted refractive index (m_t) is calculated

$$m_t = \sum_i \frac{V_i}{V_t} m_i \tag{3-11}$$

using the real part of the refractive index of the sample that is experimentally determined as shown in Eq. (3-11). The real part of the refractive index of water at 643 nm was obtained from Lavallard et al. (1996) where V_i is the volume of the component *i* and m_i is the real part of the refractive active of component *i*.[58] Only the real part of the refractive index was used since the absorption of these compounds is negligible at 643 nm. Extinction coefficients were calculated for every particle size 0.1 nm above the dry particle diameter to obtain an extinction coefficient for comparison the experimentally determined optical growth factor. The diameter that resulted in minimum variation between the calculated optical growth factor and the experimentally obtained optical growth factor was used to calculate geometric growth factor.

Eq. (3-12) is used to derive the κ factor from the growth factor

$$\kappa = ({G_f}^3 - 1)\left[\frac{RH}{100} e^{\left(\frac{4\sigma_{s/a} M_w}{RT\rho_w DG_f}\right)} - 1\right] \tag{3-12}$$

where $\sigma_{s/a}$ is the surface tension between the solution and the air, assumed to be that of water; ρ_w is the density of water, M_w is the molecular weight of water, R is the gas constant, and T is standard temperature.[59] It should be noted that these assumptions are often used for

supersaturated κ calculations, where the water content of the aerosol particles is very high but may be less than ideal for the calculation of subsaturated κ factors.

In addition to the above method for calculating κ factor, one other method was applied. Here the distinction is made between κ factors determined by Mie theory and those determined semi-empirically as $\kappa_{CRD,Mie}$ and $\kappa_{CRD,Empirical}$ respectively. This semi-empirical derivation is found in Kreidenweis and Asa-Awuku (2014).[57] In that work, geometric growth factor is related to optical growth factor via the following empirical relation and is shown here in Eq (3-13),

$$fRH(80\%RH, dry) = G_f(80\%RH, dry)^{\left(\frac{0.86}{0.28}\right)} \quad (3\text{-}13)$$

Using Eq. (3-8) in conjunction with Eq. (3-13) the following semi-empirical relation of Eq. (3-14) is derived

$$\kappa_{empirical} = \left(fRH(80\%RH, dry)^{\frac{3*0.28}{0.86}} - 1\right)\left(\frac{1-RH/100}{RH/100}\right) \quad (3\text{-}14)$$

It is noted that in the original work by Kreidenweis and Asa-Awuku (2014), the empirical correlation between growth factor and optical growth factor was determined on systems conducted at 80% RH. However, the relative humidity during our experiments was ~85% RH and also in a regime assumed to form dilute droplets.[57]

3.3 Results and Discussion

*3.3.1 Optical Growth Factors, f*RH

Optical growth factors and refractive indices were determined for each of the WSOCs: levoglucosan, trehalose, sucrose, and raffinose. The refractive indices are displayed in Table 3-1 and Supplemental Figure 3-S2. Supplemental Figure 3-S3 shows a representative plot for the optical growth factor of ammonium sulfate at 84.4% ± 2.7% RH as determined by CRDS with a

643 nm laser. These results show good agreement when compared to Mie theory using 85% RH. The *f*RH data for each of the compounds is displayed in Figure 3-2. When compared to previous studies, our values are consistently higher, which is likely the result of higher relative humidity in our experiment. Our study found that for levoglucosan, the *f*RH(82.4% RH, dry) was 2.32 ± 0.18 at an effective diameter of 250 nm, and the *f*RH(83.3% RH, dry) was 1.65 ± 0.14 at an effective diameter of 500 nm. For the same system but under different relative humidity, Garland et al. (2007) found a *f*RH(80% RH, dry) of 1.71 ± 0.05 at an effective diameter of 254 nm and a *f*RH(80% RH, dry) of 1.47 ± 0.04 at an effective diameter of 532 nm. It is noted that our study is performed with a 643 nm laser while Garland et al. (2007) used a 532 nm laser. Furthermore, measurements of water uptake are extremely sensitive to the RH of the experiment. In our study, the *f*RH(85.8% RH, dry) is 1.79 ± 0.22 for sucrose and the *f*RH(88.0% RH, dry) is 1.83 ± 0.18 for raffinose. In a different study, Robinson et al. (2014) determined the optical growth factor *f*RH(80% RH, dry) was 1.24 for sucrose and 1.25 for raffinose.[42] For sucrose, Robinson et al. (2014) found that the onset of water uptake is at 34% RH for sucrose and 40% RH for raffinose with continuous water uptake as RH increases rather than a distinct deliquescence phase transition. Like Garland et al. (2007), Robinson et al. (2014) used a 532 nm laser for their study. Optical growth factors are shown in Figure 3-2 for each of the four WSOCs. The reported errors in this measurement are quite high due to the dependence of optical growth factor on RH. Over the course of the experiment the RH within the CRDS cavity varies as much as 3%. Since *f*RH is only reported at one RH, the average RH is reported, however the variation in the measurement across those sizes results in a high error in the final reported value. This is one of the advantages to using κ since it is applicable across all RHs and can be adjusted using the RH of the measurement. The *f*RH decreases with increasing dry particle size. Since *f*RH is strongly dependent on RH, small changes (~5%) in RH can significantly modify *f*RH values. For direct comparison of optical growth, changes in RH must be considered. The conversion to κ-values (as

shown below) allows for this. Raffinose was expected to have the lowest *f*RH, and when the high RH is considered, this appears to be the case.

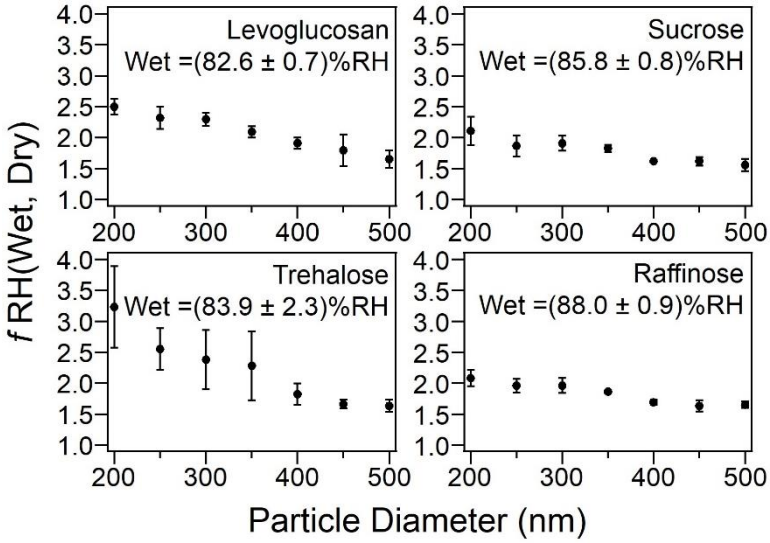

Figure 3-2: Optical growth factors for four WSOCs determined by CRDS. The average relative humidity for each compound is shown, the average relative humidity across all data points is approximately 85.1%. Over the course of the experiment the RH within the CRDS cavity varies as much as 3% resulting in higher error in the final *f*RH value. This can be clearly seen in the bottom left figure. Notably the error in individual points is not always high; this is the result of low RH variance while measuring that particle size.

3.3.2 Geometric Growth Factors, G_f

Geometric growth factors are determined for each of the WSOCs at three dry particle diameters and the average growth factor for each compound is shown in Table 3-2. The growth factors determined in this study agree with the growth factors calculated from the theoretical κ factor well across the measured particle sizes (Figure 3-3, Eq. 3-9). Trehalose and raffinose are not well studied and, to the best of our knowledge, do not have previously reported H-TDMA growth factors. H-TDMA growth factors are also strongly RH dependent and the reported values are consistent with previously reported data measured at different RH; higher saturation leads to larger geometric droplet growth. The geometric growth factor for levoglucosan at 95% RH was 1.64 ± 0.09. Svenningsson et al. (2006) reported the levoglucosan growth factor to be

approximately 1.59 at the same conditions.[15] Using a RH of 90%, Koehler et al. (2006) reported two smaller values for growth factor using H-TDMA, roughly 1.36 and 1.39.[60] The study with values closest to this study was performed by Chan et al. (2005) with an electrodynamic balance and found the growth factor to be approximately 1.6 at 96% RH.[16] Similar to Koehler et al. (2006), Mochida and Kawamura (2004) did not measure growth factor at 95%, but the trend in their data would suggest that the geometric growth factor of levoglucosan at this RH would be approximately 1.55.[19] Our work has found the growth factor of sucrose on the submicron scale to be 1.41 ± 0.02 at 95% RH.[30] Tong et al. (2011) found the growth factor of sucrose to be about 1.19 at 80% RH using optical tweezers. However, this is at a significantly lower RH than our study. Additionally, it should be noted that the particles in Tong et al., 2011 had micrometer diameters. Hodas et al. (2015) found the growth factor of sucrose to be about 1.25 at 90% using a differential aerosol sizing and hygroscopicity spectrometer probe (DASH-SP).[26] H-TDMA was also used by Estillore et al. (2017) to determine the geometric growth factor of sucrose at 90% RH and was found to be about 1.24.[25]

Table 3-2: Average Measured and Calculated Values for Each of the Water-Soluble Organic Compounds.

	fRH (%RH)	$G_{f,fRH}$ (%RH)	$G_{f,HTDMA}$ (%RH)	κ_{Ideal}	κ_{Mie}	$\kappa_{empirical}$	κ_{HTDMA}	κ_{CCNC}
Levoglucosan	2.08 ± 0.32 (82.6%)*	1.31 ± 0.01 (82.6%)*	1.64 ± 0.09 (95%)	0.190	0.277 ± 0.055	0.221 ± 0.066	0.180 ± 0.038	0.21 ± 0.03
Trehalose	2.22 ± 0.64 (83.9%)*	1.29 ± 0.03 (83.9%)*	1.33 ± 0.01 (95%)	0.083	0.221 ± 0.049	0.214 ± 0.089	0.071 ± 0.003	0.11 ± 0.02
Sucrose	1.79 ± 0.22 (85.8%)*	1.23 ± 0.01 (85.8%)*	1.41 ± 0.02 (95%)	0.084	0.144 ± 0.024	0.127 ± 0.041	0.096 ± 0.008	0.12 ± 0.02
Raffinose	2.01 ± 0.44 (88.0%)*	1.22 ± 0.01 (88.0%)*	1.20 ± 0.04 (95%)	0.064	0.117 ± 0.015	0.109 ± 0.020	0.039 ± 0.010	0.07 ± 0.01

*Note: The relative humidity used in these calculations have an associated error for each calculation. These values are found in the body of the text.

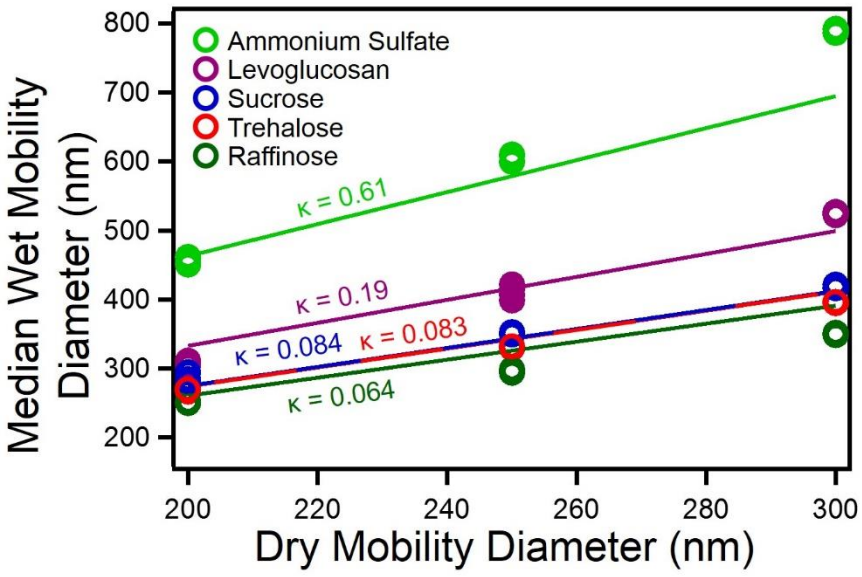

Figure 3-3: Circles indicate the measured growth factors from the H-TDMA at a relative humidity of 95%. The predicted growth factors (lines) are calculated with their theoretical κ-values (as shown).

3.3.3 CCN Activation Results – CCN Activity

The critical diameters (d_{p50}) were measured for each of the WSOCs and ammonium sulfate at varying instrument supersaturation and initial RH. Figure 3-4a shows exemplary sucrose CCN activation data measured at 0.5 L min^{-1} under dry aerosol initial conditions. The d_{p50} increases with decreasing instrument supersaturation, and κ-values remain constant over the range of instrument supersaturation (0.12 ±0.02, Table 3-2). The measured κ_{CCNC} for all four WSOCs is slightly larger but within uncertainty of ideal values. Sucrose is known to increase droplet surface tension (Supplemental Figure 3-S4).[59] However, the impact of the increase in surface tension on the droplet is negligible in this case. For small (40 nm) and large critical diameters (250 nm), the calculated hygroscopicity (accounting for changes in $\sigma_{s/a}$) remains 0.084 (Figure 3-4b). Accounting for changes in surface tension does not explain the WSOCs κ_{CCNC} values, shown in Table 3-2.

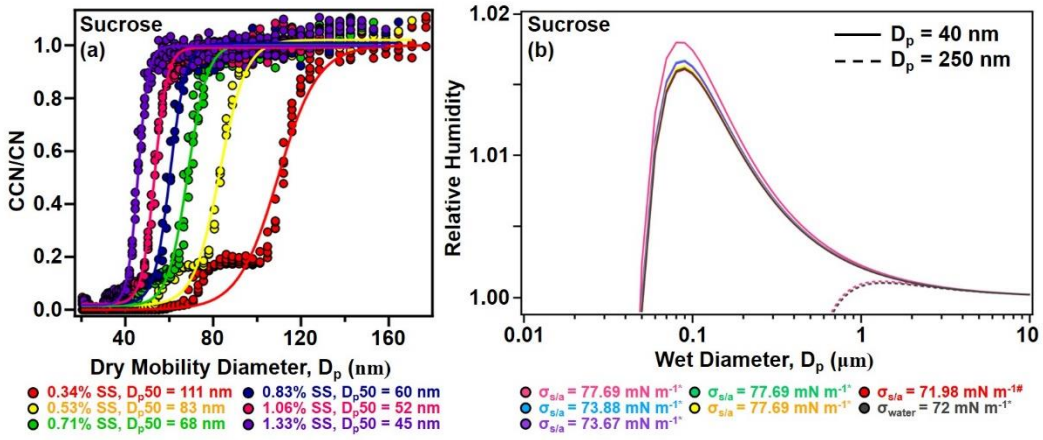

Figure 3-4: (a) Sucrose CCN activation and Mie Theory predictions. (b) Parametrized sucrose droplet growth for a 40 and 250 nm dry particle using the calculations by Pardo et al. (2007) and experimentally obtained sucrose surface tensions.[61] Sucrose increases droplet surface tension and assumptions for the interfacial droplet surface tension are modified. σ* indicates values from σ measurements (Figure 3-S4). σ# indicates value(s) obtained from Padro et al. (2007). Increases in surface tension have negligible effect on κ-values, especially for larger dry particle diameters (e.g., 250 nm). The surface tensions used in these calculations were experimentally obtained and are shown in the supplemental information.

3.3.4 Comparison of κ-values

Hygroscopicity, (κ_{Ideal}) can be calculated from known solute parameters. Four additional κ-values ($\kappa_{CRD,Mie}$, $\kappa_{CRD,Empirical}$, κ_{HTDMA}, κ_{CCNC}) are calculated from the measurement as data described above. The converted optical growth factors to $\kappa_{CRD,Mie}$ -values are shown in Fig. 3-5. In the case of the CRDS-derived κ-values, the error in individual data points is quite high due to fluctuations in relative humidity and particle concentration throughout the experiment. Generally, the highest errors occur for the larger particle sizes where particle concentration varies the most. To better interpret the data, the κ factor for each sugar is averaged across all particle sizes.

The optical growth factor is converted to κ-values with the two methods as previously discussed in Section 3.2.6. $\kappa_{CRD,Empirical}$ estimates lower values than $\kappa_{CRD,Mie}$ (Fig. 3-5). Both values are sensitive to RH. However, $\kappa_{CRD,Empirical}$ is independent of dry aerosol particle size and larger than κ_{Ideal}; $\kappa_{CRD,Empirical}$ follows the trends in the *f*RH measured data and is more sensitive to initial dry particle size. $\kappa_{CRD,Empirical}$ approaches values of κ_{Ideal} at all sizes with the greatest deviation

observed for levoglucosan. Larger particles are more likely to swell and thus approach the assumptions of dilution that are made by Köhler theory and as applied to κ_{Ideal}. There is a slight deviation between $\kappa_{CRD,Empirical}$ and $\kappa_{CRD,Mie}$ due to each having a slight size dependence, however within the range of particles sizes in this study $\kappa_{CRD,Empirical}$ serves as a good estimate for $\kappa_{CRD,Mie}$ (Fig. 3-6).

The *f*RH and G_f data from previous literature was converted into κ-values using Eq. (3-14) and Eq. (3-9), respectively. These κ-values are compared to each other and with our data for both levoglucosan and sucrose (Figure 3-7a and Figure 3-7b). In some cases, these values deviated significantly from those determined in this work. It should be noted that large deviations are not unexpected since the experimental conditions are often quite different from each other. Most notably, the RH of the experiments differs by at least five percent in many cases and the strong dependence of κ-values on RH provides justification for the deviations from literature derived values. Specifically, the κ-values derived from previous CRD literature deviated the most from our work and in these cases the *f*RH experiments were performed at 80% RH. An additional κ-value derived from Robison et al. (2014) was for raffinose which was 0.051 ± 0.008 and fits well within the range of κ-values presented in this work.[42]

κ-values that are determined by CRDS are typically higher than those determined by CCNC, likely due to the influence of the doubly charged particles, which are larger and therefore uptake more water. Doubly charged particles are not accounted for during the *f*RH analysis. Conversely, κ_{HTDMA} values are lower, ranging from 0.039 to 0.180 due to high RH (95%) in that system and κ factors' sensitivity to RH. Overall, the κ-values decrease with an increase in the molecular weight of the organic compound. According to Köhler theory, this result is expected, but notably there does not appear to be a trend with the O:C ratio within the limited range of O:C values used in this work. These data agree with the conclusions in previous literature that show a dependence of aerosol particles' physical properties on molecular weight, specifically the work

by Koop et al. (2011) who showed that the thermal glass transition was dependent upon molecular weight and with Rosenørn et al. (2006) who demonstrated that the CCN activity of various saccharides was dependent on molecular weight.[14, 32] These results suggest that molecular weight may play a larger role in κ than the relative abundance of hydroxyl groups for these systems.

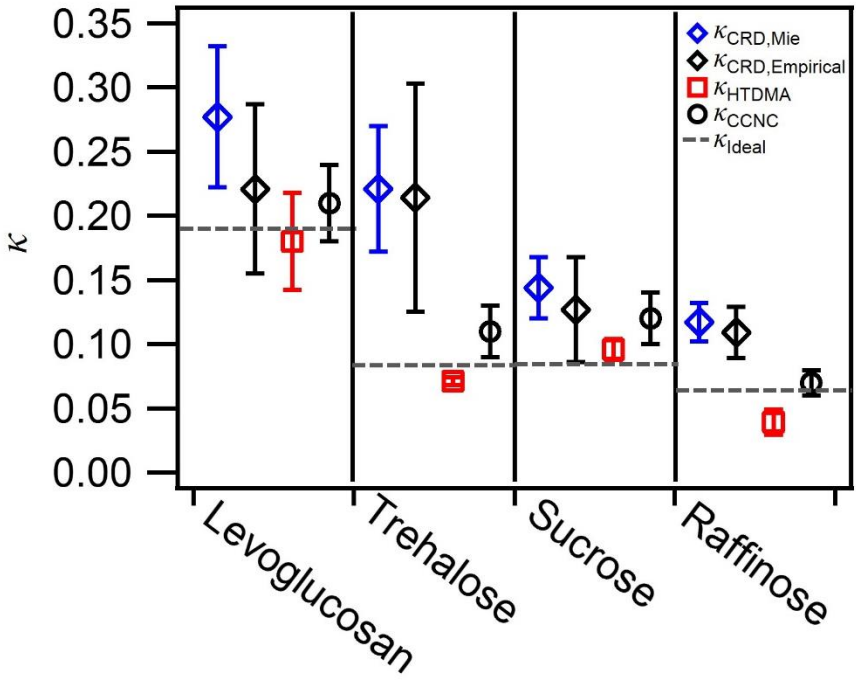

Figure 3-5: The calculated κ factors from experimental measurement are directly compaired with theory (grey dashed line). The blue and black diamonds indicate values calculated by two different methods using *f*RH measurements, red squares for values calculated from H-TDMA measurements, and black circles represent values calculated from CCNC data.

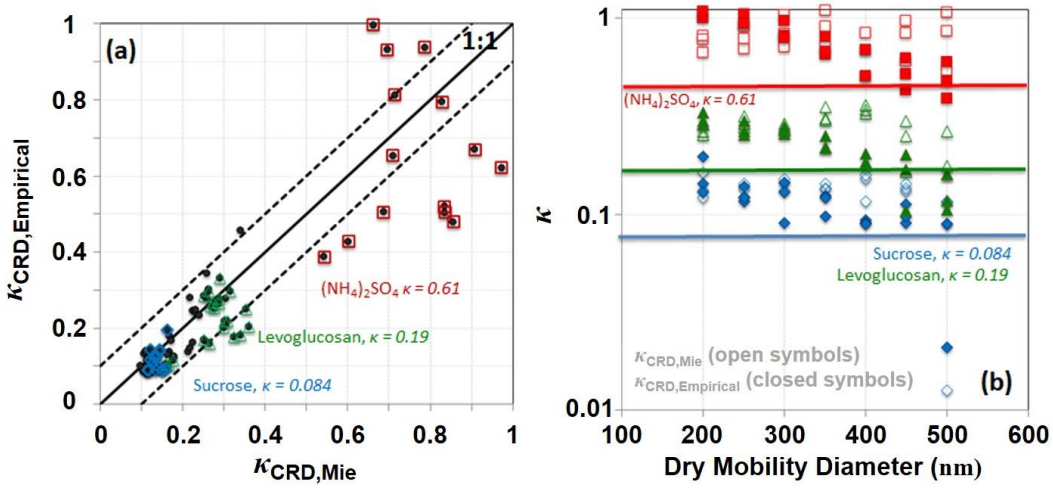

Figure 3-6: Comparison of single-κ parametrization from *f*RH data. (a) κ-values derived from Mie theory and from empirical correlation. Data (closed circles) is shown for ammonium sulfate, levoglucosan, sucrose, trehalose, and raffinose. Data for ammonium sulfate (red squares), levoglucosan (green triangles) and sucrose (blue diamonds) is highlighted. (b) Size dependence of *f*RH derived κ. Ammonium sulfate (red squares), levoglucosan (green triangles) and sucrose (blue diamonds) are highlighted. Ideal values are shown as a straight line. $\kappa_{CRD,Mie}$ is size independent and $\kappa_{CRD,Empirical}$ is size dependent, with values approaching ideal κ-values at higher diameters.

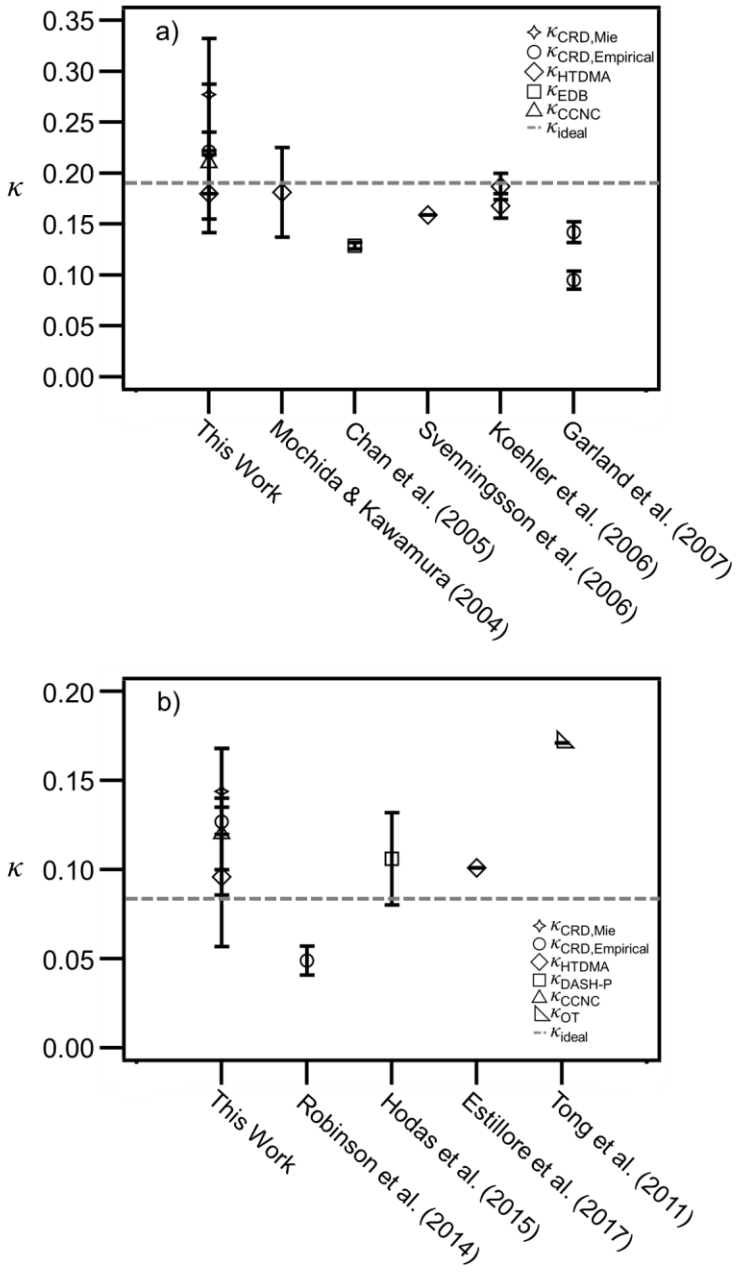

Figure 3-7: The κ-values for levoglucosan are compared to values calculated in the literature in a) and the κ-values for sucrose are compared to values calculated in the literature in b). The symbols designate the original measurement type used by the respective authors. Error is derived from those original works. Any points with an error of zero were simply not able to be derived. In most cases an online plot digitizer was used to evaluate the minimum and maximum value on each error bar, this value was then converted to κ-values with the appropriate equation and then converted into an error for the κ-values. Some information was absent in the original works that is necessary for a more rigorous error calculation to be performed. In the case of Chan et al. (2005), nearby points were grouped together and a standard deviation was calculated. Error in the works by Garland et al. (2007) and Robinson et al. (2014) were determined by using a flat 3% error that is associated with the experimental technique.

3.4 Conclusions

This work adds to the growing body of work that measures the droplet growth of WSOCs. To our knowledge, this is the only study that compares these different methods (CRDS, H-TDMA, and CCNC), which is important for comparing subsaturated and supersaturated κ and optical methods to geometric methods for determining subsaturated κ. While H-TDMA and CCNC measurements of water uptake are readily found in the literature, the use of CRDS for *f*RH measurements is less common. Here we are able to apply a parameterization to *f*RH ($\kappa_{CRD,Empirical}$), which agrees well with already published methods to obtain κ via the use of Mie theory ($\kappa_{CRD,Mie}$) with good agreement between the two. The *f*RH comparison has been shown to work well for ammonium sulfate, and now here for WSOCs measured at higher RH. The validity of the application of Köhler theory to subsaturated aerosol particles was considered due to the common assumptions used in the calculation of κ factor. Specifically, the surface tension of a sucrose-water solution was measured at varying concentrations and applied to the calculation of κ factor with no significant variation in the resulting value. Therefore, Köhler theory was applied to both CRDS and H-TDMA measurements. Each of the four determinations of κ presented in this work shows the same trend; a decrease in κ with increasing molecular weight. This result agrees with findings in previous literature and matches the theoretical predictions derived from Köhler theory. A greater understanding of this hygroscopicity parameterization will help with predictions of particle water uptake and cloud formation.

References

1. Yu, H.; Kaufman, Y. J.; Chin, M.; Feingold, G.; Remer, L. A.; Anderson, T. L.; Balkanski, Y.; Bellouin, N.; Boucher, O.; Christopher, S.; DeCola, P.; Kahn, R.; Koch, D.; Loeb, N.; Reddy, M. S.; Schulz, M.; Takemura, T.; Zhou, M., A review of measurement-based assessments of the aerosol direct radiative effect and forcing. *Atmospheric Chemistry and Physics* **2006**, *6*, (3), 613-666.

2. Haywood, J.; Boucher, O., Estimates of the direct and indirect radiative forcing due to tropospheric aerosols: A review. *Reviews of Geophysics* **2000**, *38*, (4), 513-543.

3. Lohmann, U.; Feichter, J., Global indirect aerosol effects: a review. *Atmospheric Chemistry and Physics Discussions* **2004**, *4*, (6), 7561-7614.

4. Kanakidou, M.; Seinfeld, J. H.; Pandis, S. N.; Barnes, I.; Dentener, F. J.; Facchini, M. C.; Van Dingenen, R.; Ervens, B.; Nenes, A.; Nielsen, C. J.; Swietlicki, E.; Putaud, J. P.; Balkanski, Y.; Fuzzi, S.; Horth, J.; Moortgat, G. K.; Winterhalter, R.; Myhre, C. E. L.; Tsigaridis, K.; Vignati, E.; Stephanou, E. G.; Wilson, J., Organic aerosol and global climate modelling: a review. *Atmospheric Chemistry and Physics* **2005**, *5*, (4), 1053-1123.

5. Decesari, S.; Facchini, M. C.; Fuzzi, S.; McFiggans, G. B.; Coe, H.; Bower, K. N., The water-soluble organic component of size-segregated aerosol, cloud water and wet depositions from Jeju Island during ACE-Asia. *Atmospheric Environment* **2005**, *39*, (2), 211-222.

6. Falkovich, A. H.; Graber, E. R.; Schkolnik, G.; Rudich, Y.; Maenhaut, W.; Artaxo, P., Low molecular weight organic acids in aerosol particles from Rondnia, Brazil, during the biomass-burning, transition and wet periods. *Atmospheric Chemistry and Physics* **2005**, *5*, (3), 781-797.

7. Graham, B.; Mayol-Bracero, O. L.; Guyon, P.; Roberts, G. C.; Decesari, S.; Facchini, M. C.; Artaxo, P.; Maenhaut, W.; Köll, P.; Andreae, M. O., Water-soluble organic compounds in biomass burning aerosols over Amazonia 1. Characterization by NMR and GC-MS. *Journal of Geophysical Research: Atmospheres* **2002**, *107*, (D20), LBA 14-1-LBA 14-16.

8. Mayol-Bracero, O. L.; Guyon, P.; Graham, B.; Roberts, G.; Andreae, M. O.; Decesari, S.; Facchini, M. C.; Fuzzi, S.; Artaxo, P., Water-soluble organic compounds in biomass burning aerosols over Amazonia 2. Apportionment of the chemical composition and importance of the polyacidic fraction. *Journal of Geophysical Research: Atmospheres* **2002**, *107*, (D20), LBA 59-1-LBA 59-15.

9. Chan, M. N.; Kreidenweis, S. M.; Chan, C. K., Measurements of the Hygroscopic and Deliquescence Properties of Organic Compounds of Different Solubilities in Water and Their Relationship with Cloud Condensation Nuclei Activities. *Environmental Science & Technology* **2008**, *42*, (10), 3602-3608.

10. Riipinen, I.; Rastak, N.; Pandis, S. N., Connecting the solubility and CCN activation of complex organic aerosols: a theoretical study using solubility distributions. *Atmospheric Chemistry and Physics* **2015**, *15*, (11), 6305-6322.

11. Gao, S.; Hegg, D. A.; Hobbs, P. V.; Kirchstetter, T. W.; Magi, B. I.; Sadilek, M., Water-soluble organic components in aerosols associated with savanna fires in southern Africa: Identification, evolution, and distribution. *Journal of Geophysical Research: Atmospheres* **2003**, *108*, (D13).

12. Schkolnik, G.; Rudich, Y., Detection and quantification of levoglucosan in atmospheric aerosols: a review. *Analytical and Bioanalytical Chemistry* **2006**, *385*, (1), 26-33.

13. Simoneit, B. R. T.; Schauer, J. J.; Nolte, C. G.; Oros, D. R.; Elias, V. O.; Fraser, M. P.; Rogge, W. F.; Cass, G. R., Levoglucosan, a tracer for cellulose in biomass burning and atmospheric particles. *Atmospheric Environment* **1999**, *33*, (2), 173-182.

14. Rosenørn, T.; Kiss, G.; Bilde, M., Cloud droplet activation of saccharides and levoglucosan particles. *Atmospheric Environment* **2006**, *40*, (10), 1794-1802.

15. Svenningsson, B.; Rissler, J.; Swietlicki, E.; Mircea, M.; Bilde, M.; Facchini, M. C.; Decesari, S.; Fuzzi, S.; Zhou, J.; Mønster, J.; Rosenørn, T., Hygroscopic growth and critical supersaturations for mixed aerosol particles of inorganic and organic compounds of atmospheric relevance. *Atmospheric Chemistry and Physics* **2006**, *6*, (7), 1937-1952.

16. Chan, M. N.; Choi, M. Y.; Ng, N. L.; Chan, C. K., Hygroscopicity of Water-Soluble Organic Compounds in Atmospheric Aerosols: Amino Acids and Biomass Burning Derived Organic Species. *Environmental Science & Technology* **2005**, *39*, (6), 1555-1562.

17. Lienhard, D. M.; Bones, D. L.; Zuend, A.; Krieger, U. K.; Reid, J. P.; Peter, T., Measurements of Thermodynamic and Optical Properties of Selected Aqueous Organic and Organic–Inorganic Mixtures of Atmospheric Relevance. *The Journal of Physical Chemistry A* **2012**, *116*, (40), 9954-9968.

18. Lei, T.; Zuend, A.; Wang, W. G.; Zhang, Y. H.; Ge, M. F., Hygroscopicity of organic compounds from biomass burning and their influence on the water uptake of mixed organic ammonium sulfate aerosols. *Atmospheric Chemistry and Physics* **2014**, *14*, (20), 11165-11183.

19. Mochida, M.; Kawamura, K., Hygroscopic properties of levoglucosan and related organic compounds characteristic to biomass burning aerosol particles. *Journal of Geophysical Research: Atmospheres* **2004**, *109*, (D21).

20. Decesari, S.; Fuzzi, S.; Facchini, M. C.; Mircea, M.; Emblico, L.; Cavalli, F.; Maenhaut, W.; Chi, X.; Schkolnik, G.; Falkovich, A.; Rudich, Y.; Claeys, M.; Pashynska, V.; Vas, G.; Kourtchev, I.; Vermeylen, R.; Hoffer, A.; Andreae, M. O.; Tagliavini, E.; Moretti, F.; Artaxo, P., Characterization of the organic composition of

aerosols from Rondônia, Brazil, during the LBA-SMOCC 2002 experiment and its representation through model compounds. *Atmospheric Chemistry and Physics* **2006**, *6*, (2), 375-402.

21. Pashynska, V.; Vermeylen, R.; Vas, G.; Maenhaut, W.; Claeys, M., Development of a gas chromatographic/ion trap mass spectrometric method for the determination of levoglucosan and saccharidic compounds in atmospheric aerosols. Application to urban aerosols. *Journal of Mass Spectrometry* **2002**, *37*, (12), 1249-1257.

22. Yttri, K. E.; Dye, C.; Kiss, G., Ambient aerosol concentrations of sugars and sugar-alcohols at four different sites in Norway. *Atmospheric Chemistry and Physics* **2007**, *7*, (16), 4267-4279.

23. Chenyakin, Y.; Ullmann, D. A.; Evoy, E.; Renbaum-Wolff, L.; Kamal, S.; Bertram, A. K., Diffusion coefficients of organic molecules in sucrose–water solutions and comparison with Stokes–Einstein predictions. *Atmospheric Chemistry and Physics* **2017**, *17*, (3), 2423-2435.

24. Ekdawi-Sever, N.; de Pablo, J. J.; Feick, E.; von Meerwall, E., Diffusion of Sucrose and α,α-Trehalose in Aqueous Solutions. *The Journal of Physical Chemistry A* **2003**, *107*, (6), 936-943.

25. Estillore, A. D.; Morris, H. S.; Or, V. W.; Lee, H. D.; Alves, M. R.; Marciano, M. A.; Laskina, O.; Qin, Z.; Tivanski, A. V.; Grassian, V. H., Linking hygroscopicity and the surface microstructure of model inorganic salts, simple and complex carbohydrates, and authentic sea spray aerosol particles. *Physical Chemistry Chemical Physics* **2017**, *19*, (31), 21101-21111.

26. Hodas, N.; Zuend, A.; Mui, W.; Flagan, R. C.; Seinfeld, J. H., Influence of particle-phase state on the hygroscopic behavior of mixed organic–inorganic aerosols. *Atmospheric Chemistry and Physics* **2015**, *15*, (9), 5027-5045.

27. Marshall, F. H.; Miles, R. E. H.; Song, Y.-C.; Ohm, P. B.; Power, R. M.; Reid, J. P.; Dutcher, C. S., Diffusion and reactivity in ultraviscous aerosol and the correlation with particle viscosity. *Chemical Science* **2016**, *7*, (2), 1298-1308.

28. Power, R. M.; Simpson, S. H.; Reid, J. P.; Hudson, A. J., The transition from liquid to solid-like behaviour in ultrahigh viscosity aerosol particles. *Chemical Science* **2013**, *4*, (6), 2597-2604.

29. Rothfuss, N. E.; Marsh, A.; Rovelli, G.; Petters, M. D.; Reid, J. P., Condensation Kinetics of Water on Amorphous Aerosol Particles. *The Journal of Physical Chemistry Letters* **2018**, *9*, (13), 3708-3713.

30. Tong, H. J.; Reid, J. P.; Bones, D. L.; Luo, B. P.; Krieger, U. K., Measurements of the timescales for the mass transfer of water in glassy aerosol at low relative humidity and ambient temperature. *Atmospheric Chemistry and Physics* **2011**, *11*, (10), 4739-4754.

31. Zobrist, B.; Soonsin, V.; Luo, B. P.; Krieger, U. K.; Marcolli, C.; Peter, T.; Koop, T., Ultra-slow water diffusion in aqueous sucrose glasses. *Physical Chemistry Chemical Physics* **2011**, *13*, (8), 3514-3526.

32. Koop, T.; Bookhold, J.; Shiraiwa, M.; Pöschl, U., Glass transition and phase state of organic compounds: dependency on molecular properties and implications for secondary organic aerosols in the atmosphere. *Physical Chemistry Chemical Physics* **2011**, *13*, (43), 19238-19255.

33. Lee, H. D.; Ray, K. K.; Tivanski, A. V., Directly Probing the Phase States and Surface Tension of Individual Submicrometer Particles Using Atomic Force Microscopy. In *Multiphase Environmental Chemistry in the Atmosphere*, American Chemical Society: 2018; Vol. 1299, pp 245-259.

34. Müller, A.; Miyazaki, Y.; Tachibana, E.; Kawamura, K.; Hiura, T., Evidence of a reduction in cloud condensation nuclei activity of water-soluble aerosols caused by biogenic emissions in a cool-temperate forest. *Scientific Reports* **2017**, *7*, (1), 8452.

35. Rogge, W. F.; Medeiros, P. M.; Simoneit, B. R. T., Organic marker compounds in surface soils of crop fields from the San Joaquin Valley fugitive dust characterization study. *Atmospheric Environment* **2007**, *41*, (37), 8183-8204.

36. Tang, M.; Chan, C. K.; Li, Y. J.; Su, H.; Ma, Q.; Wu, Z.; Zhang, G.; Wang, Z.; Ge, M.; Hu, M., A review of experimental techniques for aerosol hygroscopicity studies. *Atmospheric Chemistry and Physics* **2019**, *19*, 12631-12686.

37. Baynard, T.; Garland, R. M.; Ravishankara, A. R.; Tolbert, M. A.; Lovejoy, E. R., Key factors influencing the relative humidity dependence of aerosol light scattering. *Geophysical Research Letters* **2006**, *33*, (6).

38. Beaver, M. R.; Baynard, T.; Garland, R. M.; Hasenkopf, C.; Ravishankara, A. R.; Tolbert, M. A. In *Relative Humidity Dependence of Light Extinction by Mixed Organic/Sulfate Particles*, Dordrecht, 2007; Springer Netherlands: Dordrecht, 2007; pp 916-919.

39. Cappa, C. D.; Che, D. L.; Kessler, S. H.; Kroll, J. H.; Wilson, K. R., Variations in organic aerosol optical and hygroscopic properties upon heterogeneous OH oxidation. *Journal of Geophysical Research: Atmospheres* **2011**, *116*, (D15).

40. Michel Flores, J.; Bar-Or, R. Z.; Bluvshtein, N.; Abo-Riziq, A.; Kostinski, A.; Borrmann, S.; Koren, I.; Rudich, Y., Absorbing aerosols at high relative humidity: linking hygroscopic growth to optical properties. *Atmospheric Chemistry and Physics* **2012**, *12*, (12), 5511-5521.

41. Garland, R. M.; Ravishankara, A. R.; Lovejoy, E. R.; Tolbert, M. A.; Baynard, T., Parameterization for the relative humidity dependence of light extinction: Organic-ammonium sulfate aerosol. *Journal of Geophysical Research: Atmospheres* **2007**, *112*, (D19).

42. Robinson, C. B.; Schill, G. P.; Tolbert, M. A., Optical growth of highly viscous organic/sulfate particles. *Journal of Atmospheric Chemistry* **2014**, *71*, (2), 145-156.

43. Brown, S. S.; Stark, H.; Ravishankara, A. R., Cavity ring-down spectroscopy for atmospheric trace gas detection: application to the nitrate radical (NO_3). *Applied Physics B* **2002**, *75*, (2), 173-182.

44. Wex, H.; Petters, M. D.; Carrico, C. M.; Hallbauer, E.; Massling, A.; McMeeking, G. R.; Poulain, L.; Wu, Z.; Kreidenweis, S. M.; Stratmann, F., Towards closing the gap between hygroscopic growth and activation for secondary organic aerosol: Part 1 – Evidence from measurements. *Atmospheric Chemistry and Physics* **2009**, *9*, (12), 3987-3997.

45. Petters, M. D.; Kreidenweis, S. M., A single parameter representation of hygroscopic growth and cloud condensation nucleus activity. *Atmospheric Chemistry and Physics* **2007**, *7*, (8), 1961-1971.

46. Altaf, M. B.; Freedman, M. A., Effect of Drying Rate on Aerosol Particle Morphology. *The Journal of Physical Chemistry Letters* **2017**, *8*, (15), 3613-3618.

47. Veghte, D. P.; Altaf, M. B.; Haines, J. D.; Freedman, M. A., Optical properties of non-absorbing mineral dust components and mixtures. *Aerosol Science and Technology* **2016**, *50*, (11), 1239-1252.

48. Veghte, D. P.; Freedman, M. A., The Necessity of Microscopy to Characterize the Optical Properties of Size-Selected, Nonspherical Aerosol Particles. *Analytical Chemistry* **2012**, *84*, (21), 9101-9108.

49. Veghte, D. P.; Freedman, M. A., Facile Method for Determining the Aspect Ratios of Mineral Dust Aerosol by Electron Microscopy. *Aerosol Science and Technology* **2014**, *48*, (7), 715-724.

50. Freedman, M. A.; Hasenkopf, C. A.; Beaver, M. R.; Tolbert, M. A., Optical Properties of Internally Mixed Aerosol Particles Composed of Dicarboxylic Acids and Ammonium Sulfate. *The Journal of Physical Chemistry A* **2009**, *113*, (48), 13584-13592.

51. Hasenkopf, C. A.; Beaver, M. R.; Trainer, M. G.; Langley Dewitt, H.; Freedman, M. A.; Toon, O. B.; McKay, C. P.; Tolbert, M. A., Optical properties of Titan and early Earth haze laboratory analogs in the mid-visible. *Icarus* **2010**, *207*, (2), 903-913.

52. Cruz, C. N.; Pandis, S. N., Deliquescence and Hygroscopic Growth of Mixed Inorganic−Organic Atmospheric Aerosol. *Environmental Science & Technology* **2000**, *34*, (20), 4313-4319.

53. Rader, D. J.; McMurry, P. H., Application of the tandem differential mobility analyzer to studies of droplet growth or evaporation. *Journal of Aerosol Science* **1986**, *17*, (5), 771-787.

54. Swietlicki, E.; Hansson, H. C.; Hämeri, K.; Svenningsson, B.; Massling, A.; McFiggans, G.; McMurry, P. H.; Petäjä, T.; Tunved, P.; Gysel, M.; Topping, D.; Weingartner, E.; Baltensperger, U.; Rissler, J.; Wiedensohler, A.; Kulmala, M., Hygroscopic properties of submicrometer atmospheric aerosol particles measured with H-TDMA instruments in various environments—a review. *Tellus B: Chemical and Physical Meteorology* **2008**, *60*, (3), 432-469.

55. Moore, R. H.; Nenes, A., Scanning Flow CCN Analysis—A Method for Fast Measurements of CCN Spectra. *Aerosol Science and Technology* **2009**, *43*, (12), 1192-1207.

56. Wang, S. C.; Flagan, R. C., Scanning Electrical Mobility Spectrometer. *Aerosol Science and Technology* **1990**, *13*, (2), 230-240.

57. Kreidenweis, S.; Asa-Awuku, A., *Aerosol Hygroscopicity: Particle water content and its role in atmospheric processes*. 2014.

58. Lavallard, P.; Rosenbauer, M.; Gacoin, T., Influence of surrounding dielectrics on the spontaneous emission of sulforhodamine B molecules. *Physical Review A* **1996**, *54*, (6), 5450-5453.

59. Taylor, N.; Collins, D.; Spencer, C.; Lowenthal, D.; Zielinska, B.; Samburova, V.; Kumar, N., Measurement of ambient aerosol hydration state at Great Smoky Mountains National Park in the southeastern United States. *Atmospheric Chemistry and Physics Discussions* **2011**, *11*, (8), 12085-12107.

60. Koehler, K. A.; Kreidenweis, S. M.; DeMott, P. J.; Prenni, A. J.; Carrico, C. M.; Ervens, B.; Feingold, G., Water activity and activation diameters from hygroscopicity data - Part II: Application to organic species. *Atmospheric Chemistry and Physics* **2006**, *6*, (3), 795-809.

3.6 Supplemental Information

3.6.1 Summary

This supplemental document includes the method of determining relative humidity within the H-TDMA system via an ammonium sulfate standard, the presentation of refractive indices for each of the compounds of interest in this study, the comparison of experimental values obtained by our cavity ring-down system to Mie theory and subsequent demonstration of the fitting

procedure using a known standard, and an illustration of the change in surface tension of a sucrose-water solution with varying concentrations of sucrose.

Supplemental Table 3-S1: Coefficients of Determinations between the four κ Parameters and Properties of the Aerosol Species

		Property		
		M.W.	**O:C**	**Solubility**
Kappa	**Mie**	0.81	0.37	0.15
	Empirical	0.62	0.17	0.13
	H-TDMA	0.93	0.57	0.02
	CCNC	0.95	0.57	0.04

3.6.2 Hygroscopic Growth Factor Calibration

Humidity probes do not perform as well above 90% relative humidity (RH). Specifically, the humidity probes in this study (Vaisala HMP60) increase from a ±3% error to a ±5% error when above 90% RH. An ammonium sulfate calibration was done using Köhler Theory as described by the equation in the manuscript Eq. 3-9, and by using the growth factor of ammonium sulfate obtained from our experiment, and the RH obtained from Taylor et al. (2011) the RH within the H-TDMA was determined.[1] Growth factors were then determined by dividing the median particle diameter by the original dry particle mobility diameter as described in Supplemental Figure 3-S1.

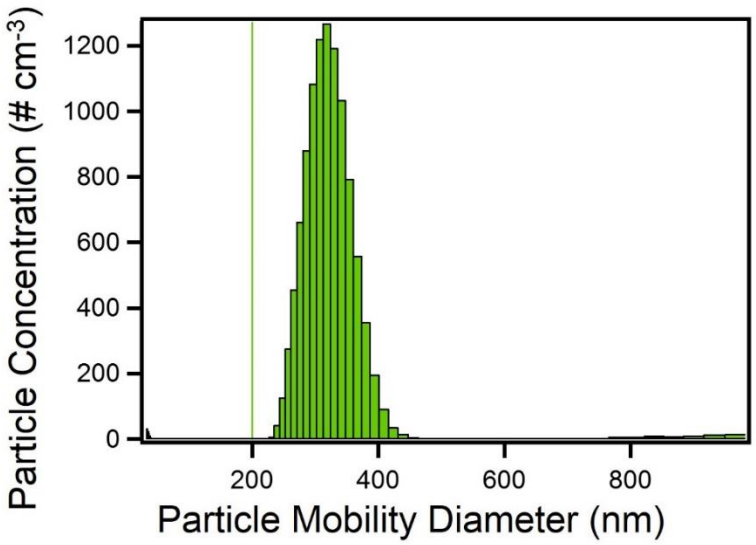

Figure 3-S1: Example of direct growth factor determination using levoglucosan. The original size is represented by a line, although the distribution of particles is determined by the transfer function. The SMPS data are the result of humidifying the dry aerosol.

3.6.3 Refractive Indices

The refractive indices were determined for each sample in the expected range for organic compounds as shown in Supplemental Figure 3-S2. The calculation for these values neglected the imaginary portion of the refractive index as these compounds have negligible absorbance at 643 nm. Even though they were dried after being atomized, these aerosolized water-soluble organic compounds become highly viscous nanoparticles rather than crystalize, and as a result, their shape is spherical and thus no shape corrections were necessary.[2,3]

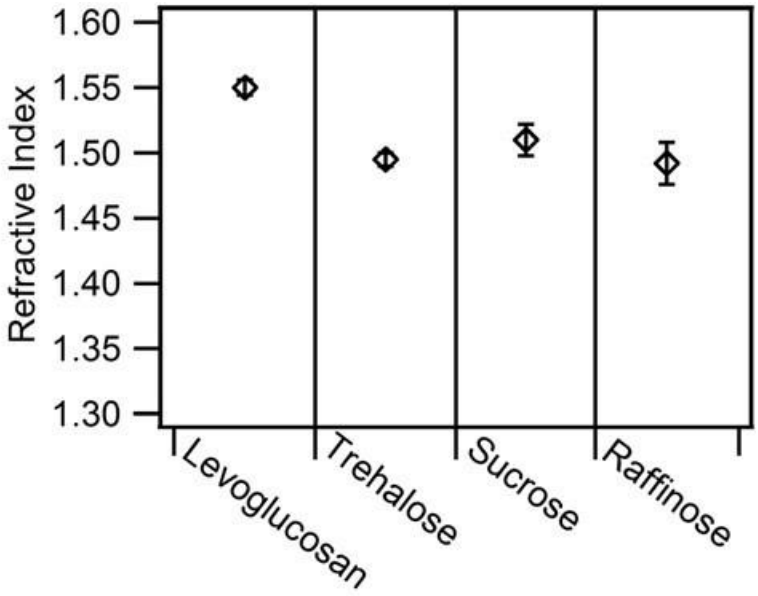

Figure 3-S2: Refractive indices of each of the four WSOC. All values ranged between 1.45 and 1.60 as expected for primarily scattering organic aerosol.

3.6.4 Optical Growth Factor of Ammonium Sulfate Standard

An ammonium sulfate standard was analyzed with the CRDS to calibrate and insure correct results.

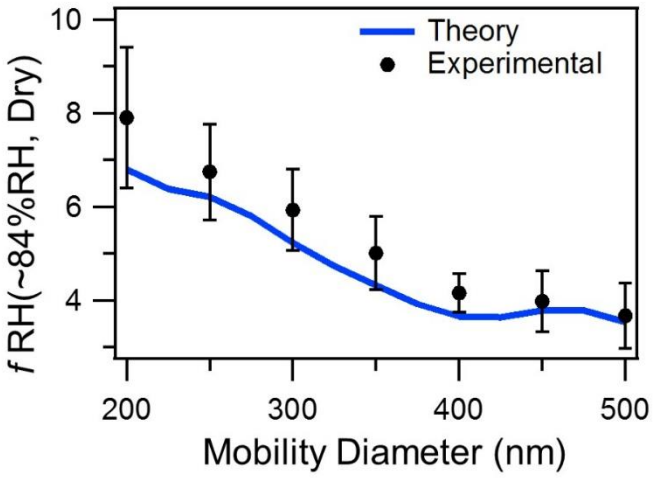

Figure 3-S3: Ammonium sulfate aerosol was measured using CRDS at a relative humidity of 84.4% ± 2.7%. The experimental data was compared to the theory line calculated from Mie theory using a relative humidity of 85%.

3.6.5 Surface Tension

The surface tension of sucrose-water solution was experimentally determined using a force tensiometer (Krüss K11). The values obtained were then used in the calculation of the surface tension of the sucrose-water solution at the point of CCN activation using a polynomial fit. The fit is shown in Supplemental Figure 3-S4.

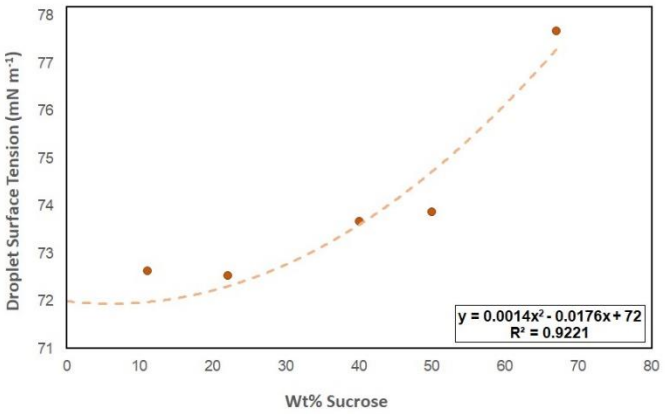

Figure 3-S4: Surface tension of sucrose-water solutions. A polynomial fit is applied to data and used to infer surface tension at the point of CCN activation.

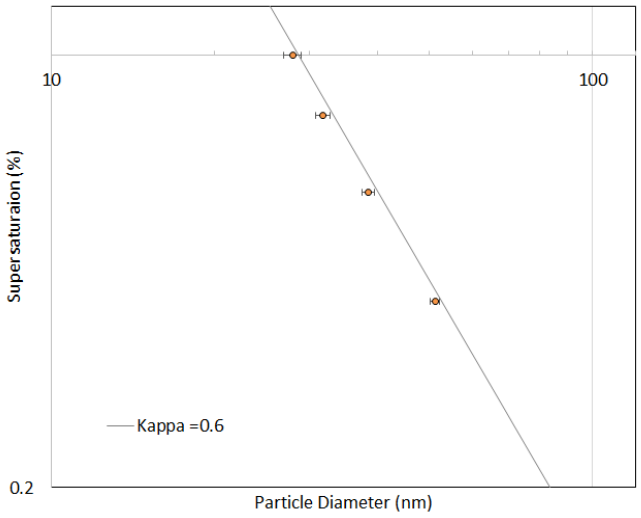

Figure 3-S5: Exemplary ammonium sulfate CCN Calibration data. The measured critical particle diameters for given instrument supersaturations are shown. The data agree well with theoretical hygroscopicity.

Supplemental References

1. Taylor, N.; Collins, D.; Spencer, C.; Lowenthal, D.; Zielinska, B.; Samburova, V.; Kumar, N., Measurement of ambient aerosol hydration state at Great Smoky Mountains National Park in the southeastern United States. *Atmospheric Chemistry & Physics Discussions* **2011**, *11*, (8), 12085-12107.

2. Power, R. M.; Simpson, S. H.; Reid, J. P.; Hudson, A. J., The transition from liquid to solid-like behaviour in ultrahigh viscosity aerosol particles. *Chemical Science* **2013**, *4*, (6), 2597-2604.

3. Veghte, D. P.; Altaf, M. B.; Haines, J. D.; Freedman, M. A., Optical properties of non-absorbing mineral dust components and mixtures. *Aerosol Science and Technology* **2016**, *50*, (11), 1239-1252.

Chapter 4

Internally Mixed SOA Hygroscopicity of SOA Formed in Wet and Dry Conditions

Author Contribution: I contributed to this work by structuring experiments, operating the CRDs, preforming relevant calculations of κ, comparing the two κ calculations derived from the CRDs results, performing the SOA reactions under each condition, operating and maintaining the laboratory equipment, and writing the manuscript.

Abstract

The influence of secondary organic aerosols (SOA) on the radiative budget, as well as the heterogeneous chemistries they undergo, is poorly understood. Specifically, the water uptake of SOA is of great interest due to the potential to lead to cloud formation. SOA is thought to be highly viscous, and it is theorized that that viscosity may inhibit water uptake, and therefore cloud formation. In this work, three techniques are used to analyze the hygroscopicity of laboratory generated SOA. α-Pinene and *trans*-caryophyllene SOA were generated via dark ozonolysis under both humid and dry conditions, and, in some cases, SOA was formed in the presence of ammonium sulfate. Each SOA sample was analyzed with three techniques: cavity ring-down spectroscopy (CRDS), hygroscopic tandem differential mobility analysis (H-TDMA), and cloud condensation nuclei counting (CCNC). The results were converted into κ-values and compared with each other. We show that *trans*-caryophyllene SOA is poorly hygroscopic when formed under both wet and dry conditions. Furthermore, when condensed onto ammonium sulfate seeds, the *trans*-caryophyllene SOA exhibited a complete inhibition of water uptake by the ammonium sulfate core. α-Pinene provided similar results under the same experimental conditions with one notable exception: when the relative humidity exceeded the deliquescence point of the seeded SOA, the particles demonstrated substantial water uptake. This indicated that when deliquesced, the ammonium sulfate core was able to take up water readily despite the SOA coating. These

results imply that highly viscous, or poorly hygroscopic SOA may play an important role in our understanding of cloud and haze formation as the SOA may need to reach supersaturated conditions in order to grow.

4.1 Introduction

A large uncertainty in how aerosol particles influence the climate through radiative forcing stems from the lack of knowledge of their water uptake.[1] Aerosol particles that uptake water can act as cloud condensation nuclei resulting in the formation of clouds or even just grow such that their optical properties change.[2] Organic compounds make up a large portion of the atmosphere and many originate from biogenic sources that can release gas phase organic compounds.[3] Volatile and semi-volatile compounds (VOCs and SVOCs), like those emitted from trees, become oxidized to form various derivative compounds and the behavior as well as the composition of these particles is poorly understood and not well characterized.[4-6] When biogenic precursors such as these react with ozone, they form secondary organic aerosol (SOA).[7] Many studies have been conducted on laboratory generated SOA with varying techniques, but rarely do studies use multiple techniques on the same sample, without which technique comparisons cannot be performed.[4-13] Several studies have shown that SOA can uptake water, modify regional visibility, and aerosol optical depth. Furthermore, several studies show SOA generated from biogenic and anthropogenic sources can act as cloud condensation nuclei (CCN).[4-7, 9, 11, 14-19] Since SOA is composed of many derivative compounds of VOCs and SVOCs, the hygroscopicity and optical properties are both poorly understood and difficult to determine. The ability for a particle to uptake water is thought to be dependent on its O:C ratio, and as a result the composition of the aerosol is important. SOA formed via the oxidation of VOCs and SVOCs are of particular interest because they are ubiquitous in the atmosphere. Furthermore, SOA can condense on existing

particles and grow them to cloud condensation nuclei (CCN) sizes.[20, 21] Yet the behavior and the composition of SOA is poorly understood.

There is a wide array of SOA studies in the current literature, but due to the different compositions of SOA, and differences in the techniques used to measure SOA, it is difficult to make comparisons between samples. In this work, multiple complimentary techniques are used on the same SOA samples to mitigate sample variation for the purpose of comparing the results from these methods. α-Pinene is a semi-volatile organic compound released by vegetation in the Western hemisphere and *trans*-caryophyllene is a semi-volatile sesquiterpene found in various oils from biogenic sources. α-Pinene SOA has been well studied. Few studies however, have measured the properties of α-pinene SOA with cavity ring-down spectroscopy (CRDS).[2, 10] H-TDMA and CCNC have been more commonly used.[1, 6, 7, 10, 11, 19, 22-24] The study of α-pinene SOA varies in terms of experimental methods most often varying in the concentrations of the precursors. Zhao et al. (2016) determined the H-TDMA derived κ-value (κ_{HTDMA}) of α-pinene SOA with a brief discussion of its discrepancy from CCN data.[25] Saathoff et al. (2003) generated α-pinene SOA on ammonium sulfate seeds and determine its geometric growth factor at several RHs using H-TDMA.[26] In some cases the SOA is generated in the presence of NO_x in addition to humidity and seeds.[27, 28] For example: various reaction conditions were used by Qi et al. (2012), including conditions similar to our own and the resulting SOA was characterized with H-TDMA.[27] *Trans*-caryophyllene SOA is another well characterized SOA, but in many cases, the composition varies between experiments.[13] Organic compounds contribute significantly to atmospheric aerosol.[3, 29]

Few studies, however, have measured the properties of α-pinene SOA with cavity ring-down spectroscopy (CRDS) .[2, 10] CRDS has more commonly been used to study the optical properties of SOA based on particle morphology and particle aging.[30, 31] Hygroscopic tandem differential mobility analyzer (H-TDMA) and cloud condensation nuclei counter (CCNC)

techniques have been more commonly used.[2, 6, 10, 11, 22-25] The study of α-pinene SOA varies in terms of experimental methods most often varying in the concentrations of the precursors. Zhao et al. (2016) determined the κ_{HTDMA} of α-pinene SOA with a brief discussion of its discrepancy from CCN data.[25] Saathoff et al. (2003) generated α-pinene SOA on ammonium sulfate seeds and determined its geometric growth factor at several RHs using H-TDMA.[26] In some cases, the SOA is generated in the presence of NO_x in addition to humidity and seeds.[27, 28] For example, various reaction conditions were used by Qi et al. (2012), and the resulting SOA was characterized with H-TDMA.[27] *Trans*-caryophyllene SOA is another well-characterized SOA, but as in many cases the composition varies between experiments.[13]

Fewer studies have explored the impact of hygroscopicity of SOA formed in the presence of water vapor. It is well known that increases in RH during SOA formation may affect overall SOA yields, oxidation products, and physical properties of the SOA phase.[32] The study of (Seinfeld et al. 2001) suggests a decrease in molecular weight may occur and the formation of hydrophilic compounds are promoted at high RH.[32] Many studies have been conducted on laboratory-generated SOA with varying techniques in an attempt to reduce sample variability, but rarely do studies use multiple techniques on the same sample. In this work, multiple complementary techniques are utilized on the same SOA samples to mitigate sample variation for the purpose of comparing the results from these methods.

4.2 Experimental Methods and Hygroscopicity Analysis

4.2.1 SOA Generation

Laboratory generated SOA was produced with a 1 m^3 Tedlar® chamber (Welsh Fluorocarbon®). Before each experiment, the chamber was cleaned with excess ozone (~ 100

ppm) and then purged with a continuous flow of purified air for 8 hours. Ozone was generated via a corona discharge tube ozone generator (Ozotech Inc. Poseidon Model). The chamber was first filled with purified air and ozone at the beginning of each experiment. The target ozone concentrations were 200 or 300 ppb depending on the aerosol precursor.

SOA was generated under four conditions: dry (< 10% RH unseeded), wet (humidified between 75% and 80% RH unseeded), dry seeded (SOA condensed on $(NH_4)_2SO_4$ particles), and wet seeded (SOA formed in humidified conditions in the presence of $(NH_4)_2SO_4$ particles). The humidification in the chamber is kept below 80% to prevent the deliquescence of $(NH_4)_2SO_4$ particles in wet seeded experiments. For humidified experiments, the filtered air was humidified with a bubbler containing ultrapure water (Millipore™ Water < 18 MΩ). For seeded experiments, a dilute solution of the $(NH_4)_2SO_4$ (ammonium sulfate, 98%, Fisher Chemical™) was atomized by a 3.6 L min^{-1} carrier gas of purified air. The particles were dehydrated via a silica gel diffusion dryer (Figure 4-1). Ammonium sulfate seed particles were added to the chamber at < 10% RH, which is considered to be “dry” conditions.

Two volatile organic carbon precursors were then added to the well-mixed chamber system (dry, wet and or seeded). Specifically, two precursors, α-pinene (Aldrich™, 98%) and *trans*-caryophyllene precursors (Sigma™, >98.5%) were injected into the environmental chamber to initiate nucleation and particle formation. α-Pinene SOA was generated using 200 ppb of ozone and 150 ppb of α-pinene and *trans*-caryophyllene SOA was formed in the presence of 300 ppb of ozone and 400 ppb of the *trans*-caryophyllene precursor. In the text below, α-pinene SOA and *trans*-caryophyllene SOA experiments are referred to as dry, wet, dry seeded and wet seeded experiments.

After nucleation, SOA concentrations were monitored with a scanning mobility particle sizer (SMPS, TSI 3081) and a condensation particle counter (TSI 3776). SOA is measured with three separate hygroscopicity techniques; cavity ring-down spectroscopy (CRDS), humidified

tandem differential mobility analysis (HTDMA), and cloud condensation nuclei counting (CCNC). All three analytical techniques used in this study have been previously reported and are briefly described below.

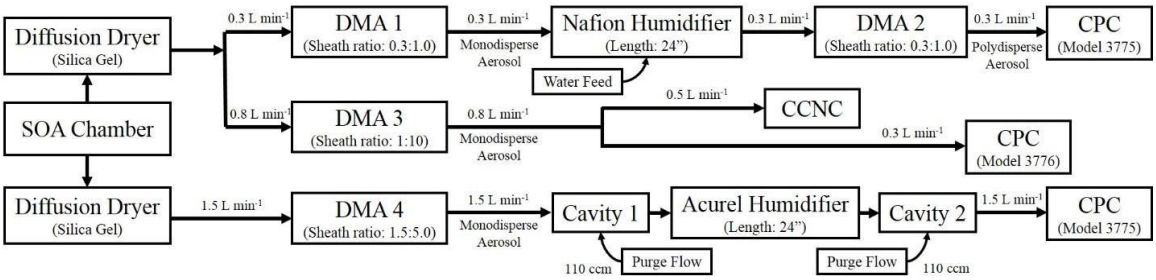

Figure 4-1: Box diagram of the experimental set-up consisting of three complementary methods: HTDMA, CCNC, and CRDS.

4.2.2 Cloud Condensation Nuclei Droplet Growth

The cloud condensation nuclei (CCN) activity is immediately measured after particle formation for each SOA experiment. The aerosol particles were dried upon exiting the chamber with a diffusion drier. Dry particles are sampled from the chamber and then size selected with an electrostatic classifier (SMPS, TSI 3081). The monodisperse aerosol sample is then split into two parallel streams. A condensation particle counter (CPC, TSI 3776) samples at a flow rate of 0.3 L min^{-1} and measures the total particle concentration for a given size. A continuous flow streamwise thermal gradient cloud condensation nuclei counter (CCNC; Droplet Measurement Technologies, DMT©) samples aerosol at 0.5 L min^{-1} and measures the CCN concentration simultaneously. The CCNC is calibrated before the experiment with $(NH_4)_2SO_4$. The aerosol size (from 8 to 352 nm) and CCN distribution is measured every 2 minutes and 15 sec and the CCN concentration is measured for a given instrument supersaturation for ~ 10 minutes and supersaturations in the DMT CCNC varied from 0.4% to 0.8% as the size distribution moved to larger sizes.

The critical diameter, dp_{50}, is defined by the 50% efficiency of the ratio of CCN to total particle concentration. This method, scanning mobility CCN analysis (SMCA) has been previously used to measure α-pinene SOA and *trans*-caryophyllene SOA CCN.[4, 9, 14, 18, 33] Supersaturation and dp_{50} data are used to calculate single-parameter hygroscopicity, κ, in the supersaturated RH regime using Eq. (4-1),

$$\kappa = \frac{4(A)^2}{27\left(D_{dry}\right)^3 ln^2 s_c} \quad (4\text{-}1)$$

where s_c is the instrument supersaturation, D_{dry} is the dp_{50}, and A is a constant based on the physical properties of water.[34] CCN measurement ends when all particle sizes activate at the lowest instrument supersaturation.

4.2.3 Humidified Tandem Differential Mobility Droplet Growth

Subsaturated geometric growth factors of the laboratory-generated SOA were measured with an H-TDMA. The H-TDMA is commonly used for aerosol hygroscopic measurement and a detailed setup has been previously described in previous publications.[33, 35-39] H-TDMA measures the growth of particles greater than 100 nm, thus H-TDMA sampling began about two hours after SOA particle formation, when sufficient aerosol had shifted to larger sizes (≥ 200 nm). As with CCN measurement, sampled dry aerosol particles are first separated by their electrical mobility diameter with a differential mobility analyzer (DMA, TSI 3081). The sample flow to sheath flow was maintained at a ratio of 0.3:1.0 and allowed for the selection of the 200, 250, and 300 nm particles used in this analysis. The selected distributions were then humidified with a Nafion humidification line (PermaPure® MH series) to 95% RH. The humidified distribution was then measured with a scanning particle mobility sizer (SMPS, TSI 3081/TSI 3775). The peak of the

second distribution was then used to calculate the geometric growth factor as has been previously described using a simple geometric growth factor calculation,

$$G_f(a,b) = \frac{D_a}{D_b} \quad (4\text{-}2)$$

where D_a is the mode mobility diameter of the humidified particles, and D_b is the mobility diameter of the dried particles before humidification. Similar H-TDMA measurement techniques have measured α-pinene SOA and *trans*-caryophyllene SOA.[2, 6, 7, 10-13, 16, 22, 23, 39]

4.2.4 Cavity Ring-Down Spectroscopy

Three hours after the SOA was generated, the particles grew to large enough sizes to be analyzed with CRDS. Again, the aerosol particles were dried upon exiting the chamber with a diffusion drier (Figure 4-1). The sample was then size selected with an electrostatic classifier (DMA, TSI 3080) and a differential mobility analyzer (DMA, TSI 3081) to a dry mobility diameter that was studied (eg. 200 nm, 225 nm, 250 nm, 275 nm, 300 nm, 350 nm, or 400 nm). The aerosol flow to sheath flow ratio was set to 1.5:5.0 to maintain this range of particle mobility diameters without changing the sheath flow. The CRDS system has been previously described and as such, only relevant portions of the system are addressed here.[40] The CRDS in this work consists of two cavities, a dry cavity and a humidified cavity. As size selected aerosol particles are introduced into either cavity, the extinction of light by those particles is measured. The extinction of the humidified aerosol particles is then divided by the extinction of the dry particles to obtain an optical growth factor for each dry mobility size. Optical growth factor (*f*RH) is then converted to geometric growth factor using Mie scattering theory and the basis of Eq. 4-2 where D_b is the dry particle mobility diameter selected by the DMA, and D_a is the diameter of the humidified particle derived from the humidified particle extinction coefficient and the refractive index of the particle. This method has been discussed before and is only briefly describe here

where extinction coefficients are calculated for particle size 0.1 nm above the original dry particle size until a calculated extinction coefficient if found that best matches the extinction coefficient of the humidified particle that was experimentally determined. In the CRDS chamber studies, the flow of sample through the system is governed by the CPC (TSI 3775) which was operated at 1.5 L min^{-1} flow rate. The actual flow from the chamber was slightly less than this value as each of the mirrors in the CRDS had a purge flow of 110 sccm which was maintained across them throughout the experiment. Each measurement technique was calibrated with ammonium sulfate (Millipore™, 99%) aerosol particles which were generated by a constant output atomizer (TSI 3076).

4.2.5 Hygroscopicity Analysis

The measured CCN activity, sub-saturated droplet growth, and optical growth can be converted to single hygroscopicity parameter, κ. Briefly, we present equations used to calculate hygroscopicity from the above three experimental methods.

κ-values can be derived from H-TDMA, G_f and RH measurements. Specifically, at relative humidities (>80%), the vapor pressure of water approaches that of a flat surface. As such droplet water activity can be approximated with RH. Thus, G_f simplifies to

$$G_f{}^3 = 1 + \kappa \frac{RH/100}{1 - RH/100} \tag{4-3}$$

and for supersaturated CCN measurement, κ is calculated via

$$\kappa = \frac{4\left(\frac{4\sigma_{s/a} M_w}{RT\rho_w}\right)^2}{27\left(D_{dry}\right)^3 ln^2 s_c} \tag{4-4}$$

where $\sigma_{s/a}$ is the surface tension of the droplet at the air droplet interface and is assumed to be that of pure water, D_{dry} is the dry particles diameter, s_c is the critical supersaturation, R is the universal

gas constant, T is the temperature of the droplet, and M_w and ρ_w are the molecular weight and density of water, respectively.[34, 41] Henceforth, we refer to κ-values derived in Eq. (3) and Eq. (4) as κHTDMA and κCCNC, respectively, and determined by the instrument measurement.

Contrary to the H-TDMA and CCNC κ-values, the equations for single hygroscopicity optical growth measurements have not been explicitly derived. Previous studies have proposed two and three empirical parameter relationships between *f*RH and RH.[41-43] Currently, two techniques are available to obtain a single hygroscopicity parameter with *f*RH data. The first method converts optical growth factor to geometric growth factor, G_f, using Mie theory, and the experimentally derived refractive indices.[43] The conversion to κ, Eq. (4-5) is thus similar to the Eq. (4-3) and is used to derive the κ factor from the growth factor

$$\kappa = ({G_f}^3 - 1)\left[\frac{RH}{100}e^{\left(\frac{4\sigma_{s/a}M_w}{RT\rho_w DG_f}\right)} - 1\right] \quad (4\text{-}5)$$

where $\sigma_{s/a}$ is the surface tension between the solution and the air, assumed to be that of water; ρ_w is the density of water, M_w is the molecular weight of water, R is the gas constant, and T is standard temperature.[34]

The second *f*RH method applies an empirical relationship to solve for G_f, and is shown by Eq. (4-6),

$$\kappa_{CRD,empirical} = \left(fRH(80\%RH, dry)^{\frac{3*0.28}{0.86}} - 1\right)\left(\frac{1-RH/100}{RH/100}\right) \quad (4\text{-}6)$$

where $\kappa_{CRD,Empirical}$, is the empirically derived κ-value.[41] Here the distinction is made between κ-factors determined by Mie theory and that determined semi-empirically as $\kappa_{CRD,Mie}$ and $\kappa_{CRD,Empirical}$, respectively. $\kappa_{CRD,Mie}$ has been shown to be particle size-independent, and $\kappa_{CRD,Empirical}$, exhibits a similar size dependence as *f*RH data. $\kappa_{CRD,Empirical}$, approaches κ-values of known aerosol compounds at larger particle sizes and both values have been shown to estimate slightly higher values than κ_{CCNC} and κ_{HTDMA} for water-soluble organic sugars.

4.3 Results and Discussion

4.3.1 Sub-Saturated Geometric Growth Factors

Geometric growth factors were determined for both α-pinene and *trans*-caryophyllene SOA under four conditions: dry, humidified, seeded dry and seeded humidified. The geometric growth factor for the dry α-pinene SOA at 95% RH is 1.28 ± 0.07. Juranyi et al. (2009) found the geometric growth factor of α-pinene SOA to range from about 1.43 to 1.63 at an RH of 97% and the κ_{HTDMA} to be between 0.074 and 0.126.[6] The geometric growth factor data obtained by and converted to κ_{HTDMA} by Zhao et al. (2016) ranged from 0.03 to 0.06 for α-pinene SOA.[19] The experimental conditions reported by Qi et al. varied too greatly from our own data for direct comparison; however, all reported α-pinene SOA (without further reactants than ozone) had a geometric growth factor less than 1.10.[27] The presence of water vapor during the formation of the α-pinene SOA did not appear to have an effect on the geometric growth factor which is 1.19 ± 0.01 at 95% RH. On the other hand, the seeded α-pinene SOA did exhibit a change in geometric growth factor where the dry, seeded SOA is 1.59 ± 0.09 and the wet seeded SOA is 2.08 ± 0.16, both at 95% RH. This is likely due to the deliquescence of α-pinene at relative humidities above 90%. Saathoff et al. (2003) reported a geometric growth factor for α-pinene SOA coated ammonium sulfate to be 1.106 ± 0.002 at 85% RH.[26] Meyer et al. (2009) used HTDMA at an RH of 75% and found geometric growth of seeded α-pinene SOA to be between 1.07 and 1.25 over the course of their experiment.[11]

The geometric growth factor for the *trans*-caryophyllene SOA at 95% RH is 1.12 ± 0.02. In the work by Hamilton et al. (2011), it was shown that the geometric growth factor of β-caryophyllene was less than 1.1 at an RH of 90%.[13] Changing the reaction conditions of the *trans*-caryophyllene SOA did little to change the geometric growth factor, specifically, when the SOA

was generated at 76% RH the geometric growth factor at 95% RH is 1.02 ± 0.04. Likewise, seeding the *trans*-caryophyllene under both wet and dry conditions did not significantly change the geometric growth factors which are 1.07 ± 0.02 and 0.99 ± 0.01, respectively. Overall *trans*-caryophyllene SOA effectively shows no geometric growth when humidified.

It is important to note that SOA generated under humidified conditions has some core concerns. One major concern is the inability to maintain the RH in the chamber. Once an RH of > 70% was measured within the chamber, we were unable to check the humidity during reaction without risk of contaminating our sample. The resultant changes in the chemical and physical properties of SOA generated in humid conditions could also pose a problem. Particles that are "stickier" could more readily stick to the walls of the chamber, and some unstable/semivolatile organics formed during the formation of the SOA may be removed when the SOA is dried.

4.3.2 Optical Growth Factors

The optical growth factors and refractive indices for each array of systems, both α-pinene and *trans*-caryophyllene SOA, are shown in Table 4-1. The expected result with the addition of ammonium sulfate seeds was a significant increase in *f*RH resulting from the very hygroscopic nature of ammonium sulfate; however, this increase was not observed within the limits of our system for either the α-pinene or *trans*-caryophyllene SOA.

Table 4-1: Tabulated values for the array of SOA samples for both optical growth factor and refractive index.

*f*RH	Dry	Wet	Seeded Dry	Seeded Wet
α-Pinene	1.30 ± 0.45	1.84 ± 0.27	1.27 ± .028	1.77 ± 0.46
trans-caryophyllene	1.11 ± 0.15	1.14 ± 0.12	1.16 ± 0.13	1.22 ± 0.13
RI	Dry	Wet	Seeded Dry	Seeded Wet
α-Pinene	1.474 ± 0.029	1.471 ± 0.029	1.478 ± 0.030	1.461 ± 0.029
trans-caryophyllene	1.490 ± 0.030	1.465 ± 0.029	1.448 ± 0.029	1.477 ± 0.030

Optical growth factors were determined for the α-pinene SOA and are displayed in Figure 4-2. The optical growth factor for the α-pinene SOA that was neither humidified nor seeded with

ammonium sulfate, *f*RH(85.9 ± 0.2%, dry), is 1.30 ± 0.04. For the α-pinene SOA, an increase in *f*RH was observed when the sample was generated under high RH conditions with an *f*RH(88.7 ± 0.6%, dry) value of 1.84 ± 0.74. The addition of ammonium sulfate seeds prior to the formation of the α-pinene SOA had little effect on the optical growth factors. Specifically, the dry seeded SOA has an *f*RH(88.3 ± 2.2%, dry) of 1.28 ± 0.08 and the wet seeded SOA has an *f*RH(87.8 ± 1.6%, dry) of 1.77 ± 0.18.

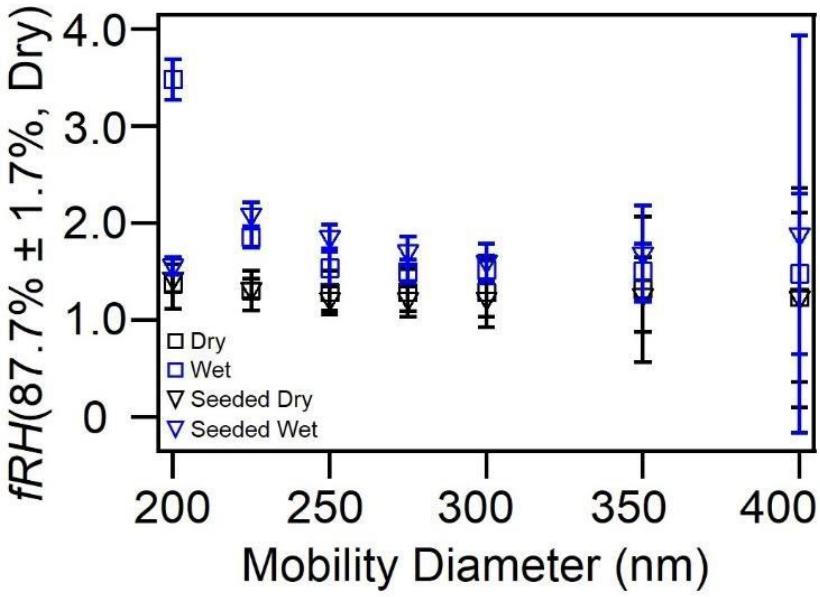

Figure 4-2: Size-resolved optical growth factors determined for α-pinene SOA under each of the four conditions. At the smaller particle diameters, the humidified (blue) points are higher than the dry (black points) with the differences becoming less apparent at larger particle sizes.

For the *trans*-caryophyllene samples, all *f*RH the data points were often within error of one another Figure 4-3. This includes the wet and dry generated SOA, as well as, the seeded SOA. However, some of the wet generated SOA has a higher *f*RH than the dry generated counterparts. Previous studies have shown that SOA generated in humid conditions can have their optical properties changed, which may play into the observed difference. The error in the *f*RH measurements is greater with the larger particles sizes as the influence of doubly charged particles becomes more apparent. The unseeded, dry generated *trans*-caryophyllene SOA has an *f*RH(89.8

± 1.9%, dry) of 1.11 ± 0.01. Comparatively the humified SOA has an *f*RH(89.0 ± 0.2%, dry) of 1.14 ± 0.01. When seeded, the dry SOA had an *f*RH(88.5 ± 1.7%, dry) of 1.16 ± 0.08 and the humidified SOA had an *f*RH(88.0 ± 1.6%, dry) of 1.22 ± 0.07.

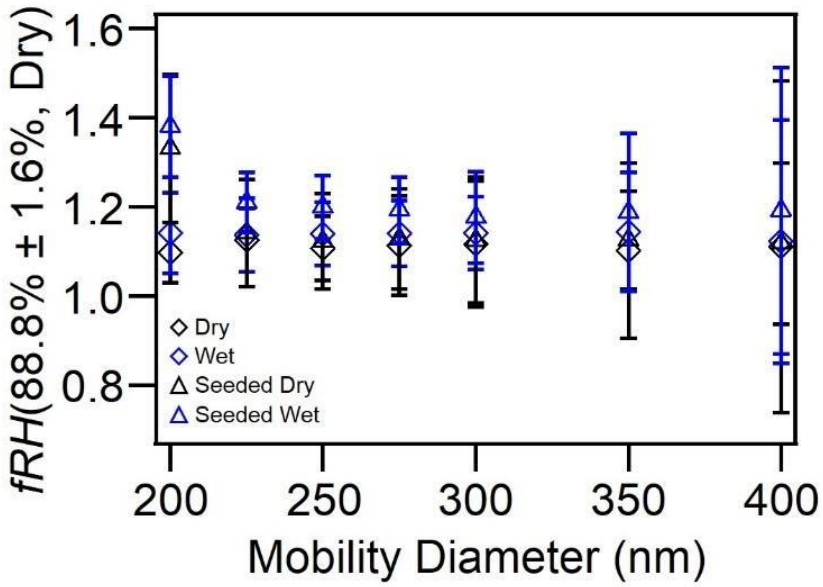

Figure 4-3: Size-resolved optical growth factors determined for *trans*-caryophyllene SOA under each of the four conditions. All points are within error of each other despite seeding or humidification.

4.3.3 Comparison of κ-values

Four *κ*-values were calculated from the data collected in the experiments above and from known solute parameters. It is of note that that there is some overlap in the measurements during the experiment, and we assume that the composition of aerosols remains constant and uniform throughout the distribution. An example of the particle size evolution is shown in Figure 4-4. However, the acquisition of these results occurs over the course of about 2 hours during which the aerosol particles continually interact with each other and grow. CCN activation and HTDMA results are well documented for dry and seeded dry α-pinene SOA and *trans*-caryophyllene SOA

systems. The unseeded α-pinene SOA κ_{CCNC} is 0.12 ± 0.02 as measured over the course of the experiment. This value is consistent with previously reported values of α-pinene SOA.[2, 4-9] Two of these values were calculated from the CRDS experiments, one based on the calculations by Asa-Awuku et al. (2008) ($\kappa_{CRDS,Empirical}$) and one from the methods described in previous literature ($\kappa_{CRDS,Mie}$). The two calculations are in good agreement with each other suggesting that both methods are viable. In general, the κ-values derived from the CRDS were lower than those from other methods (Figure 4-5 and Figure 4-6). This is likely due to the lower RH within the system (85% to 90% RH). H-TDMA data was also used to calculate a κ-value (κ_{HTDMA}). In this case, the values were often in agreement with the other technique that operate in the subsaturated regime, CRDS. It is of note that in the case of the α-pinene SOA that was generated under dry conditions but seeded with ammonium sulfate the κ-value was closer to the value of the technique that operated in the supersaturated regime, CCNC (Figure 4-6). We propose that since α-pinene SOA deliquesces around 90 – 95% RH, the ammonium sulfate core was able to uptake water whereas in the CRDS experiment it was not. This resulted in greater water uptake.

Hygroscopicity data was calculated from the CCNC data (κ_{CCNC}). These values were often higher than either the CRDS- or H-TDMA-derived κ-values which is likely a result of the supersaturated conditions of the experiment. This result is not surprising since the core principle of the CCNC technique is the generation of water vapor in a thermodynamically unstable state. The supersaturated water vapor will condense onto particles, where it can be more readily absorbed. In general, the *trans*-caryophyllene SOA exhibited little to no hygroscopic growth regardless of the experiment type. This is despite the presence of the very hygroscopic ammonium sulfate within some of the experiments. Most likely the *trans*-caryophyllene is coating the ammonium sulfate seeds and completely inhibiting water uptake by the core, at least within the time frame of our experiments.

The α-pinene SOA exhibited a change in hygroscopicity when generated under humid conditions. Seeding the SOA with ammonium sulfate resulted in a key observation: at lower RH (<90%) the addition of ammonium sulfate seeds did not increase the hygroscopicity. As with the *trans*-caryophyllene SOA, this is likely due to the SOA thoroughly coating the seed and inhibiting water uptake. However, with the techniques that operated at higher RH, the α-pinene SOA did exhibit an increase in hygroscopicity with the addition of ammonium sulfate seeds while the *trans*-caryophyllene with ammonium sulfate seeds did not. It has been shown that α-pinene SOA deliquesces around 90 – 95% RH and therefore when humidified past this point, the water would have access to the core, resulting in increased hygroscopic growth. This result suggests that the deliquescence of the inorganic solute does not contribute to the depression of water vapor pressure at the surface of the droplet or that most of the SOA generated is by seeded growth rather than new particle formation which is in terms of thermodynamics, most likely.

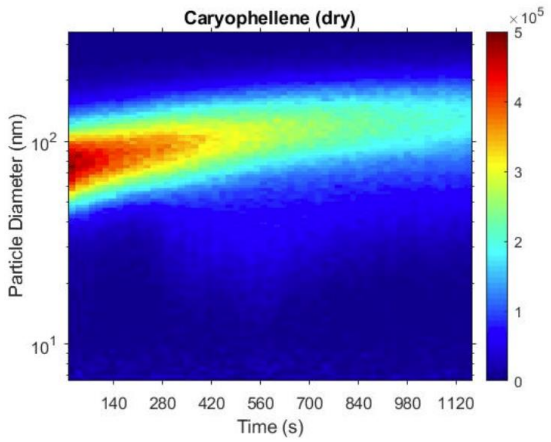

Figure 4-4: Evolution of particle sizes for dry generated *trans*-caryophyllene SOA over the course of each of the hygroscopicity measurements.

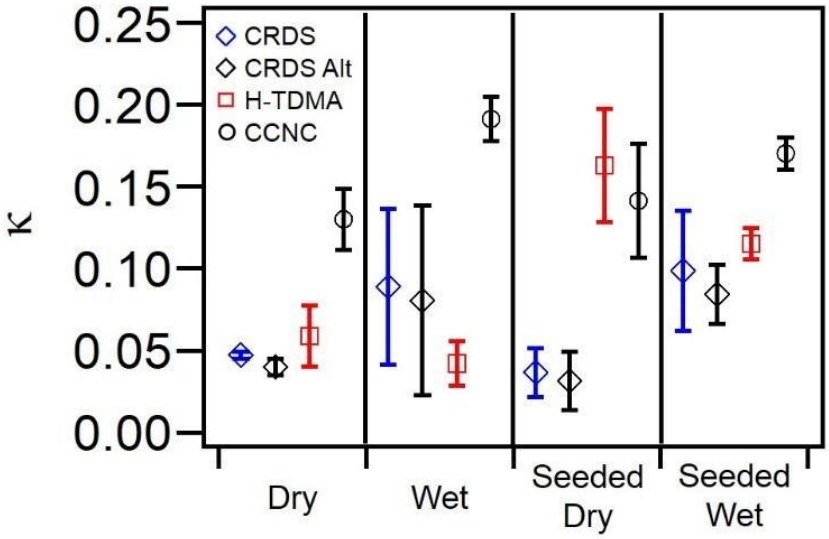

Figure 4-5: Four calculations of kappa factor for α-pinene SOA derived from the three experimental methods. In each case, the calculations were performed on the four experimental conditions. In some cases, an enhancement is observed when the particles were humidified prior to SOA formation, which is most notably observed in the CRDS derived data.

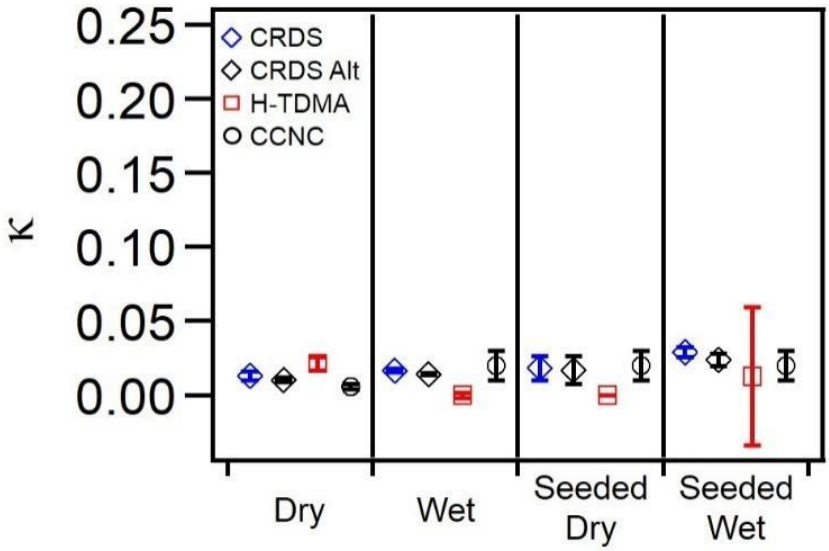

Figure 4-6: Four calculations of kappa factor for *trans*-caryophyllene SOA derived from the three experimental methods. In each case, the calculations were performed on the four experimental conditions. These data clearly exhibit a profound lack of change despite humidification and seeding of the SOA.

4.5 Conclusions

SOA is capable of taking up water, changing both its direct and indirect optical properties. Using three complementary techniques we determined the κ-values for laboratory-generated SOA. The differences between κ-values for the α-pinene and *trans*-caryophyllene SOA emphasize the importance of composition on hygroscopicity. The lack of hygroscopic growth by seeded particles indicates inhibition of water uptake by the ammonium sulfate core likely due to limited solubility or viscosity of the SOA. Once the deliquescence point of the SOA has been reached however, the ammonium sulfate core is free to take up water. As in previous publication, we continue to show the close approximation that the work of Kreidenweis and Asa-Awuku (2014)'s calculations of κ-factor from optical growth factor gives.[41] This indicates that it may be a viable method for calculating the κ-factor. Hygroscopicity of aerosol particles plays an important role in the determination of their optical properties and the formation of clouds and haze. By comparing subsaturated and supersaturated methods of determining the hygroscopicity of SOA, we may be able to reduce the high error associated with models which use the reported κ-values.

References

1. Stocker, T. F.; Qin, D.; Plattner, G.-K.; Tignor, M. M.; Allen, S. K.; Boschung, J.; Nauels, A.; Xia, Y.; Bex, V.; Midgley, P. M., Climate Change 2013: *The physical science basis. contribution of working group I to the fifth assessment report of IPCC the intergovernmental panel on climate change*. In Cambridge University Press: 2014.

2. Wex, H.; Petters, M. D.; Carrico, C. M.; Hallbauer, E.; Massling, A.; McMeeking, G. R.; Poulain, L.; Wu, Z.; Kreidenweis, S. M.; Stratmann, F., Towards closing the gap between hygroscopic growth and activation for secondary organic aerosol: Part 1 – Evidence from measurements. *Atmospheric Chemistry and Physics Discussions* **2009**, *9*, (12), 3987-3997.

3. Kanakidou, M.; Seinfeld, J. H.; Pandis, S. N.; Barnes, I.; Dentener, F. J.; Facchini, M. C.; Van Dingenen, R.; Ervens, B.; Nenes, A.; Nielsen, C. J.; Swietlicki, E.; Putaud, J. P.; Balkanski, Y.; Fuzzi, S.; Horth, J.; Moortgat, G. K.; Winterhalter, R.; Myhre, C. E. L.; Tsigaridis, K.; Vignati, E.; Stephanou, E. G.; Wilson, J., Organic aerosol and global climate modelling: a review. *Atmospheric Chemistry and Physics Discussions* **2005**, *5*, (4), 1053-1123.

4. Engelhart, G. J.; Asa-Awuku, A.; Nenes, A.; Pandis, S. N., CCN activity and droplet growth kinetics of fresh and aged monoterpene secondary organic aerosol. *Atmospheric Chemistry and Physics Discussions* **2008**, *8*, (1), 95-135.

5. Huff Hartz, K. E.; Rosenørn, T.; Ferchak, S. R.; Raymond, T. M.; Bilde, M.; Donahue, N. M.; Pandis, S. N., Cloud condensation nuclei activation of monoterpene and sesquiterpene secondary organic aerosol. *Journal of Geophysical Research: Atmospheres* **2005**, *110*, (D14).

6. Jurányi, Z.; Gysel, M.; Duplissy, J.; Weingartner, E.; Tritscher, T.; Dommen, J.; Henning, S.; Ziese, M.; Kiselev, A.; Stratmann, F.; George, I.; Baltensperger, U., Influence of gas-to-particle partitioning on the hygroscopic and droplet activation behaviour of α-pinene secondary organic aerosol. *Physical Chemistry Chemical Physics* **2009**, *11*, (36), 8091-8097.

7. Massoli, P.; Lambe, A. T.; Ahern, A. T.; Williams, L. R.; Ehn, M.; Mikkilä, J.; Canagaratna, M. R.; Brune, W. H.; Onasch, T. B.; Jayne, J. T.; Petäjä, T.; Kulmala, M.; Laaksonen, A.; Kolb, C. E.; Davidovits, P.; Worsnop, D. R., Relationship between aerosol oxidation level and hygroscopic properties of laboratory generated secondary organic aerosol (SOA) particles. *Geophysical Research Letters* **2010**, *37*, (24).

8. Frosch, M.; Bilde, M.; DeCarlo, P. F.; Jurányi, Z.; Tritscher, T.; Dommen, J.; Donahue, N. M.; Gysel, M.; Weingartner, E.; Baltensperger, U., Relating cloud condensation nuclei activity and oxidation level of α-pinene secondary organic aerosols. *Journal of Geophysical Research: Atmospheres* **2011**, *116*, (D22).

9. Lambe, A.; Onasch, T.; Massoli, P.; Croasdale, D.; Wright, J.; Ahern, A.; Williams, L.; Worsnop, D.; Brune, W. H.; Davidovits, P., Laboratory studies of the chemical composition and cloud condensation nuclei (CCN) activity of secondary organic aerosol (SOA) and oxidized primary organic aerosol (OPOA). *Atmospheric Chemistry & Physics* **2011**, *11*, (17).

10. Denjean, C.; Formenti, P.; Picquet-Varrault, B.; Pangui, E.; Zapf, P.; Katrib, Y.; Giorio, C.; Tapparo, A.; Monod, A.; Temime-Roussel, B.; Decorse, P.; Mangeney, C.; Doussin, J. F., Relating hygroscopicity and optical properties to chemical composition and structure of secondary organic aerosol particles generated from the ozonolysis of α-pinene. *Atmospheric Chemistry and Physics Discussions* **2015**, *15*, (6), 3339-3358.

11. Meyer, N. K.; Duplissy, J.; Gysel, M.; Metzger, A.; Dommen, J.; Weingartner, E.; Alfarra, M. R.; Prevot, A. S. H.; Fletcher, C.; Good, N.; McFiggans, G.; Jonsson, Å. M.; Hallquist, M.; Baltensperger, U.; Ristovski, Z. D., Analysis of the hygroscopic and volatile properties of ammonium sulphate seeded and unseeded SOA particles. *Atmospheric Chemistry and Physics Discussions* **2009**, *9*, (2), 721-732.

12. Alfarra, M. R.; Hamilton, J. F.; Wyche, K. P.; Good, N.; Ward, M. W.; Carr, T.; Barley, M. H.; Monks, P. S.; Jenkin, M. E.; Lewis, A. C.; McFiggans, G. B., The effect of photochemical ageing and initial precursor concentration on the composition and hygroscopic properties of β-caryophyllene secondary organic aerosol. *Atmospheric Chemistry and Physics Discussions* **2012**, *12*, (14), 6417-6436.

13. Hamilton, J. F.; Rami Alfarra, M.; Wyche, K. P.; Ward, M. W.; Lewis, A. C.; McFiggans, G. B.; Good, N.; Monks, P. S.; Carr, T.; White, I. R.; Purvis, R. M., Investigating the use of secondary organic aerosol as seed particles in simulation chamber experiments. *Atmospheric Chemistry and Physics Discussions* **2011**, *11*, (12), 5917-5929.

14. Asa-Awuku, A.; Engelhart, G. J.; Lee, B. H.; Pandis, S. N.; Nenes, A., Relating CCN activity, volatility, and droplet growth kinetics of β-caryophyllene secondary organic aerosol. *Atmospheric Chemistry and Physics Discussions* **2008**, *8*, (3), 10105-10151.

15. Asa-Awuku, A.; Nenes, A.; Gao, S.; Flagan, R.; Seinfeld, J. H., Water-soluble SOA from Alkene ozonolysis: composition and droplet activation kinetics inferences from analysis of CCN activity. *Atmospheric Chemistry and Physics* **2010**, *10*, (4), 1585.

16. Prenni, A. J.; Petters, M. D.; Kreidenweis, S. M.; DeMott, P. J.; Ziemann, P. J., Cloud droplet activation of secondary organic aerosol. *Journal of Geophysical Research: Atmospheres* **2007**, *112*, (D10).

17. Vizenor, A.; Asa-Awuku, A., Gas-phase kinetics modifies the CCN activity of a biogenic SOA. *Physical Chemistry Chemical Physics* **2018**, *20*, (9), 6591-6597.

18. Tang, X.; Cocker Iii, D.; Asa-Awuku, A., Are sesquiterpenes a good source of secondary organic cloud condensation nuclei (CCN)? Revisiting B-caryophyllene CCN. *Atmospheric Chemistry and Physics Discussions* **2012**, *12*, (18).

19. Zhao, D. F.; Buchholz, A.; Kortner, B.; Schlag, P.; Rubach, F.; Kiendler-Scharr, A.; Tillmann, R.; Wahner, A.; Flores, J. M.; Rudich, Y.; Watne, Å. K.; Hallquist, M.; Wildt, J.; Mentel, T. F., Size-dependent hygroscopicity parameter (κ) and chemical composition of secondary organic cloud condensation nuclei. *Geophysical Research Letters* **2015**, *42*, (24), 10,920-10,928.

20. Riipinen, I.; Pierce, J.; Yli-Juuti, T.; Nieminen, T.; Hakkinen, S.; Ehn, M.; Junninen, H.; Lehtipalo, K.; Petaja, T.; Slowik, J., Organic condensation: a vital link connecting aerosol formation to cloud condensation nuclei (CCN) concentrations. *Atmospheric Chemistry and Physics Discussions* **2011**, *11*, 3865-3878.

21. Pierce, J.; Leaitch, W.; Liggio, J.; Westervelt, D.; Wainwright, C.; Abbatt, J.; Ahlm, L.; Al-Basheer, W.; Cziczo, D.; Hayden, K., Nucleation and condensational growth to CCN sizes during a sustained pristine biogenic SOA event in a forested mountain valley. *Atmospheric Chemistry and Physics Discussions* **2012**, *12*, 3147-3163.

22. Varutbangkul, V.; Brechtel, F. J.; Bahreini, R.; Ng, N. L.; Keywood, M. D.; Kroll, J. H.; Flagan, R. C.; Seinfeld, J. H.; Lee, A.; Goldstein, A. H., Hygroscopicity of secondary organic aerosols formed by oxidation of cycloalkenes, monoterpenes, sesquiterpenes, and related compounds. *Atmospheric Chemistry and Physics Discussions* **2006**, *6*, (1), 1121-1177.

23. Duplissy, J.; Gysel, M.; Sjogren, S.; Meyer, N.; Good, N.; Kammermann, L.; Michaud, V.; Weigel, R.; dos Santos, S. M.; Gruening, C., Intercomparison study of six HTDMAs: results and general recommendations for HTDMA operation. *Atmospheric Measurement Techniques Discussion* **2008**, *1*, 1-507.

24. Duplissy, J.; Gysel, M.; Alfarra, M. R.; Dommen, J.; Metzger, A.; Prevot, A. S. H.; Weingartner, E.; Laaksonen, A.; Raatikainen, T.; Good, N.; Turner, S. F.; McFiggans, G.; Baltensperger, U., Cloud forming potential of secondary organic aerosol under near atmospheric conditions. *Geophysical Research Letters* **2008**, *35*, (3).

25. Zhao, D. F.; Buchholz, A.; Kortner, B.; Schlag, P.; Rubach, F.; Fuchs, H.; Kiendler-Scharr, A.; Tillmann, R.; Wahner, A.; Watne, Å. K.; Hallquist, M.; Flores, J. M.; Rudich, Y.; Kristensen, K.; Hansen, A. M. K.; Glasius, M.; Kourtchev, I.; Kalberer, M.; Mentel, T. F., Cloud condensation nuclei activity, droplet growth kinetics, and hygroscopicity of biogenic and anthropogenic secondary organic aerosol (SOA). *Atmospheric Chemistry & Physics* **2016**, *16*, (2), 1105-1121.

26. Saathoff, H.; Naumann, K. H.; Schnaiter, M.; Schöck, W.; Möhler, O.; Schurath, U.; Weingartner, E.; Gysel, M.; Baltensperger, U., Coating of soot and (NH4)2SO4 particles by ozonolysis products of α-pinene. *Journal of Aerosol Science* **2003**, *34*, (10), 1297-1321.

27. Qi, L.; Nakao, S.; Cocker, D. R., Aging of secondary organic aerosol from α-pinene ozonolysis: Roles of hydroxyl and nitrate radicals. *Journal of the Air & Waste Management Association* **2012**, *62*, (12), 1359-1369.

28. Chu, B.; Wang, K.; Takekawa, H.; Li, J.; Zhou, W.; Jiang, J.; Ma, Q.; He, H.; Hao, J., Hygroscopicity of particles generated from photooxidation of α-pinene under different oxidation conditions in the presence of sulfate seed aerosols. *Journal of Environmental Sciences* **2014**, *26*, (1), 129-139.

29. Zhang, Q.; Jimenez, J. L.; Canagaratna, M. R.; Ulbrich, I. M.; Ng, N. L.; Worsnop, D. R.; Sun, Y., Understanding atmospheric organic aerosols via factor analysis of aerosol mass spectrometry: a review. *Analytical and Bioanalytical Chemistry* **2011**, *401*, (10), 3045-3067.

30. Fard, M. M.; Krieger, U.; Rudich, Y.; Marcolli, C.; Peter, T., *Morphology and Optical Properties of Mixed Aerosol Particles*. In 2016; pp EPSC2016-6587.

31. Li, C.; He, Q.; Schade, J.; Passig, J.; Zimmermann, R.; Meidan, D.; Laskin, A.; Rudich, Y., Dynamic changes in optical and chemical properties of tar ball aerosols by atmospheric photochemical aging. *Atmospheric Chemistry & Physics* **2019**, *19*, (1).

32. Seinfeld, J. H.; Erdakos, G. B.; Asher, W. E.; Pankow, J. F., Modeling the Formation of Secondary Organic Aerosol (SOA). 2. The Predicted Effects of Relative Humidity on Aerosol Formation in the α-Pinene-, β-Pinene-, Sabinene-, Δ3-Carene-, and Cyclohexene-Ozone Systems. *Environmental Science & Technology* **2001**, *35*, (9), 1806-1817.

33. Moore, R. H.; Nenes, A., Scanning Flow CCN Analysis—A Method for Fast Measurements of CCN Spectra. *Aerosol Science and Technology* **2009**, *43*, (12), 1192-1207.

34. Petters, M. D.; Kreidenweis, S. M., A single parameter representation of hygroscopic growth and cloud condensation nucleus activity. *Atmospheric Chemistry & Physics* **2007**, *7*, (8), 1961-1971.

35. Cruz, C. N.; Pandis, S. N., Deliquescence and Hygroscopic Growth of Mixed Inorganic−Organic Atmospheric Aerosol. *Environmental Science & Technology* **2000**, *34*, (20), 4313-4319.

36. Rader, D. J.; McMurry, P. H., Application of the tandem differential mobility analyzer to studies of droplet growth or evaporation. *Journal of Aerosol Science* **1986**, *17*, (5), 771-787.

37. Swietlicki, E.; Hansson, H. C.; Hämeri, K.; Svenningsson, B.; Massling, A.; McFiggans, G.; McMurry, P. H.; Petäjä, T.; Tunved, P.; Gysel, M.; Topping, D.; Weingartner, E.; Baltensperger, U.; Rissler, J.; Wiedensohler, A.; Kulmala, M., Hygroscopic properties of submicrometer atmospheric aerosol particles measured with H-TDMA instruments in various environments—a review. *Tellus B: Chemical and Physical Meteorology* **2008**, *60*, (3), 432-469.

38. Taylor, N.; Collins, D.; Spencer, C.; Lowenthal, D.; Zielinska, B.; Samburova, V.; Kumar, N., Measurement of ambient aerosol hydration state at Great Smoky

Mountains National Park in the southeastern United States. *Atmospheric Chemistry & Physics Discussions* **2011**, *11*, (8), 12085-12107.

39. Duplissy, J.; DeCarlo, P. F.; Dommen, J.; Alfarra, M. R.; Metzger, A.; Barmpadimos, I.; Prevot, A. S. H.; Weingartner, E.; Tritscher, T.; Gysel, M.; Aiken, A. C.; Jimenez, J. L.; Canagaratna, M. R.; Worsnop, D. R.; Collins, D. R.; Tomlinson, J.; Baltensperger, U., Relating hygroscopicity and composition of organic aerosol particulate matter. *Atmospheric Chemistry & Physics* **2011**, *11*, (3), 1155-1165.

40. Veghte, D. P.; Altaf, M. B.; Haines, J. D.; Freedman, M. A., Optical properties of non-absorbing mineral dust components and mixtures. *Aerosol Science and Technology* **2016**, *50*, (11), 1239-1252.

41. Kreidenweis, S.; Asa-Awuku, A., *Aerosol Hygroscopicity: Particle water content and its role in atmospheric processes*. 2014.

42. Cappa, C. D.; Che, D. L.; Kessler, S. H.; Kroll, J. H.; Wilson, K. R., Variations in organic aerosol optical and hygroscopic properties upon heterogeneous OH oxidation. *Journal of Geophysical Research: Atmospheres* **2011**, *116*, (D15).

43. Garland, R. M.; Ravishankara, A. R.; Lovejoy, E. R.; Tolbert, M. A.; Baynard, T., Parameterization for the relative humidity dependence of light extinction: Organic-ammonium sulfate aerosol. *Journal of Geophysical Research: Atmospheres* **2007**, *112*, (D19).

Chapter 5

Ultrafine Nanoparticles Emitted Through Routine Operation of a Hairdryer

Abstract

Particulate matter is a large concern for human health. Current regulation targets the size of the particles, but composition also impacts toxicity. Indoor sources of air pollution pose unique challenges for human health due to the potential for human exposure to high concentrations in confined spaces. In this work, six hairdryers were each operated within a Plexiglass chamber, and their emissions were analyzed with transmission electron microscopy and energy dispersive spectroscopy (EDS). Each hairdryer emitted particles in the ultrafine range, and EDS revealed that two of the six hairdryers emitted silver nanoparticles. All hairdryers were found to emit ultrafine iron, carbon, and copper. The particle size distribution and compositions of these two hairdryers were analyzed. Emissions from both hairdryers primarily contained silver nanoparticles in the ultrafine range (<100 nm). These particles can easily enter into the blood steam after inhalation and pose long term health effects.

5.1 Introduction

In 1977 the U. S. Clean Air Act was amended to reflect the growing concern of the influence of inhalable particulate matter on human health. Since then, particulate air pollution has been classified into three main categories: coarse particles, fine particles, and ultrafine particles. Coarse, fine, and ultrafine particulate matter consist of particles less than 10 microns (PM_{10}), 2.5 microns ($PM_{2.5}$), and 100 nm ($PM_{0.1}$) in diameter, respectively.[1] These divisions are made to

reflect the potential health impact of each size regime. The Harvard Six Cities study outlined a correlation between fine particulate matter and mortality.[2] Those results have been confirmed and expounded upon revealing that $PM_{2.5}$ is capable of entering deep into the lungs and becomes embedded in the alveolar sacs, increasing the burden of cardiopulmonary disease.[3-5] In addition to the negative health effects caused by particulate matter, it is currently estimated that the aggregate social cost of particulate matter in the United States is $330 billion per year.[6] The aggregate social cost is the financial cost associated with treating the diseases caused by particulate matter.[6] In more recent years, ultrafine particulate matter has been identified as a cause for concern. Studies in rats revealed that when inhaled, these particles can enter into the bloodstream in as little as fifteen minutes.[7] Upon entering the bloodstream, particles can interact with the body on a cellular level. This cellular interaction is dependent on the composition, size, and surface properties of the nanoparticle, but few studies of the dependence of composition on toxicity have been performed. While the field of nanotoxicology is fairly new, the effect of metal nanoparticles, such as, gold, silver, titanium dioxide, and iron oxide have been investigated.[8] Once absorbed into the bloodstream, metal nanoparticles have been shown to cause oxidative stress and mitochondrial damage.[9] As concern over the impact of particulate matter continues to rise, compositional information will be key to understanding the full health effects of ultrafine particles.

Americans spend approximately 87% of their time indoors, and daily activities like cooking and cleaning release particulate matter into the air.[10] Additionally, particulate matter from outside can transfer indoors where it can dwell for long periods of time. High particle number concentrations and large particle surface areas result in an increased number of particles being absorbed into the bloodstream, or otherwise condensed onto tissues.[11, 12] Many household items and activities, such as cigarette smoking, candle burning gas stove operation and heated surfaces, serve as sources of ultrafine particles.[3, 12-17] Indoor sources of particulate matter

generally generate much less particulate matter than outdoor/industrial sources, but because these particles are confined in small room volumes they can quickly exceed the EPA's National Ambient Air Quality Standards (NAAQS).[17, 18] Ultrafine particles have high mobility and quickly coagulate to form larger particles. The risk associated with these particles is therefore dependent on the rates of emission, aggregation, and deposition.[12, 17, 19] These rates determine the number and size of the particles as a function of distance from the source. A recent study (HOMEChem) has used a test home to investigate the gas, particle and surface chemistry in the indoor environment.[20] This study focused on the impacts of ventilation and addressed influence of organic aerosol particles and gas phase pollutants.

Due to the ability of nanoparticles to enter into the blood stream, size distribution information alone is not enough to fully understand their impact on human health. The emerging field of nanotoxicology attempts to elucidate the health impacts of nanoparticles based on their composition and size.[8, 21, 22] Understanding the full effects of indoor air pollution lies in the composition of the ultrafine particulate matter. Recent literature has focused on household sources of silver nanoparticles. Silver nanoparticles are well known antimicrobial agents and many products seek to benefit from those properties.[23, 24] Quadros and Marr identified various household antimicrobial sprays as containing silver nanoparticles.[25] Further work has been done by Taylor et al. on types of hairdryers that are marketed for containing antimicrobial silver nanoparticles, as potential sources of silver nanoparticles.[26] As an antimicrobial agent, silver nanoparticles induce oxidative stress within the body. There are no guidelines established by the EPA to regulate the inhalation of silver nanoparticles, however OSHA has a set exposure limit of 0.01 mg m^{-3} for metallic silver and recent literature has highlighted the cytotoxilogical effects of silver nanoparticles.[12, 22, 27] The close proximity of hairdryers to human airways during operation could allow an increase in the localized concentration of silver nanoparticles.

5.2 Experimental Methods

5.2.1 Hairdryers

Six hairdryers were selected for investigation based on the "most popular" listing of hairdryers on Amazon.com at the time of purchase. These included five new and unused hairdryers, and one heavily used hairdryer. The following unused hairdryers were tested: Revlon 1875-watt ceramic, ion hairdryer (Model RV484), Remington Pro (Model D3190), Ovonni (Model BST-808I), Ionic Turbo (Model HTDR5577SN2), and ConAir 1875 Watt (Model 247). The heavily used, approximately five-year-old hairdryer was a Revlon 1875-watt hairdryer (Model RVDR5034). The older hairdryer was used in an attempt to see if a different distribution of particle was observed after long term use.

5.2.2 Particle Generation and Collection

A 127.5 L Plexiglas chamber was built to house the hairdryers during operation to eliminate the influence of ambient aerosol particles (Figure 5-1).[28] In contrast, a previous study with hairdryers was performed in open air without a chamber, where the background levels of aerosol particles are high.[26] Our chamber was purged with prepurified nitrogen gas at a flow rate of 1.5 L min^{-1} for approximately 30 min. Afterward, a condensation particle counter (TSI 3775, Shoreview, MN) was used to verify that the concentration of particles within the chamber had reached a minimum. Each hairdryer was then operated on the lowest setting for 1 min while maintaining a constant 1.5 L min^{-1} flow of prepurified nitrogen. Using a cascade impactor (PIXE International Corp., Tallahassee, FL, USA) particles were collected onto 200 mesh copper TEM grids coated with a continuous carbon coating (Electron Microscopy Science, Hatfield, PA). It

was assumed that the fan within the hairdryer was sufficient to maintain a well-mixed chamber and thus a mixing fan was not used.

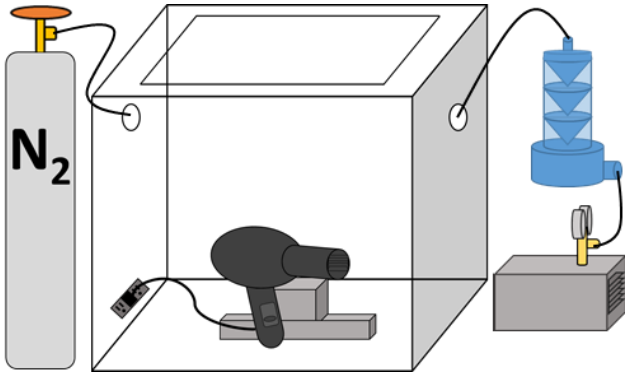

Figure 5-1: Schematic figure of hairdryer experimental set-up showing nitrogen input, impactor, and pump.

5.2.3 Characterization of Chamber and Emission Calculations

To determine the emission rates of the hairdryers, the 127.5 L Plexiglass chamber had to be characterized. First, the air exchange rate (AER) was determined by first filling the chamber with 2500 ppmv CO_2 and then flowing clean air into the chamber at a rate of 1.5 L min^{-1}. A vacuum pump was used to match the flowrate entering the chamber by pulling on the chamber at a rate of 1.5 L min^{-1}. The concentration of CO_2 was monitored with a HOBOware Onset data logger. The rate of decay was for the CO_2 was determined and is the AER. Next the particle deposition rate within the chamber was determined. This was done by filling with chamber with aerosolized 200 nm polystyrene spheres latex beads (PSLs) using an atomizer (TSI 3075) and an air flow rate of 1.5 L min^{-1}. The chamber was continually filled with these aerosolized PSLs until the concentration of particles was stable. The particle concentration was monitored and recorded using a condensation particle counter (CPC, TSI 3775). Once the concentration stabilized, the generation of aerosol was halted but a clean purge flow at a rate of 1.5 L min^{-1} was maintained. The rate of decay of the particles while a purge flow was maintained was then determined. To determine the particle deposition rate, the air exchange rate was subtracted from the particle

decay rate with a purge flow. Each hairdryer was operated at its lowest setting in the chamber while maintaining a purge flow of 1.5 L min^{-1} for 30 min, which exceeded the time required for the particle concentration to reach a maximum and steady value. After 30 min the hairdryer would be turned off while the purge flow continued for another 30 min. Particle emission rates (S) were calculated by

$$S = \frac{V(a+k)C_{peak}}{1-e^{(a+k)t}} \quad (5\text{-}1)$$

where V is the volume of the chamber, C_{peak} is maximum concentration of the particles before they began to decay, a is the air exchange rate, k is the particle deposition rate, and t is the time at C_{peak}.[28] These emission rates were determined for the particles in the ultrafine range, therefore particles greater than 100 nm in diameter were not included in the particle counts.

5.2.4 Particle Characterization

A Tecnai G20 20 XTWIN transmission electron microscope (FEI, Hillsboro, OR) with an accelerating voltage of 200 keV was used to acquire images of particles generated by the hairdryer. This electron microscope is equipped with an EDAX Apollo XLT 30mm^2 silicon drift detector energy dispersive spectrometer (EDS) with a super ultra-thin window. This EDS detector was used to obtain point EDS spectra to quickly characterize particle composition. EDS maps were obtained with a FEI Talos F200X scanning/transmission electron microscope (FEI, Hillsboro, OR) with an accelerating voltage of 200 keV using the Super-X EDS windowless, quad silicone drift detector system at a current of -0.15 nA and a solid angle of 0.9 srad. ImageJ software (NIH) was used to determine the area equivalent diameters of each particle analyzed from the digital micrographs. To determine the source of the silver nanoparticles coming from the hairdryers, their components were studied. The Revlon 1875-watt hairdryer (Model RVDR5034) was disassembled and its components isolated for analysis with inductively coupled plasma

emission spectrometry (ICP-AES). Small samples were obtained from each unique component. Each sample was digested in acid and analyzed via a Perkin-Elmer Optica 5300 UV ICP-AES for silver concentration. Additionally, a duplicate hairdryer of the same model that had never been operated was analyzed in the same manner.

5.3 Results and Discussion

The air exchange rate for the 127.5 L Plexiglass chamber was found to be 0.754 ± 0.060 Hr^{-1} and the particle deposition rate was found to be 0.234 ± 0.190 Hr^{-1}. High errors in particle deposition rates are common and not unexpected in this case. The emission rate of ultrafine particles was determined for four of the hairdryers. The emission rate for the Remington Pro (Model D3190) was found to be 2.60 x 10^{12} ± 1.47 x 10^{12} Hr^{-1}, for the Ovonni (Model BST-808I) it was 1.64 x 10^{12} ± 0.07 x 10^{12} Hr^{-1}, for the ConAir 1875 Watt (Model 247) it was 4.25 x 10^{12} ± 0.36 x 10^{12} Hr^{-1}, and for the Ionic Turbo (Model HTDR5577SN2) it was 1.27 x 10^{12} Hr^{-1} ± 0.42 x 10^{12} Hr^{-1}. Due to the destructive nature of ICP-AES, the emission rates for the Revlon hairdryers were not determined, however since the other four hairdryers produced ultrafine particles on the same order of magnitude, we expect these untested hairdryers to be in the same range. The concentration of ultrafine particles generated by the hairdryers were on the same order of magnitude as ultrafine particle emissions by gas stoves and electric burners, and an order of magnitude higher than ultrafine particle emissions by candles.[29]

Table 5-2: Hairdryer emissions rates determined by the chamber studies and compositions of particles determined by EDS for the six hairdryers in this study.

Hairdryer	Emission Rate ($x10^{12}$ Hr^{-1})	Size Distribution Comments	Composition
Remington Pro (Model D3190)	2.60 ± 1.47	N/A	Iron, Carbon, Copper
Ovonni (Model BST-808I)	1.64 ± 0.07	N/A	Iron, Carbon, Copper
ConAir 1875 Watt (Model 247)	4.25 ± 0.36	N/A	Iron, Carbon, Copper
Ionic Turbo (Model HTDR5577SN2)	1.27 ± 0.42	N/A	Iron, Carbon, Copper
Revlon 1875-watt hairdryer (Model RVDR5034)	N/A	Bimodal	Silver, Nickle, Carbon, Iron
Revlon 1875-watt ceramic, ion hairdryer (Model RV484)	N/A	Bimodal	Silver, Nickle, Carbon, Iron

Of the six hairdryers investigated all emitted particles in the ultrafine range. Emission rates, particle compositions, and distribution types for these hairdryers are tabulated in Table 5-1. Each of the hairdryers emitted particles composed of iron and likely particles composed of copper and carbon. Due to the presence of copper and carbon in the grid however, the determination of copper and carbon in the sample may be unreliable. It should be noted that the relative intensity of the EDS signals does strongly suggest that the particles were composed of carbon and/or copper. Most notably, two of the hairdryers, the Revlon 1875-watt ceramic, ion hairdryer (Model RV484) and the Revlon 1875-watt hairdryer (Model RVDR5034) primarily emitted silver nanoparticles. Resultingly, these hairdryers were analyzed more rigorously. The other four hairdryers had a primary emission of carbon containing nanoparticles, which were likely organic compounds reemitted from the heating elements within the hairdryers. A representative TEM image of the hairdryer emissions of the Revlon Model RV484 is shown in Figure 5-2a. 92.3 % of imaged particles from this hairdryer were nanoparticles in the ultrafine range. The particles are well ordered, exhibiting lattice fringes. The high contrast in the images indicates that they are composed of atoms with a high Z-number. The smallest particles that were observed in this analysis were about 1.5 nm in area equivalent diameter, and the largest particles were about 250

nm. These large particles that are outside the ultrafine range were shown to be the result of aggregation as the impaction stages removed most of the larger particles during operation. This was done because we only had interests in the particles in the ultrafine range. Larger particles are more easily filtered and thus pose less of a health risk. Of the observed particles, sizes were as small as 4 nm. Figure 5-2b shows one such large aggregate surrounded by many much smaller particles that are believed to have deflocculated from the aggregate.[30] Unlike with the previously unused Revlon Model RV484, silver nanoparticles greater than 60 nm were observed in the emissions from the used Revlon Model RVDR5034. This result is likely due to the aforementioned aggregates of particles.

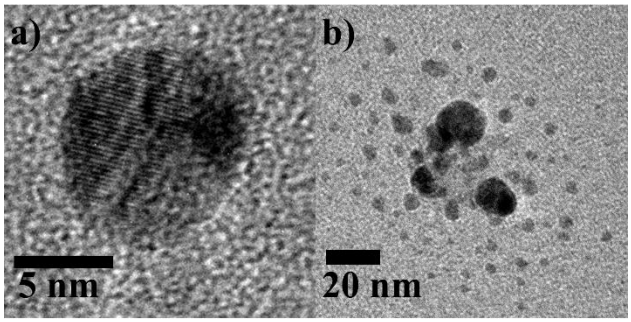

Figure 5-2: a) Representative TEM image of a single silver nanoparticle. b) Representative TEM image of a broken silver nanoparticle aggregate.

EDS spectra were acquired with the EDAX Apollo XLT system and the spectra were used to characterize the composition of each particles from the two Revlon hairdryers. From the EDS spectra, particles were found to contain silver and nickel (Figure 5-3). The unlabeled peaks in the EDS spectra are those of silicon, carbon, copper, lithium, and oxygen; each of these elements are from either the TEM grids and/or the EDS detector used in the analysis. Of the 283 particles analyzed, 81% of particles contained silver. This result is in contrast to the work of Taylor et al. who used scanning electron microscopy paired with EDS. This technique was limited to particles greater than 56 nm and as a result, no silver was detected during their study.[26] It should be noted that the hairdryers used in this study were not marketed as containing silver

nanoparticles, while the study performed by Taylor et al. included hairdryers marketed in this manner.[26]

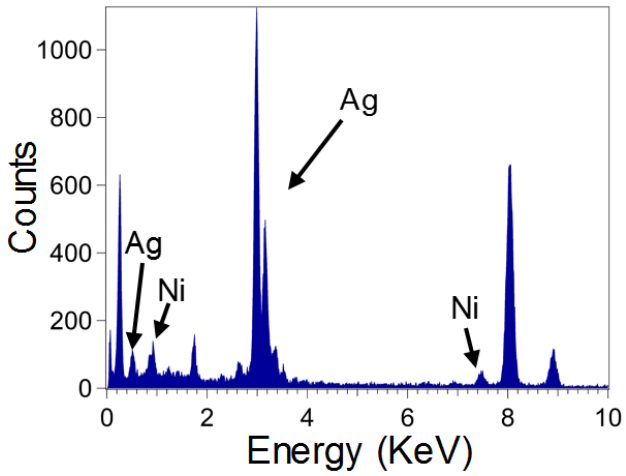

Figure 5-3: A representative EDS spectra of particles emitted by the hairdryer.

To gain a more comprehensive understanding of particle composition and to subtract out background signals from the detector and grids, select, representative particles from the Revlon hairdryers were characterized with EDS mapping. The mapping software (ESpirit) allows for a quantitative elimination of background signal and the mapping itself allows for spatial resolution of particle composition. EDS mapping revealed that particles from the used hairdryer were primarily composed of silver with some nickel on the edges. A representative map of one of these particles is shown in Figure 5-4.

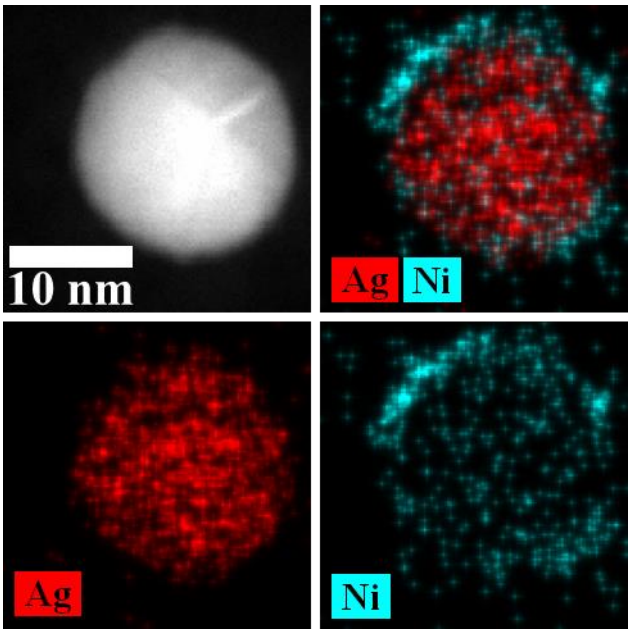

Figure 5-4: EDS map of a representative silver nanoparticle emitted by the used Revlon 1875-watt ceramic, ion hairdryer (Model RV484).

Using the data from the point EDS spectra, size resolved histograms were generated for the silver nanoparticles. The particles had a bimodal distribution centered on the 5 nm and 25 nm bins (Figure 5-5a). The 5 nm bin is exceptionally high compared to the larger size bins. The large population in this bin is hypothesized to be due to loosely aggregated particles breaking free from one another upon impaction with the TEM grid (Figure 5-2b). This behavior has previously been observed when quartz is impacted onto scanning electron microscopy substrates.[31] This hypothesis is further supported by the morphology of particles that did not deflocculate, as shown in Figure 5-6. We theorize that this is representative of how the aggregates will behave upon inhalation.[30, 32]

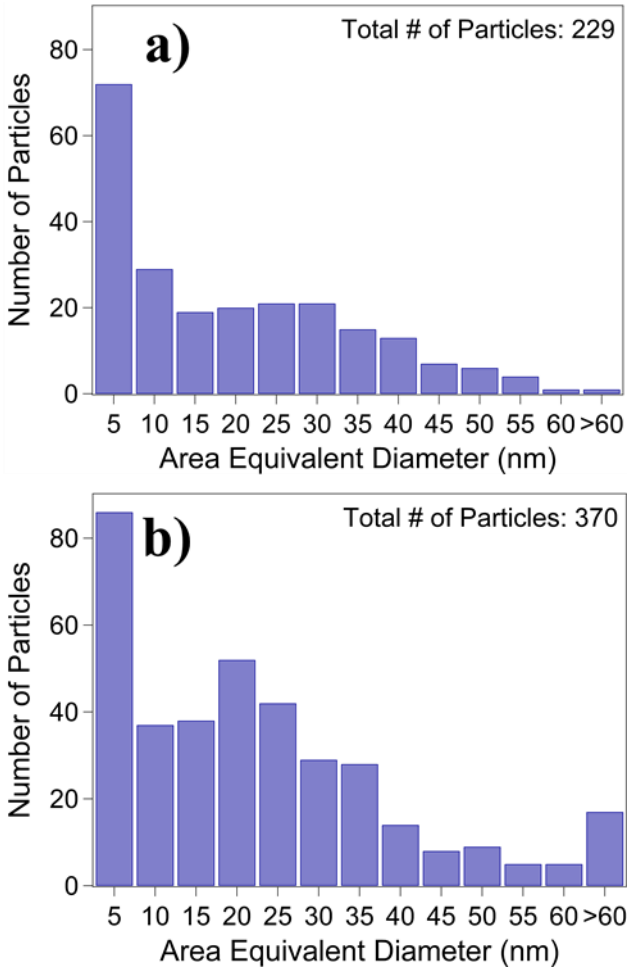

Figure 5-5: a) Histogram of particle sizes emitted by the Revlon Model RVDR5034 (new) hairdryer. B) Histogram of particle sizes emitted by the Revlon Model RV484 (used) hairdryer.

Similar results were obtained from the used hairdryer with the bimodal distribution again centered on the 5 nm and 25 nm size bins (Figure 5-5b). In contrast to the new hairdryer, this sample contained a significant number of particles greater than 60 nm in diameter. A representative image of one of these large aggregates is shown in Figure 5-6a. Again, point EDS revealed that the particles from the used hairdryer were primarily composed of silver. Interestingly, particles that were greater than 60 nm were found to be composed of Ni aggregated with small silver particles, as indicated by EDS mapping (Figure 5-6b). This kind of aggregation was not observed in the hair dryers that did not contain silver; however, the some of the particles primarily composed of iron appeared to be coated in a carbon containing compound.

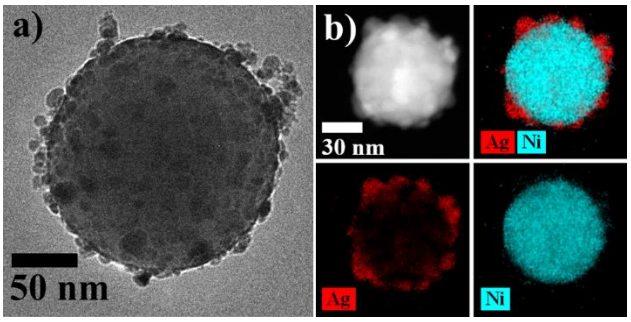

Figure 5-6: a) TEM image of large aggregates emitted by the Revlon Model RVDR5034 hairdryer. b) EDS maps showing that the large aggregates emitted by the Revlon Model RVDR5034 hairdryer are nickel nanoparticles with smaller silver nanoparticles aggregated to them.

To determine the origin of the silver nanoparticles generated by the Revlon Model RVDR5034 hairdryer, it was carefully disassembled and each of the components were separated. All samples contained some silver, as expected due to the extended operation of the hairdryer. When the hairdryer is powered on and silver particles are generated, it is very likely that they are able to travel throughout the hairdryer and accumulate on all components.

The two components with the highest weight percent silver were the solder connecting the power cord to the switches in the handle of the hairdryer with 0.029 ± 0.001 wt% silver, and the metallic, foil-like cover surrounding the heating coil in the head of the hairdryer with 0.038 ± 0.002 wt% silver, marking these two components as the possible primary sources of silver nanoparticles. The heating coil cover has the largest surface area of all components and covers most of the interior of the hairdryer head, raising the possibility that the majority of silver particles settle on this component during operation of the hairdryer as opposed to originating here. A second Revlon 1875-watt hairdryer (Model RVDR5034) was purchased, and immediately, without any operation of the hairdryer after distribution, samples of the same components were isolated and submitted for ICP-AES analysis. Unlike the first analysis, neither the metallic cover nor the solder contained the highest concentrations of silver. This validates the theory that the cover is accumulating silver nanoparticles during operation. Even without operating the device there was evidence of silver, ranging from 0.003 wt% to 0.020 wt%, in many

different components indicating that there may not be any one major source of silver within the hairdryer, but rather multiple smaller sources. After continual operation, much of the silver collects onto the foil-like cover. The size scale of the particles emitted by the hairdryers is alarming as the particles in this range are easily inhaled and can enter the bloodstream. While we cannot directly compare the two hairdryers, it is to be noted that despite heavy usage over a long period, the used hairdryer still produced silver nanoparticles. This result indicates that long term exposure to silver is possible.

5.4 Conclusions

The emissions from six different hairdryers were analyzed. All of the hairdryers were found to emit particles in the ultrafine range. Particles in the ultrafine range are known to cause adverse health effects such as cardiovascular and pulmonary diseases.[4] The hairdryer ultrafine emissions were found to be on the same order of magnitude as the ultrafine emissions of gas and electric stoves. Primarily, the particles measured with TEM were observed to be spherical. Knowing the shape of these nanoparticles may be beneficial for the future of toxicological studies of indoor air pollution.[33] While in general, the hairdryers emitted particles composed of iron, copper, and carbon; the two Revlon hairdryers were shown to generate silver nanoparticles is the ultrafine particle range. Ultrafine silver nanoparticles have been shown to pose additional negative health effects in addition to those caused by uncategorized ultrafine particles.[24] Specifically, silver nanoparticles can cause oxidative stress within cells which can lead to cellular death.[12] Additionally, the nickel was observed as well as possible organic coatings. These two compositions may also pose unique health effects when in the body, and while they were in lower amounts than the silver, they were often on the surface where most chemical reactions will take place. Larger silver containing particles were found to be the result of aggregation of ultrafine

particles. The Revlon 1875-watt hairdryer (Model RVDR5034) used in the study and a duplicate hairdryer were both disassembled and the components were tested for silver with ICP-AES. While no one component was the main source of silver, many components were found to contain silver. Due to their antimicrobial properties, silver nanoparticles can be harmful if they enter into the bloodstream and the particles observed in this study were small enough to pass through the blood-air barrier if inhaled. Indoor air pollution sources are potentially harmful when operated in locations with poor ventilation. Without a removal method, ultrafine particulate matter produced by indoor sources can reach high concentrations. Sources, such as hairdryers, are often operated close to human airways and thus even when ventilation is available the proximity to pollution source may result in exposure to high concentrations of particles.

References

1. Miller, F. J.; Gardner, D. E.; Graham, J. A.; Lee, R. E.; Wilson, W. E.; Bachmann, J. D., Size Considerations for Establishing a Standard for Inhalable Particles. *Journal of the Air Pollution Control Association* **1979**, *29*, (6), 610-615.

2. Dockery, D. W.; Pope, C. A.; Xu, X.; Spengler, J. D.; Ware, J. H.; Fay, M. E.; Ferris, B. G.; Speizer, F. E., An Association between Air Pollution and Mortality in Six U.S. Cities. *New England Journal of Medicine* **1993**, *329*, (24), 1753-1759.

3. Pope III, C. A.; Thun, M. J.; Namboodiri, M. M.; Dockery, D. W.; Evans, J. S.; Speizer, F. E.; Clark W. Heath, J., Particulate Air Pollution as a Predictor of Mortality in a Prospective Study of U.S. Adults. *American Journal of Respiratory and Critical Care Medicine* **1995**, *151*, (3), 669-674.

4. Pope III, C. A.; Burnett, R. T.; Thun, M. J.; Calle, E. E.; Krewski, D.; Ito, K.; Thurston, G. D., Lung Cancer, Cardiopulmonary Mortality, and Long-term Exposure to Fine Particulate Air Pollution. *JAMA* **2002**, *287*, (9), 1132-1141.

5. Miller, K. A.; Siscovick, D. S.; Sheppard, L.; Shepherd, K.; Sullivan, J. H.; Anderson, G. L.; Kaufman, J. D., Long-Term Exposure to Air Pollution and Incidence of Cardiovascular Events in Women. *New England Journal of Medicine* **2007**, *356*, (5), 447-458.

6. Heo, J.; Adams, P. J.; Gao, H. O., Public Health Costs of Primary PM2.5 and Inorganic PM2.5 Precursor Emissions in the United States. *Environmental Science & Technology* **2016**, *50*, (11), 6061-6070.

7. Oberdörster, G.; Celein, R. M.; Ferin, J.; Weiss, B., Association of Particulate Air Pollution and Acute Mortality: Involvement of Ultrafine Particles? *Inhalation Toxicology* **1995**, *7*, (1), 111-124.

8. Nel, A. E.; Mädler, L.; Velegol, D.; Xia, T.; Hoek, E. M. V.; Somasundaran, P.; Klaessig, F.; Castranova, V.; Thompson, M., Understanding biophysicochemical interactions at the nano–bio interface. *Nature Materials* **2009**, *8*, (7), 543-557.

9. Oberdörster, G.; Oberdörster, E.; Oberdörster, J., An emerging discipline evolving from studies of ultrafine particles supplemental web sections. *Environmental Health Perspectives* **2005**, *113*, (7), 823-839.

10. Klepeis, N. E.; Nelson, W. C.; Ott, W. R.; Robinson, J. P.; Tsang, A. M.; Switzer, P.; Behar, J. V.; Hern, S. C.; Engelmann, W. H., The National Human Activity Pattern Survey (NHAPS): a resource for assessing exposure to environmental pollutants. *Journal of Exposure Science & Environmental Epidemiology* **2001**, *11*, (3), 231-252.

11. Nel, A.; Xia, T.; Mädler, L.; Li, N., Toxic Potential of Materials at the Nanolevel. *Science* **2006**, *311*, (5761), 622-627.

12. Verma, A.; Stellacci, F., Effect of Surface Properties on Nanoparticle–Cell Interactions. *Small* **2010**, *6*, (1), 12-21.

13. Hussein, T.; Glytsos, T.; Ondráček, J.; Dohányosová, P.; Ždímal, V.; Hämeri, K.; Lazaridis, M.; Smolík, J.; Kulmala, M., Particle size characterization and emission rates during indoor activities in a house. *Atmospheric Environment* **2006**, *40*, (23), 4285-4307.

14. Géhin, E.; Ramalho, O.; Kirchner, S., Size distribution and emission rate measurement of fine and ultrafine particle from indoor human activities. *Atmospheric Environment* **2008**, *42*, (35), 8341-8352.

15. Pagels, J.; Wierzbicka, A.; Nilsson, E.; Isaxon, C.; Dahl, A.; Gudmundsson, A.; Swietlicki, E.; Bohgard, M., Chemical composition and mass emission factors of candle smoke particles. *Journal of Aerosol Science* **2009**, *40*, (3), 193-208.

16. Wallace, L.; Wang, F.; Howard-Reed, C.; Persily, A., Contribution of Gas and Electric Stoves to Residential Ultrafine Particle Concentrations between 2 and 64 nm: Size Distributions and Emission and Coagulation Rates. *Environmental Science & Technology* **2008**, *42*, (23), 8641-8647.

17. Rim, D.; Choi, J.-I.; Wallace, L. A., Size-Resolved Source Emission Rates of Indoor Ultrafine Particles Considering Coagulation. *Environmental Science & Technology* **2016**, *50*, (18), 10031-10038.

18. U.S. EPA National Ambient Air Quality Standards for Particulate Matter. www.epa.gov/criteria-air-pollutants/naaqs-table (September 27, 2020).

19. Nazaroff, W. W., Indoor particle dynamics. *Indoor Air* **2004**, *14*, (Supplement 7), 175-183.

20. Farmer, D. K.; Vance, M. E.; Abbatt, J. P.; Abeleira, A.; Alves, M. R.; Arata, C.; Boedicker, E.; Bourne, S.; Cardoso-Saldaña, F.; Corsi, R., Overview of HOMEChem: House observations of microbial and environmental chemistry. *Environmental Science: Processes & Impacts* **2019**, *21*, (8), 1280-1300.

21. Blaser, S. A.; Scheringer, M.; MacLeod, M.; Hungerbühler, K., Estimation of cumulative aquatic exposure and risk due to silver: Contribution of nano-functionalized plastics and textiles. *Science of The Total Environment* **2008**, *390*, (2), 396-409.

22. Rai, M.; Yadav, A.; Gade, A., Silver nanoparticles as a new generation of antimicrobials. *Biotechnology Advances* **2009**, *27*, (1), 76-83.

23. Maillard, J.-Y.; Hartemann, P., Silver as an antimicrobial: facts and gaps in knowledge. *Critical Reviews in Microbiology* **2013**, *39*, (4), 373-383.

24. Yang, X.; Gondikas, A. P.; Marinakos, S. M.; Auffan, M.; Liu, J.; Hsu-Kim, H.; Meyer, J. N., Mechanism of Silver Nanoparticle Toxicity Is Dependent on Dissolved

Silver and Surface Coating in Caenorhabditis elegans. *Environmental Science & Technology* **2012**, *46*, (2), 1119-1127.

25. Quadros, M. E.; Marr, L. C., Silver Nanoparticles and Total Aerosols Emitted by Nanotechnology-Related Consumer Spray Products. *Environmental Science & Technology* **2011**, *45*, (24), 10713-10719.

26. Taylor, A. A.; Khan, M. Y.; Helbley, J.; Walker, S. L., Safety evaluation of hair-dryers marketed as emitting nano silver particles. *Safety Science* **2017**, *93*, 121-126.

27. U.S. Dept. of Labor. OSHA Permissible Exposure Limits / OSHA Annotated Table Z-1. www.osha.gov/dsg/annotated-pels/tablez-1.html (November 28, 2019).

28. Afshari, A.; Matson, U.; Ekberg, L. E., Characterization of indoor sources of fine and ultrafine particles: a study conducted in a full-scale chamber. *Indoor Air* **2005**, *15*, (2), 141-150.

29. Rim, D.; Green, M.; Wallace, L.; Persily, A.; Choi, J.-I., Evolution of Ultrafine Particle Size Distributions Following Indoor Episodic Releases: Relative Importance of Coagulation, Deposition and Ventilation. *Aerosol Science and Technology* **2012**, *46*, (5), 494-503.

30. El-Gendy, N.; Desai, V.; Berkland, C., Agglomerates of ciprofloxacin nanoparticles yield fine dry powder aerosols. *Journal of Pharmaceutical Innovation* **2010**, *5*, (3), 79-87.

31. Veghte, D. P.; Altaf, M. B.; Haines, J. D.; Freedman, M. A., Optical properties of non-absorbing mineral dust components and mixtures. *Aerosol Science and Technology* **2016**, *50*, (11), 1239-1252.

32. Shi, L.; Plumley, C. J.; Berkland, C., Biodegradable Nanoparticle Flocculates for Dry Powder Aerosol Formulation. *Langmuir* **2007**, *23*, (22), 10897-10901.

33. Pal, S.; Tak, Y. K.; Song, J. M., Does the Antibacterial Activity of Silver Nanoparticles Depend on the Shape of the Nanoparticle? A Study of the Gram-Negative Bacterium *Escherichia coli*. *Applied and Environmental Microbiology* **2007**, *73*, (6), 1712-1720.

Chapter 6

Conclusions and Future Directions

6.1 Conclusions

In this dissertation the physics and chemistry of aerosol particles have been explored with regard to their atmospheric implications and health effects. Aerosol particles affect the global radiative budget through their interactions with light. These particles can further affect the environment by leading to cloud formation, or haze formation. Aerosol particles, specifically submicron particles, have a negative effect on human health when inhaled. We have demonstrated the effect of molecular weight on the single hygroscopicity term, κ, in accordance to κ-Kohler theory. To investigate this relation, we measure the hygroscopicity of WSOCs with CRDS, H-TDMA, and CCNC. The results from these complimentary techniques were then compared to establish what factors result in their differences. We explored the influence of viscosity on particle hygroscopicity, but observed no trend. The WSOCs used in this study were not surface active and as a result matched the theory trend quite well since surface active species are known to deviate.

SOA particles are formed by gas-phase reactions in the atmosphere. Due to the diversity of gaseous species in the atmosphere, the composition of SOA is poorly understood, and this lack of compositional knowledge leads to uncertainty in the hygroscopic properties of SOA. We have shown that poorly soluble SOA coatings limit the water uptake of hygroscopic cores, and that the composition of SOA plays a role in its hygroscopicity. It was discovered that κ-values from subsaturated hygroscopicity measurement techniques can often vary from supersaturated techniques, especially when the deliquescence point of the compound being studied is greater

than 90% RH. These results suggest that the hygroscopic growth of external mixtures may be governed by the water uptake of SOA coatings.

An understanding of the differences between hygroscopic measurement techniques is necessary to standardize reported hygroscopicity values. At present, κ-values are used by modelers to determine the radiative forcing of aerosol particles in a humid environment or otherwise determine what conditions are required for those particles to act as cloud condensation nuclei. Reducing the variance in reported κ-values is therefore important to reduce the error in the radiative forcing calculations. One of the largest uncertainties in atmospheric chemistry for radiative forcing stems from both the influence of aerosol particles and clouds formed by aerosol particles.

The negative health effects of aerosol particles are magnified when they are in high concentrations. Within indoor environments humans can be exposed to relatively high concentrations of ultrafine aerosol particles. Ultrafine particles in particular are those that are smaller than 100 nm in diameter and can enter into the bloodstream if inhaled. The full extent of these adverse health effects cannot be evaluated by size alone; composition plays a large role. We have shown that hairdryers emit concentrations of ultrafine aerosol particles similar to other household sources such as gas burning stoves. These particles were characterized using TEM and EDS analysis to obtain further size and composition information. It was discovered that some hairdryers emit silver nanoparticles. The presences of silver nanoparticles emitted by hairdryers is important due to their specific cytological toxicity resulting from oxidative stress. The nanotoxilogical effects of aerosol particles is very poorly understood. Composition, shape and phase state all play important roles in the degree of toxicity of aerosol particles.

6.2 Future Directions

The atmosphere contains a large number of aerosol particle species of varying complexity. Up to this point, my work has focused on overly-simplified systems that are not truly representative of atmospheric systems. This approach focuses on studying the more fundamental properties of aerosolized particles and observing trends that can be applied to more complicated systems. A continuation of this work is therefore two-fold. The first is to continue to study fundamental properties, such as the effect of particle morphology on water uptake and a broader study of how populations of aerosol particles behave based on their mixing states. The second approach to continuing this work is to use the trends we have observed and apply them to more atmospherically relevant systems.

One of the most meaningful conclusions from my work is in the comparison of multiple techniques. In this comparison we observed that values obtained by the supersaturated technique CCNC were generally higher than those obtained by the sub-saturated technique of H-TDMA. CRDS trended very high, likely due to the influence of double charged particles. By applying a more rigorous study of these differences, a methodology can be established to relate values obtained by one method to values obtained by a differing method. As such, a standardized approach to reporting κ-values may be established. While this is seemingly trivial, the result is a reduction of variance in reported κ-values and ultimately a reduction in error in climate models that calculate radiative forcing based on those values.

An important trend observed from the WSOCs study was the importance of molecular weight on hygroscopicity for non-surface active species in accordance to κ-Kohler theory.[1] However, κ-Kohler theory breaks down when surface active species are present. Another fundamental study to be performed, then, is to see if molecular weight still correlates strongly

with hygroscopcity when using systems that are surface active. Such an approach would involve κ measurements of saponificants of increasing molecular weights with similar surface activities.

Previous work by our group has shown that particles of the same composition can have differing morphologies based on size.[2] Large particles may be phase-separated with an organic coating on an inorganic core, while smaller particles remain homogenous. The range of sizes where this transition occurs is dependent on the particles' compositions and the environment surrounding the particles. The results presented in this work indicate that organic coatings may inhibit water uptake. To explore this effect, the hygroscopicity of phase separated particles can be compared to the hygroscopicity of homogeneous particles with similar physical properties such as molecular weight, surface activity, degree of oxidation, and density.

The atmosphere is more complex than simple internal mixtures, or even internal mixtures of phase-separated particles. In truth, the atmosphere contains a large external mixture of aerosol particles that often interact with each other, either directly, or by desorbing and absorbing semi-volatile organic compounds.[3] As such, another fundamental study to be performed is to observe populations of aerosol particles that are internally mixed and compare their behavior to populations that are externally mixed, such that the overall composition of the populations remains the same. Understanding these complex systems is necessary for predicting the behavior of atmospheric aerosol systems.

The study of health effects of indoor aerosol pollution is a somewhat fledgling field. As previously discussed, most studies only consider particle size when determining the impact particles have on human health.[4-6] My work focused on categorizing indoor aerosol particles by composition, with some consideration to shape. The scope of this work was very limited, resulting in a focus on hairdryers since they operate near the face, and thus have a high likelihood of directly influencing the user's health. However, indoor air pollution sources vary greatly and are not only generated from primary sources like stoves and hairdryers. The continuation of this

work will focus on oxidative reactions that occur with semivolatile and volatile compounds that are released indoors, such as the compounds responsible for scents from candles and laundry detergents. It has been shown that ozone can react with the squalene on human skin to form secondary organic aerosol within confined areas, such as on aircraft.[7] This work will use the 127.5 L Plexiglass chamber from chapter 5 and an ozone generator to expose household products to highly oxidizing environments.

My work with indoor air pollutants can be expanded beyond the brute force method of studying various indoor sources. Specifically, techniques can be developed to improve how we study the populations of indoor aerosol particles. As previously mentioned, most studies focus on size resolving the populations, however another major concern is particle morphology.[8, 9] A solid aerosol and a liquid aerosol will behave differently within the human body, and as such, developing techniques to differentiate between these types of particles is key.[10, 11] Bounce factor studies have been applied in other areas of atmospheric chemistry with exactly this consideration in mind.[12, 13] The development of an experimental system that is able to resolve size and morphology of indoor aerosol pollutants may be a next step in analyzing particle populations. Identifying these potential pollutants will expand our understanding of the various compositions of particles within the indoor environment. Additionally, the development of new methodologies may allow for a better understanding of the health impacts of particle populations. These understandings are crucial for the development of guidelines to improve indoor air quality.

References

1. Petters, M. D.; Kreidenweis, S. M., A single parameter representation of hygroscopic growth and cloud condensation nucleus activity. *Atmospheric Chemistry and Physics* **2007**, *7*, (8), 1961-1971.

2. Veghte, D. P.; Altaf, M. B.; Freedman, M. A., Size Dependence of the Structure of Organic Aerosol. *Journal of the American Chemical Society* **2013**, *135*, (43), 16046-16049.

3. Pöhlker, C.; Wiedemann, K. T.; Sinha, B.; Shiraiwa, M.; Gunthe, S. S.; Smith, M.; Su, H.; Artaxo, P.; Chen, Q.; Cheng, Y.; Elbert, W.; Gilles, M. K.; Kilcoyne, A. L. D.; Moffet, R. C.; Weigand, M.; Martin, S. T.; Pöschl, U.; Andreae, M. O., Biogenic Potassium Salt Particles as Seeds for Secondary Organic Aerosol in the Amazon. *Science* **2012**, *337*, (6098), 1075-1078.

4. U.S. EPA National Ambient Air Quality Standards for Particulate Matter. www.epa.gov/criteria-air-pollutants/naaqs-table (September 27, 2020),

5. Dockery, D. W.; Pope, C. A.; Xu, X.; Spengler, J. D.; Ware, J. H.; Fay, M. E.; Ferris, B. G.; Speizer, F. E., An Association between Air Pollution and Mortality in Six U.S. Cities. *New England Journal of Medicine* **1993**, *329*, (24), 1753-1759.

6. Pope III, C. A.; Thun, M. J.; Namboodiri, M. M.; Dockery, D. W.; Evans, J. S.; Speizer, F. E.; Clark W. Heath, J., Particulate Air Pollution as a Predictor of Mortality in a Prospective Study of U.S. Adults. *American Journal of Respiratory and Critical Care Medicine* **1995**, *151*, (3), 669-674.

7. Weisel, C.; Weschler, C. J.; Mohan, K.; Vallarino, J.; Spengler, J. D., Ozone and Ozone Byproducts in the Cabins of Commercial Aircraft. *Environmental Science & Technology* **2013**, *47*, (9), 4711-4717.

8. Rim, D.; Choi, J.-I.; Wallace, L. A., Size-Resolved Source Emission Rates of Indoor Ultrafine Particles Considering Coagulation. *Environmental Science & Technology* **2016**, *50*, (18), 10031-10038.

9. Géhin, E.; Ramalho, O.; Kirchner, S., Size distribution and emission rate measurement of fine and ultrafine particle from indoor human activities. *Atmospheric Environment* **2008**, *42*, (35), 8341-8352.

10. Verma, A.; Stellacci, F., Effect of Surface Properties on Nanoparticle–Cell Interactions. *Small* **2010**, *6*, (1), 12-21.

11. Nel, A.; Xia, T.; Mädler, L.; Li, N., Toxic Potential of Materials at the Nanolevel. *Science* **2006**, *311*, (5761), 622-627.

12. Chang, M.; Kim, S.; Sioutas, C., Experimental studies on particle impaction and bounce: effects of substrate design and material. *Atmospheric Environment* **1999**, *33*, (15), 2313-2322.

13. Virtanen, A.; Kannosto, J.; Kuuluvainen, H.; Arffman, A.; Joutsensaari, J.; Saukko, E.; Hao, L.; Yli-Pirilä, P.; Tiitta, P.; Holopainen, J. K.; Keskinen, J.; Worsnop, D. R.; Smith, J. N.; Laaksonen, A., Bounce behavior of freshly nucleated biogenic secondary organic aerosol particles. *Atmospheric Chemistry and Physics* **2011**, *11*, (16), 8759-8766.

VITA

Joseph Nelson Dawson

Education

Doctor of Philosophy in Chemistry September 2020
The Pennsylvania State University | University Park, PA
GPA: 3.39 on a 4.00 scale

Bachelor of Science in Chemistry May 2015
University of North Alabama | Florence, AL
Minor in Mathematics. GPA: 3.69 on a 4.00 scale

Associate of Science in Chemistry May 2013
Northwest Shoals Community College | Muscle Shoals, AL
GPA: 3.77 on a 4.00 scale

Professional Associations, Awards & Highlighted Outreach

Co-Chair, Graduate Women in Science Fall 2016 - Fall 2018
GWIS Affiliates Chapter | The Pennsylvania State University

President, Chemistry Club April 2014 - April 2015
ACS Affiliates Chapter | University of North Alabama

Recipient, NSF Graduate Research Fellowship March 2017 - May 2020
National Science Foundation | The Pennsylvania State University

Recipient, Analytical Chemistry Award May 2014
Department of Chemistry and Industrial Hygiene | University of North Alabama

Recipient, Scholastic Honors in Chemistry Award May 2013
Department of Science | Northwest Shoals Community College

Organizer and Invited Lecturer, Grad School 101 Lecture September 2017
Department of Science | Northwest Shoals Community College

Publication History

• **J. N. Dawson,** K. A. Malek, P. N. Razafindrambina, T. M. Raymond, D. D Dutcher, A. Asa-Awuku, M. A. Freedman. Direct Comparison of the Hygroscopicity of Water-Soluble Sugars. *ACS Earth and Space Chemistry*. ***Article ASAP***.

• **J. N. Dawson**, K. A. Malek, P, N, Razafindrambina, K. DiMonte, T. M. Raymond, D. D Dutcher, A. Asa-Awuku, M. A. Freedman. Simultaneous Measurements of Laboratory Generated SOA's Hygroscopicity, CCN Activity, and Optical Properties. *In Prep.*

• **J. N. Dawson**, K. DiMonte, M. Griffin, M. A. Freedman. Silver Nanoparticles Emitted Through Routine Operation of a Hairdryer. *In Prep.*

• T. M. Kucinski, **J. N. Dawson**, M. A. Freedman. Size-Dependent Liquid-Liquid Phase Separation in Atmospherically Relevant Complex Systems. *Journal of Physical Chemistry Letters*. **10**(21), 6915-6920 (2019)

• V. J. Alstadt, **J. N. Dawson**, D. J. Losey, S. K. Sihvonen, M. A. Freedman. Heterogeneous Freezing of Carbon Nanotubes: A Model System for Pore Condensation and Freezing in the Atmosphere. *Journal of Physical Chemistry A.* **121**(42), 8166-8175 (2017)

• X. Fan, **J. Dawson**, M. Chen, C. Qiu, A. Khalizov. Thermal Stability of Particle-Phase Monoethanolamine Salts. *Environmental Science and Technology*. **52** (4), 2409-2417 (2018)